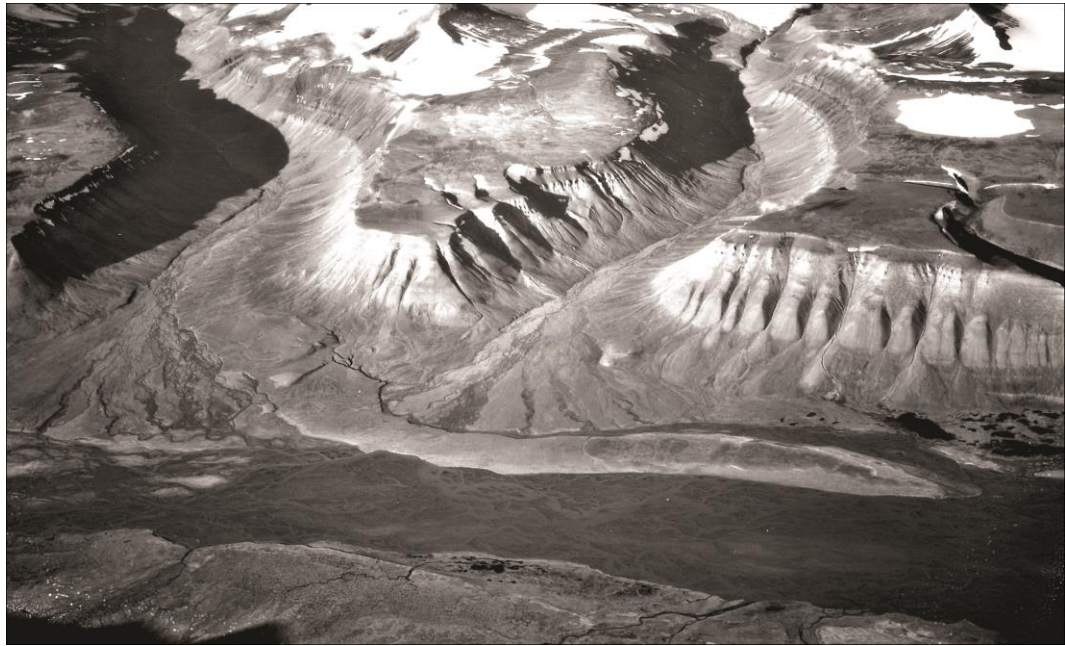


**Master Thesis, Department of Geosciences**

**Sedimentology and geocryology of an  
Arctic fjord head delta  
(Adventdalen, Svalbard)**

**Graham Lewis Gilbert**



**UNIVERSITY OF OSLO**

**FACULTY OF MATHEMATICS AND NATURAL SCIENCES**



# **Sedimentology and geocryology of an Arctic fjord head delta (Adventdalen, Svalbard)**

**Graham Lewis Gilbert**



Master Thesis in Geosciences

Discipline: Physical Geography, Hydrology, and Geomatics

Department of Geosciences

Faculty of Mathematics and Natural Sciences

University of Oslo

**June 1<sup>st</sup> 2014**

© Graham Lewis Gilbert, 2014

Supervisors: Prof. Henning Dypvik (UiO); Prof. Hanne H. Christiansen (UNIS/KU)

This work is published digitally through DUO – Digitale Utgivelser ved UiO

<http://www.duo.uio.no>

It is also catalogued in BIBSYS (<http://www.bibsys.no/english>)

All rights reserved. No part of this publication may be reproduced or transmitted, in any form or by any means, without permission.



*Cover photo: A south-facing perspective over lower Adventdalen and the study site. The Endalen Valley and its associated alluvial fan are situated in the center of the image. The Adventelva River is in the foreground. Study site is indicated by the black arrow. Aerial photograph taken in 1936 by the Norwegian Polar Institute.*

## ABSTRACT

The evolution of sedimentary environments and permafrost in Adventdalen during the late Quaternary period has been reconstructed using cryostratigraphic and sedimentary evidence from a 60 m ice-bonded sediment core. Results are contextualized with existing knowledge regarding sea-level variations and glacial history. Sediment properties (facies, grain size distribution, bioturbation intensity, and trace fossils), ground-ice characteristics (gravimetric moisture content, excess ice content, and cryostructures), and age determinations are utilized to identify sedimentary environments and subenvironments.

This core was retrieved in September 2012 as part of the investigations undertaken by the UNIS CO<sub>2</sub> Lab at the Adventdalen well park (9 m.a.s.l., 78°12'N, 15°49'E). Encompassing the interval between the ground surface and Cretaceous bedrock (Carolinefjellet Formation) at ca. 60 m depth, this core forms the basis for the first comprehensive description of Holocene permafrost and sedimentary development in Adventdalen. This is the deepest core obtained from Svalbard with the express purpose of reconstructing permafrost conditions and development.

The presence of cryostructures allows for the determination of the nature of permafrost aggradation and conditions under which the sediment has accumulated. In addition to cryostratigraphy, detailed sediment analysis has resulted in a facies model, permitting inference of changes in depositional environments. To establish temporal variations in sedimentation rates ca. 42 samples were taken for dating. Optically stimulated luminescence (OSL) was the primary method used; however, a few samples were selected for Accelerator Mass Spectrometry radiocarbon (AMS <sup>14</sup>C) dating in order to obtain a more robust chronostratigraphy.

Three main cryostructures have been identified in the Adventdalen permafrost core: pore ice, layered ice, and ice lenses. The distribution of these ice types in combination with the dating results indicates that permafrost aggradation at this site began ca. 3 kya – once the ground was exposed subaerially. Core sedimentology and chronology indicates that during the Last Glacial Maximum, a fast-moving ice stream, located in Adventdalen, removed all unconsolidated sediments, leaving only a thin layer of till. Following deglaciation, marine conditions dominated during the early Holocene. The transitioning to delta-driven sedimentation occurred at ca. 6.8 kya during which time a sedimentation rate of ca. 20 m ky<sup>-1</sup> is reconstructed. Establishment of the modern, aeolian dominated environment took place ca. 3 kya, and coincides with the onset of conditions favorable to permafrost aggradation. This conclusion suggests that permafrost in the Adventdalen valley bottom is likely a Holocene phenomenon.

## SAMMENDRAG

Utviklingen av sedimentære miljøer og permafrost i Adventdalen i sen kvartær er rekonstruert ved å bruke kryostratigrafiske og sedimentologiske data fra en 60 meter dyp sedimentkjerne i permafrosten. Resultatene blir satt sammen med eksisterende kunnskap om havnivåendringer og glasiasjoner. Sedimentegenskaper (facies, kornstørrelsesfordeling, intensitet i bioturbasjon og sporfossiler), kjennetegn på is i kjernen (andel vann av total masse, andel is som overgår porevolum i tint tilstand, og isstrukturer) og ulike dateringer er anvendt for å identifisere større og mindre avsetningsmiljø.

Kjernen ble tatt opp i september 2012 i Adventdalen brønnpark (9 m. o. h., 78°12'N, 15°49'Ø) som en del av undersøkelser foretatt av UNIS CO<sub>2</sub> Lab. Den strekker seg fra overflaten og ned til krittlagene (Carolinefjellformasjonen) på ca. 60 meters dybde. Kjernen danner grunnlaget for den første omfattende beskrivelsen av sen kvartær sedimentærutvikling i Adventdalen og permafrost dannet i Holosen. Dette er den dypeste kjernen som er tatt opp fra løsmasser på Svalbard med formål om å rekonstruere permafrostforhold og utvikling.

Isstrukturer gjør det mulig å bestemme hvordan permafrosten har utviklet seg over tid og hvilke sedimentære egenskaper som er av særlig betydning. I tillegg til kryostratigrafi, har detaljerte sedimentologiske analyser resultert i en faciesmodell, som gjør det mulig å rekonstruere endringer i avsetningsmiljøet. Ca. 42 prøver ble datert for å fastslå variasjoner i sedimentasjonshastigheter over tid. Hovedmetoden som ble benyttet var optisk stimulert luminescens (OSL), men for å oppnå en mer pålitelig kronostratigrafi ble i tillegg noen prøver datert ved <sup>14</sup>C-metoden (AMS <sup>14</sup>C).

I kjernen ble det identifisert tre hovedformer for isstrukturer; poreis, lagdelt is og islinser. Fordelingen av disse tre istypene, i kombinasjon med dateringsresultatene, indikerer at akkumulasjon av permafrost på dette stedet startet for ca. 3000 år siden, da terrenget ble eksponert for luft. Kjerneanalysen og kronostratigrafiske bestemmelser indikerer at en raskt bevegende isstrøm i løpet av siste istids maksimum fjernet alle ukonsoliderte sedimenter og bare et lite lag med morene ble liggende igjen. Etter påfølgende isavsmelting dominerte marine forhold i Adventdalen gjennom tidlig Holosen. Overgangen til deltaisk sedimentasjon skjedde omkring 6 800 år siden, og i denne tidsperioden er det estimert en sedimentasjonshastighet på ca. 20 meter per tusen år. Dannelsen av det moderne eolisk dominerte miljøet skjedde for omkring 3000 år siden. Dette faller sammen med begynnende permafrostdannelse. Disse resultatene viser at permafrosten i Adventdalen mest sannsynlig er fra Holosen.

## ACKNOWLEDGEMENTS

The supervision of Dr. Henning Dypvik (UiO) and Dr. Hanne H. Christiansen (UNIS/KU) is gratefully acknowledged. Their continuing support during this investigation and input to preliminary presentations and manuscripts has greatly improved all elements of this investigation.

Many individuals at the University Centre on Svalbard and University of Oslo provided assistance during this investigation. Mufak Naoroz provided an introduction to the laboratory methods pertaining to grain size analysis. Dr. Jenö Nagy contributed to my understanding of trace fossil analysis and gave much needed corrections to initial attempts to classify ichnogenera. Elisabeth Tønnessen kindly read and considered early versions of the chapters contained in this thesis, providing comments and corrections. First-class field assistance was provided by Katja Baum in September 2012. Wesley Farnsworth, Sara Cohen, Mikkel Kristiansen, Helge Gjelberg, Stefanie Härtel, and Alexander Hovland were an invaluable source of scientific discussion and companionship during my time in Longyearbyen.

The Optically Stimulated Luminescence dating included in this thesis was conducted by Dr. Christine Thiel in collaboration with Dr. Jan-Pieter Buylaert and Dr. Andrew Murray at the Nordic Centre for Luminescence Research (Risø, Denmark). I am particularly grateful to Christine for her willingness to travel to Svalbard and introducing me to luminescence dating and the sampling techniques for this method.

Financial support for this investigation was provided by the UNIS CO<sub>2</sub> Laboratory (<http://co2-ccs.unis.no/>). The realization of this project is thanks largely to the willingness of Dr. Alvar Braathen, Dr. Snorre Olausen, and Trygve Dahl to incorporate the retrieval of this core into the summer 2012 drilling programme. Personal financial support was provided by the Natural Sciences and Engineering Research Council of Canada (NSERC). As a Canadian, I am proud of NSERC's commitment to supporting the scientific pursuits of young Canadians abroad.

Finally, I would like to thank Åse and my immediate family for their support these past two years. I am particularly grateful to Åse for her patience during my extended periods on Svalbard and tolerance during the completion of this thesis.

## Contents

ABSTRACT.....	I
SAMMENDRAG.....	II
ACKNOWLEDGEMENTS.....	III
Chapter 1 INTRODUCTION .....	1
1.1. Motivation, hypothesis, and objectives .....	3
1.2. Thesis structure .....	3
Chapter 2 PERMAFROST, GROUND ICE, AND CRYOSTRATIGRAPHY .....	5
2.1. Climate and permafrost .....	5
2.2. Ground ice .....	6
2.3. Cryostratigraphy.....	11
Chapter 3 REGIONAL SETTING AND SEDIMENTARY ENVIRONMENTS.....	14
3.1. Regional Quaternary history .....	14
3.1.1. Last Glacial Maximum (LGM).....	14
3.1.2. Deglaciation .....	16
3.1.3. Post-LGM sea level changes.....	16
3.1.4. Implications for permafrost development.....	17
3.2. Climate and meteorology .....	17
3.2.1. Holocene palaeoclimate .....	17
3.2.2. Meteorology.....	19
3.3. Adventdalen region .....	19
3.3.1. Geology.....	20
3.3.2. Quaternary geology and geomorphology.....	23
3.3.3. Permafrost.....	23
3.4. Modern sedimentary environments.....	26
Chapter 4 MATERIALS AND METHODS.....	31
4.1. Core retrieval.....	31
4.2. Analysis of core samples.....	31
4.2.1. Sedimentary log .....	31
4.2.2. Facies, facies associations, bioturbation, and trace fossils .....	34
4.2.3. Grain size determination and statistical parameters.....	34
4.2.4. Excess ice content and gravimetric moisture content .....	36
4.2.5. Cryostratigraphy and cryostructures .....	37
4.2.6. Chronology (OSL and AMS <sup>14</sup> C) .....	37
Chapter 5 RESULTS: SEDIMENTOLOGY .....	40
5.1. Facies and Facies Associations .....	40
5.2. Grain size distribution and statistical parameters.....	47
5.2.1. Grain size distribution.....	47
5.2.2. Grain size statistical parameters.....	47
5.3. Bioturbation and trace fossil characteristics.....	49
5.3.1. Bioturbation .....	49
5.3.2. Trace fossils .....	50
5.4. Age and sedimentation rates .....	52
5.5. Summary .....	54
Chapter 6 RESULTS: GROUND ICE AND CRYOSTRATIGRAPHY .....	55
6.1. Gravimetric moisture content and excess ice content .....	55
6.2. Cryostratigraphy of the Adventdalen core .....	55
6.3. Summary .....	60
Chapter 7 DISCUSSION.....	62
7.1. Facies associations .....	62



7.2.	General discussion.....	73
7.2.1.	Lithostratigraphic correlations .....	73
7.2.2.	Ice-rafted debris (IRD).....	75
7.2.3.	Grain size distributions .....	77
7.3.	Permafrost in lower Adventdalen.....	81
7.3.1.	Permafrost in saline sediments.....	81
7.3.2.	Formation of ice layers in epigenetic permafrost .....	82
7.3.3.	Timing and nature of permafrost aggradation .....	83
7.3.4.	Implications for permafrost aggradation in Spitsbergen valley deposits.....	85
Chapter 8	SUMMARY AND CONCLUSIONS .....	86
8.1.	Summary: sedimentary and permafrost development of the Adventdalen Valley....	86
8.2.	Conclusions .....	92
8.3.	Research implications and directions for further investigations .....	93
LITERATURE	.....	95
Appendix A:	Sedimentary log .....	103
Appendix B:	Images of additional facies .....	106
Appendix C:	Core ichnology .....	107
Appendix D:	Grain size results .....	115
Appendix E:	Results of AMS <sup>14</sup> C and OSL dating.....	119
Appendix F:	Gravimetric moisture content and excess ice content results .....	121
Appendix G:	Core photographs (CD) .....	124

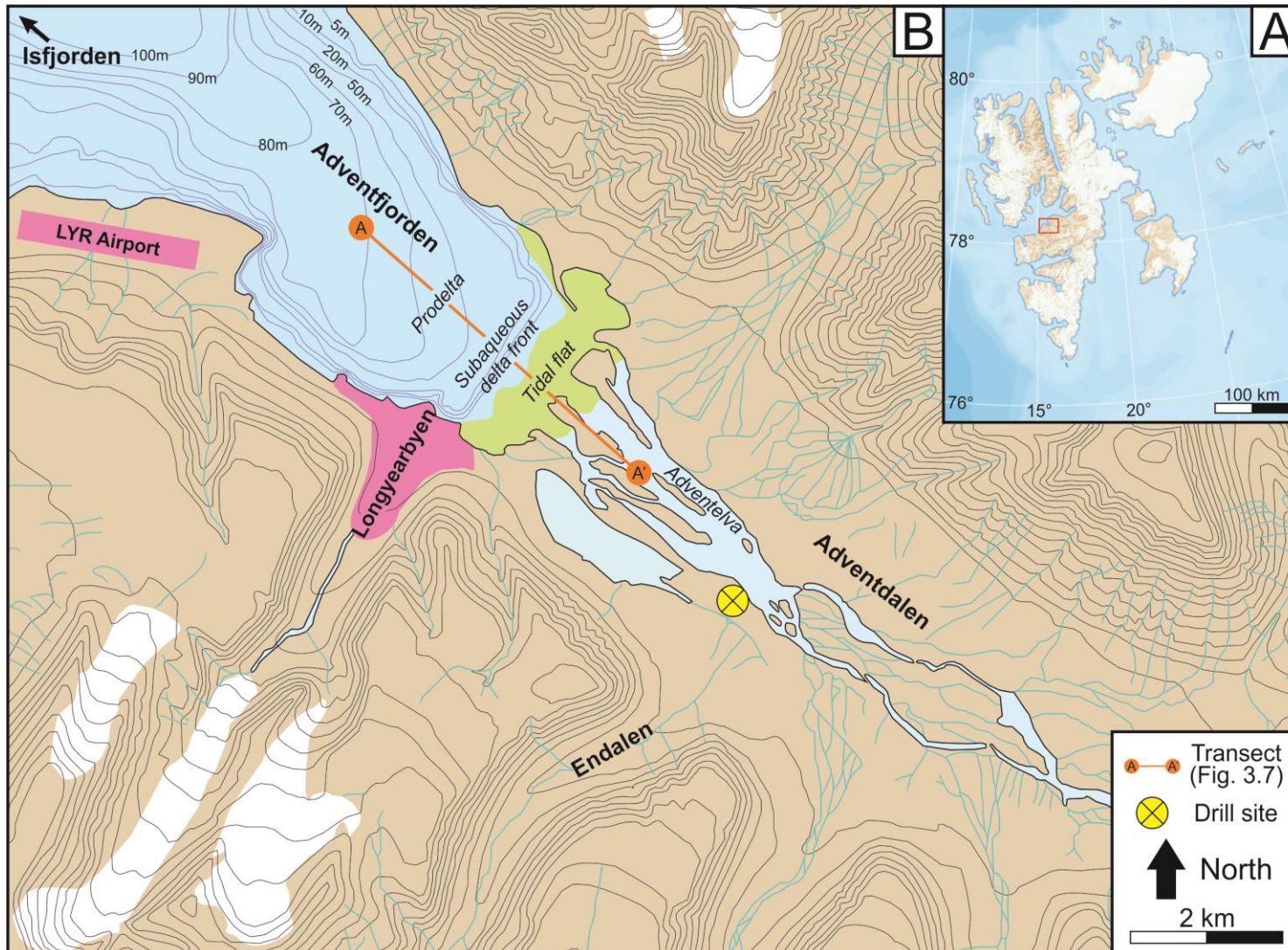
## CHAPTER 1 INTRODUCTION

This thesis examines the sedimentary and permafrost development of the lower Adventdalen valley (Svalbard, Norway). The investigation is founded on the analysis of a 60 m ice-bonded sediment core retrieved from the UNIS CO<sub>2</sub> Project Well Park (9 m.a.s.l., 78°12'N, 15°49'E; Braathen et al. 2012; **Figure 1.1**). Encompassing the interval between the ground surface and bedrock at ca. 60 m depth, this core forms the basis for the first comprehensive description of the late Quaternary permafrost and sedimentary development in the Adventdalen valley deposits.

Adventdalen is a glacially and periglacially modified, side-entry tributary valley to the Isfjorden system (**Figure 1.1**). During the late Quaternary period, this region was repeatedly inundated by large, marine-based ice sheets which have formed and disintegrated over glacial-interglacial cycles (Mangerud et al. 1998; Ingólfsson and Landvik 2013). These glaciations have acted to remove much of the terrestrial sedimentary record from preceding glacial and interglacial periods (Elverhøi et al. 1995).

Surficial deposits in the Adventdalen valley bottom primarily reflect the activity of fluvial and eolian processes (Tolgensbakk et al. 2000). Steep slopes are draped by allochthonous weathering deposits which are largely affected by solifluction (Harris et al. 2011). The Adventelva River runs through the valley, forming a braided network of migrating channels which are active during the melt season. The transition from Adventdalen to Adventfjord is characterized by a fjord-wide tidal flat and subaqueous delta (Zajączkowski and Włodarska-Kowalczyk 2007; **Figure 1.1**). Since the early Holocene, this delta has prograded ca. 10 km to its present position (Johansen et al. 2003; Lønne and Nemeč 2004).

The study area is further characterized by the presence of permafrost – a geologic phenomenon associated with cold climates. Permafrost is generally defined as ground which remains at or below 0 °C for two or more consecutive years (Williams and Smith 1989). Svalbard is situated within the continuous permafrost zone meaning that permafrost is both spatially and temporally continuous; greater than 90% of the ice-free, terrestrial surface of Svalbard is believed to be underlain by perennially frozen ground (Humlum 2005; French 2007). Extensive previous permafrost research from this environment makes it an ideal location for further studies of the overall permafrost and landscape development since the Late Weichselian Glaciation.



**Figure 1.1** A) Overview map of the Svalbard Archipelago (study area denoted by red box). B) The Adventdalen area. Deltaic subdivision from description by Zajączkowski & Włodarska-Kowalczyk (2007). Bathymetry after Zajączkowski (2008: 62). Contour lines after Norsk Polarinstitutt (2013). Topographic contour lines in 50 m increments.

## **1.1. Motivation, hypothesis, and objectives**

Research was initially focused on the aggradational history and characterization of permafrost in the valley deposits. The scope of this investigation was expanded to include sedimentology following the retrieval and examination of the sediment core. The motivation for a broader, multidisciplinary study came from two sources. First, the understanding of sedimentary processes operating during the Holocene provides the key to estimating the timing of permafrost development in valley bottoms throughout Spitsbergen. Second, the fjord-fill deposits in Adventdalen contain a high-resolution depositional history from the Late Weichselian Glaciation to present.

The purpose of this study is to investigate the sedimentary and geocryological characteristics of the deposits in lower Adventdalen using observations from a 60 m ice-bonded sediment core. A working hypothesis, informed by previous studies of permafrost and Quaternary sedimentology, has been employed during this investigation. This hypothesis is that the Late Weichselian glaciation removed unconsolidated sediments from lower Adventdalen and temporarily established conditions conducive to permafrost degradation. Therefore, sedimentary deposits and permafrost likely post-date the Last Glacial Maximum and reflect glacial, glaciomarine, paraglacial, and Holocene processes, the most important of which relates to the progradation of the Adventelva delta.

The specific objectives of this thesis are to:

- (1) Provide a detailed description and interpretation of the Adventdalen valley fill deposits with emphasis on sedimentological and geocryological attributes;
- (2) Determine the timing and nature of permafrost aggradation in these sediments;
- (3) Combine these observations to construct a sedimentological and geocryological model for the landscape development of lower Adventdalen.

## **1.2. Thesis structure**

This thesis is organized into eight chapters. Chapter Two provides a background to the elements of geocryology pertinent to this investigation. An overview of the late Quaternary history of the study region is provided in Chapter Three. The modern sedimentary environments along a seaward transect from Adventelva to Adventfjord are also described in this chapter. These two chapters establish the theoretical and historical context for this study. The field and laboratory methods utilized in this investigation are described in Chapter Four. Results are divided into two chapters. The focus of Chapter Five is the sedimentary characteristics of the core. Facies and facies associations are presented along with results

from grain size, trace fossil analysis, and dating investigations. Chapter Six presents the vertical distribution of ground ice and the cryostratigraphy of the sediments. A discussion of these results is given in Chapter Seven. Chapter Eight presents a summary of the sedimentary and geocryological development of the study area. Conclusions, research implications, and recommendations for continuing investigations are presented at this time.

## CHAPTER 2 PERMAFROST, GROUND ICE, AND CRYOSTRATIGRAPHY

### 2.1. Climate and permafrost

Permafrost is a geological expression of climate and is prevalent in high latitude and altitude environments. Permafrost is defined as ground that remains at or below 0 °C for two or more consecutive years (Williams and Smith 1989). The spatial extent to which permafrost occurs has been used to identify zones in which perennially frozen ground is spatially continuous, widespread, sporadic, or isolated in occurrence (Smith and Riseborough 2002). Continuous, widespread, sporadic, and isolated correspond to regions wherein greater than 90%, 50-90%, 10-50%, and less than 10% of the subaerial surface is underlain by permafrost, respectively. At a continental scale, the presence or absence of permafrost is determined by climate. Within permafrost areas, differences in topography, vegetation, snow cover, and ground characteristics yield temperature variations over smaller distances (Smith and Riseborough 2002). Permafrost may range up to many hundreds of meters in thickness (French 2007). Depth is a function of ground thermal properties and the duration of conditions conducive to permafrost formation.

Permafrost may also be classified in relation to the deposition of the host material. *Epigenetic* permafrost is that which has aggraded following the deposition of the host material. French and Shur (2010) note the time lag between substrate genesis and permafrost aggradation may be substantial (up to millions of years). Conversely, the development of *syngenetic* permafrost is concurrent with sediment deposition. Syngenetic permafrost is characteristic of permafrost landscapes influenced by fluvial, colluvial, and aeolian deposition (Burn and Kokelj 2009). In reality, most permafrost bodies consist of both epigenetic and syngenetic components and are so termed *polygenetic* (French and Shur 2010).

The active layer is defined as the zone overlying permafrost subject to summer thaw and winter freezing (Williams and Smith 1989). Active-layer thickness is influenced by the height and thermal properties of vegetation, organic-layer thickness, summer precipitation, snow cover, substrate texture and thermal properties, and topography (Hinkel and Nelson 2003). In unconsolidated sediments, permafrost below the active layer is characteristically rich in ground ice (Burn 1988). This form of ground ice has been termed ‘aggradational ice’ by Mackay (1972). Its formation is attributed to upfreezing associated with a rising permafrost table (Burn 1988). The presence of aggradational ice is of particular importance

when considering the application of cryostructures to the sedimentary and permafrost development of Adventdalen as will be discussed below.

## 2.2. Ground ice

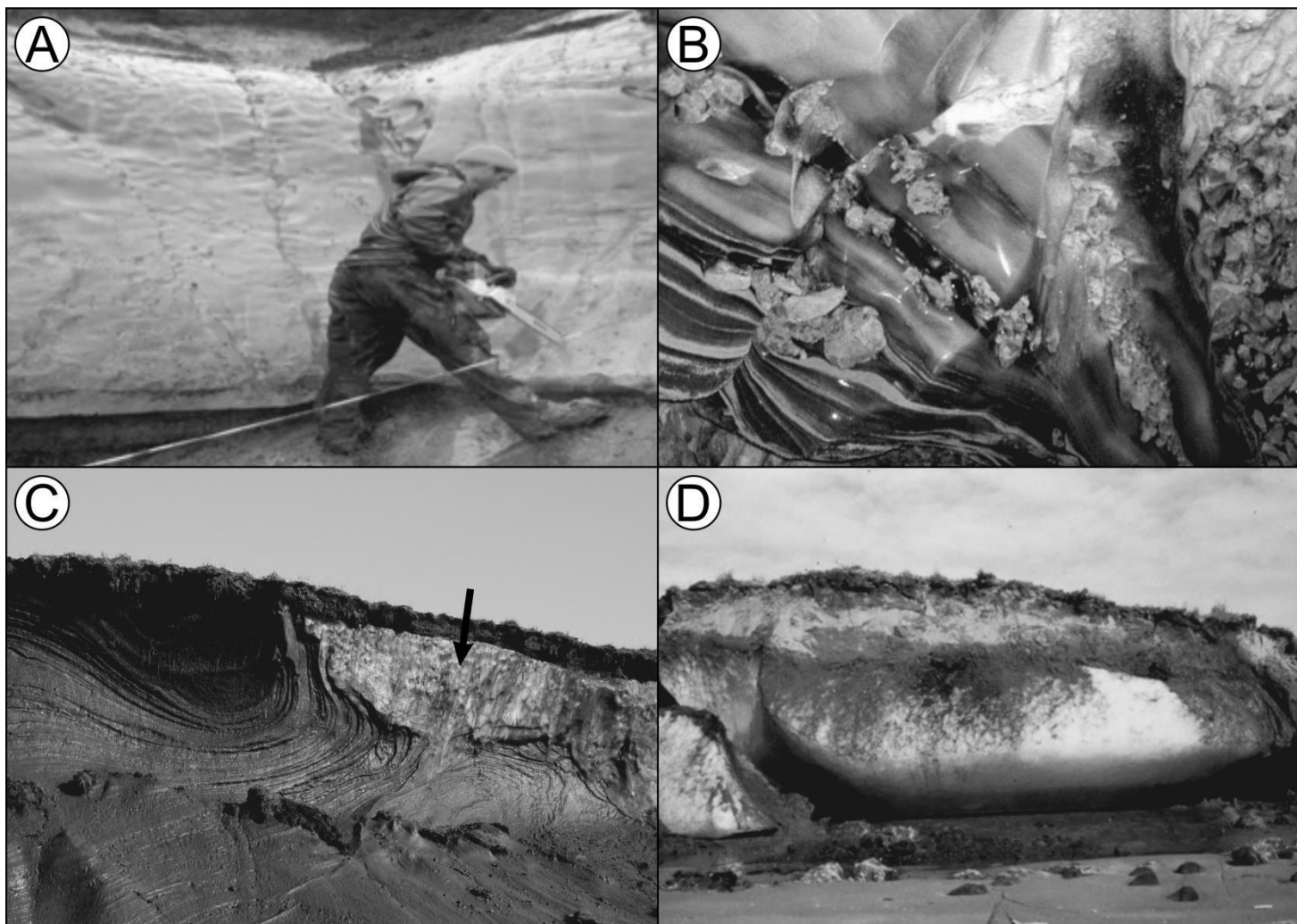
Ground ice is defined as moisture frozen below the ground surface (French 2007). In permafrost settings, such ice bodies may be preserved indefinitely. Ground ice is of particular importance when considering the geomorphological development of permafrost environments as most periglacial landforms are directly related to the development or degradation of ground ice. Ground ice can be classified as buried or intrasedimental in origin (French and Harry 1990). Buried ice masses are those which have been subject to burial following formation on the ground surface. Ice sources include sea, river, and lake ice, glacier ice, snow banks, and icings (**Figure 2.1a**; French 2007). With the exception of ice-cored moraines (Sletten et al. 2001) and some rock glaciers (**Figure 2.1b**; Humlum et al. 2007), buried ice is not known to occur widely in the Svalbard environment. Therefore, most ground ice is intrasedimental in origin.

Intrasedimental ice includes vein ice (**Figure 2.1c**), intrusive ice (**Figure 2.1d**), pore ice, and segregated ice<sup>1</sup> (French 2007). Though all ice types are significant from a geomorphological perspective, it is variations in the expression of segregated ice and pore ice which result in the cryostructures described in this thesis. *Vein ice* forms from melt water infiltrating into vertical thermal contraction cracks (Mackay 1972; French 2007). Ice wedges develop in environments where this process is repeated over many years (**Figure 2.1c**). The interaction of many such wedges creates polygons with each side underlain by an ice wedge (Mackay 1972). Ice-wedge polygon networks are a characteristic permafrost landform present on terraces in lower Adventdalen (Christiansen 2005). *Intrusive ice* is formed by injection or expulsion of water into permafrost. Pingos, present in the Adventdalen area, provide local evidence of intrusive ice development (Yoshikawa and Harada 1995).

The two most significant ice types with respect to this investigation are segregated ice and pore ice. In permafrost environments, *pore ice* acts as a bonding agent; holding individual grains together in otherwise unconsolidated sediments. Pore ice occupies voids between grains and is considered to occur ubiquitously where moisture is present (French 2007). The existence of *segregated ice* is typically determined by the presence of supernatant water following thawing (French 2007). Ice lenses can be observed in cores and exposures of

---

<sup>1</sup> Images of pore ice, segregated (lenticular) ice, and ice layers (a form of intrusive ice) are provided in **Figure 6.3** or Chapter Six.



**Figure 2.1** Images of select ice types. (A) Buried glacier ice, Herschel Island, Yukon Territory, Canada (Fox 2011). (B) Rock-glacier interior exposed below the Larsbreen rock glacier (Spitsbergen; Humlum et al. 2007). (C) Ice wedge (vein ice) exposed in a retrogressive thaw slump (Herschel Island, Yukon Territory). Arrow indicating the center of the ice wedge. Note the deformation of surrounding sediments resulting from ice-wedge development. (D) Pingo ice-core (intrusive ice) exposed in McKinley Bay, N.W.T. by coastal erosion (Mackay 1972). The exposure is approximately 30 m in height.



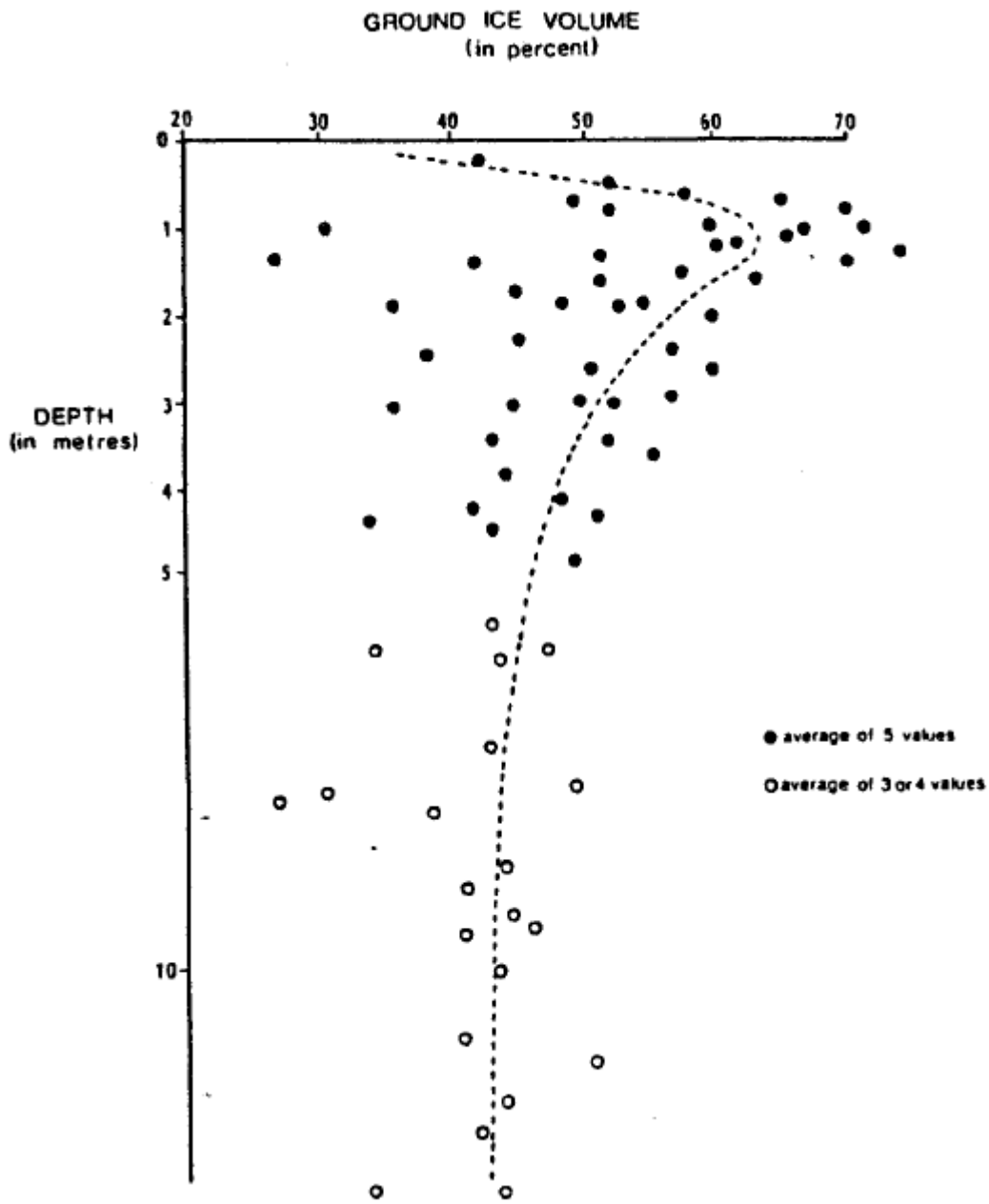
sediments containing segregated ice without difficulty (**Figure 2.2**). Segregated ice formation is typically associated with fine-grained (silty) deposits where moisture is abundant (French 2007). For this reason, such deposits are commonly referred to as frost susceptible.

As mentioned above, permafrost below the bottom of the active layer is characteristically rich in aggradational ice (**Figure 2.3**; Mackay 1972; Burn 1988). According to Mackay (1972), the development of aggradational ice results from a rise in the permafrost table, incorporating ice-lenses which were formerly present in the base of the active layer. Such changes in the permafrost table may be the result of climatic variations, vegetation development, or sedimentation. Mackay's (1972) hypothesis suggests that in order to develop an ice-rich zone below the active layer the permafrost table must rise, resulting in permafrost aggradation. An alternative, though complementary, hypothesis has been proposed by Cheng (1983) implying that aggradational ice results from net moisture migration into the top permafrost zone due to seasonal variations in temperature induced suction gradients (cryosuction). Overtime, these processes result in ice enrichment of the top of permafrost (Burn 1988).

Two parameters are typically used to quantify ground-ice conditions in unconsolidated material: gravimetric moisture content and excess ice content. *Gravimetric moisture content* (occasionally termed ice content), expressed as a percentage, represents the weight of moisture (ice and unfrozen water) to dry sediment. Low moisture contents are regarded as those below ca. 50%. High moisture contents range between 50% and ca. 150% (though may be considerably higher) and are associated with fine-grained sediments and deposits rich in organic material (French 2007; Morse et al. 2009). *Excess ice* refers to the volume of supernatant water present following the thaw of frozen sediment (French 2007). The volume of supernatant water is expressed as a percentage of the total volume of sediment and water. Water volumes are typically multiplied by 1.09 to approximate the equivalent volume of ice (Kokelj and Burn 2005). The geotechnical significance of permafrost is principally derived from the presence of excess ice. This parameter provides implication of morphological changes as the thaw of sediments characterized by excess ice presence will experience subsidence and a decrease in shear strength (French 2007). On hills, this may result in slope failure along the thaw table (Mackay 1970).



**Figure 2.2** Segregated ice lenses at the top of permafrost. Core drilled in aeolian sediments of the lower Adventdalen valley (ca. 3 km from the study site). A few ice lenses are indicated by arrows. Photo: S. Härtel.



**Figure 2.3** Vertical distribution of ground ice, Richards Island, N.W.T., Canada. The dashed line indicates the average values. Note the peak in ground ice at the top of permafrost (ca. 1.0 m depth). From Pollard and French (1980).

### 2.3. Cryostratigraphy

Cryostratigraphy involves the description of, and relationship between, ground ice and sediment. The value of cryostratigraphy in landscape reconstruction stems from the fact that ice within sediments produces structures unique from those in unfrozen deposits (French and Shur 2010). The distribution of ground ice within sediments determines the morphological expression of these structures – termed cryostructures. As in sedimentology, ‘structure’ denotes the macroscopic features of the ice/sediment complex. A simplified North American classification framework, initially presented by Murton and French (1994), encompasses the range of ice structures observed in permafrost (**Figure 2.4**).

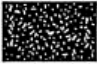



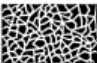


Three of the structures presented in **Figure 2.4** are of particular relevance to the present study: structureless, lenticular, and layered cryostructures. Frozen sediments containing *structureless cryostructures* (termed porous cryostructures in this thesis<sup>2</sup>) are defined by the absence of visible ice and other cryostructures. In such sediments, pore ice acts to bond the otherwise unconsolidated sediments but has no distinct morphological expression. In near surface sediments, porous cryostructures are typically associated with sands and gravels without a significant mud component (Murton and French 1994). The occurrence of porous cryostructures in other lithologies has not been widely reported in the North American or European literature. Intervals characterized by the presence of *lenticular cryostructures* contain discrete, lens-shaped bodies of ice (French and Shur 2010). Lenses may vary in geometry and are described by inclination, thickness, length, shape, and relationship to each other (Murton and French 1994). Lenticular cryostructures are commonly attributed to segregation processes (introduced above) and are oriented normal to the direction of the freezing front. *Layered cryostructures* are typified by continuous bands of ice though the degree of continuity is difficult to assess when working with sediment cores. The origin of ice layers is attributed to segregation or intrusion processes. Layers may range in thickness from millimeters to meters (Murton and French 1994).

Cryostructures can be applied when interpreting the depositional and freezing history of sediments in permafrost environments. French and Shur (2010) note, particular cryostructures, are diagnostic of syngenetic and epigenetic permafrost aggradation. Syngenetic permafrost is characterized by the presence of rhythmically organized layered or lenticular cryostructures (Shur et al. 2004). These structures are essentially segregated,

---

<sup>2</sup> This cryostructure has been renamed in order to avoid confusion with the sedimentological meaning of ‘structureless’.

aggradational ice which reflect an aggrading depositional surface (French and Shur 2010). Porous cryostructures are usually associated with epigenetic permafrost development as they result from the *in situ* freezing of pore water and low soil moisture conditions (Bray et al. 2006; French 2007; French and Shur 2010).

CRYOSTRUCTURE AND CODE	SEDIMENT	ICE	OCCURRENCE AS OR WITHIN
 structureless (SI)	sand gravel	pore	ice in sand + gravel
 lenticular (Le)	muddy peat mud (fine sand)	sand segregated	crack infill ice/sediment lenses massive ice icy sediments (ice wedges) (composite sand-ice wedges) (dilation-crack ice)
 layered (La)	muddy peat mud (fine sand)	sand segregated intrusive	crack infill ice/sediment layers massive ice icy sediments ice wedges composite sand-ice wedges dilation-crack ice
 regular reticulate (Rr)	mud	segregated	ice in mud
 irregular reticulate (Ri)	mud	segregated	ice in mud
 crustal (Cr)	mud frost-susceptible clasts	segregated	
 suspended (Su)	mud sand gravel mud sand gravel	segregated intrusive	icy layer at top of permafrost ice dykes in mud ice lenses massive ice icy sediments ice dykes

**Figure 2.4** Classification of cryostructures proposed by Murton and French (1994). Ice is shown in white and sediment in grey or black. Modified from French and Shur (2010).

## CHAPTER 3 REGIONAL SETTING AND SEDIMENTARY ENVIRONMENTS

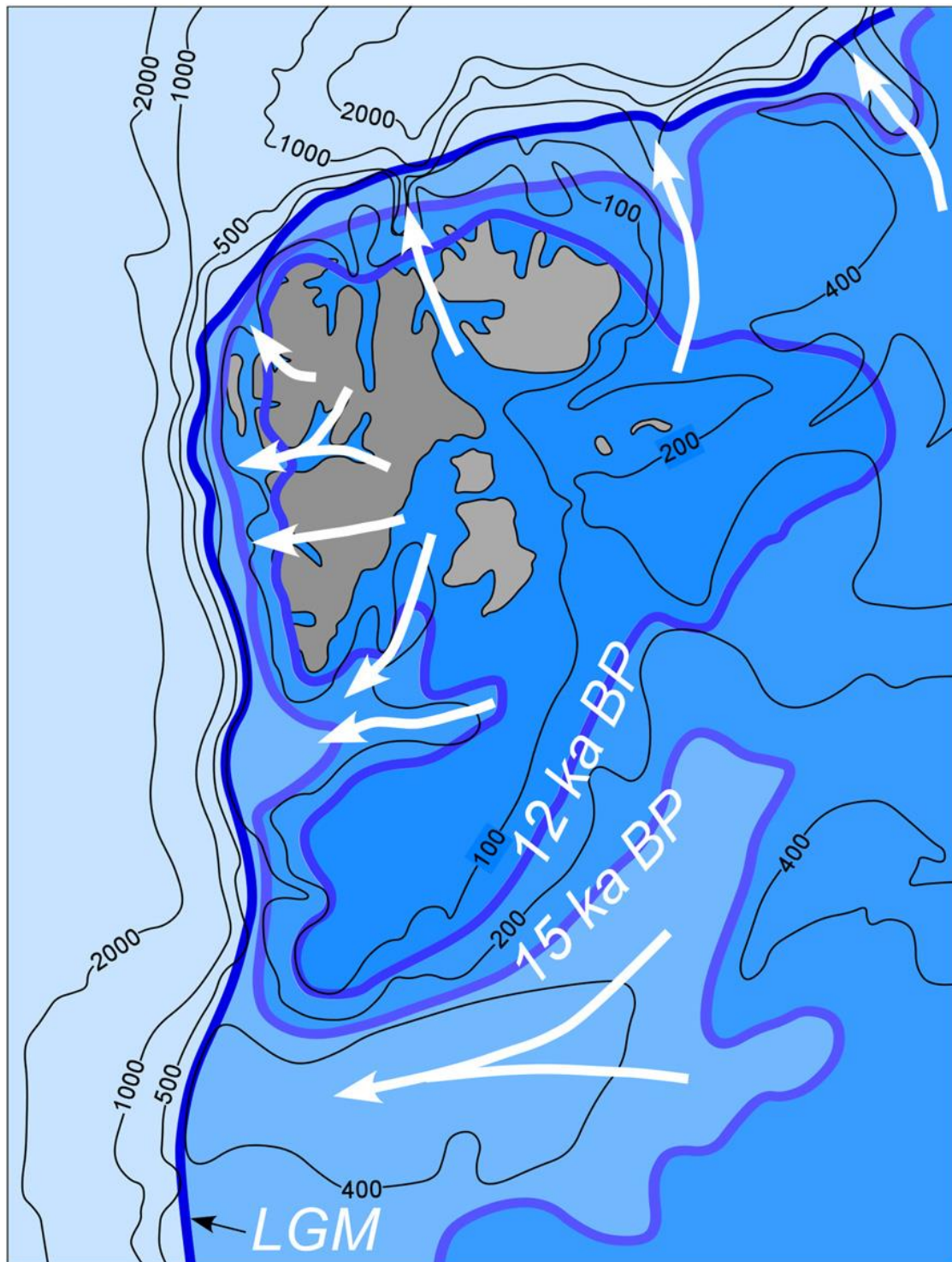
### 3.1. Regional Quaternary history

Svalbard is a high-arctic archipelago located on the north-western margin of the Barents Sea. Throughout the late Pleistocene, this region has been repeatedly inundated by large marine-based ice sheets which have formed and disintegrated over glacial-interglacial cycles (Mangerud et al. 1998; Ingólfsson and Landvik 2013). During the Weichselian, three major glacial advances, separated by two interstadials, have been identified on western Svalbard (Mangerud et al. 1998). The earliest Weichselian glaciation occurred between ca. 118 kya and ca. 108 kya and was followed by the Phantomodden Interstadial. A mid-Weichselian glaciation, occurring between ca. 56 kya and ca. 40 kya is additionally recorded on western Spitsbergen (Mangerud et al. 1998). The timing and spatial extent of these preceding glaciations are problematic as sedimentary evidence is spatially discontinuous, and deposits are beyond the range of radio-carbon dating. The most recent, and best documented, glaciation occurred during the late Weichselian (ca. 30 kya– ca. 12 kya) following the Kapp Ekholm Interstadial (Mangerud et al. 1998).

#### 3.1.1. *Last Glacial Maximum (LGM)*

The Late Weichselian advance of the Svalbard –Barents Sea ice sheet started from a mid-Weichselian interstadial minimum (ca. 30 – 25 kya) when ice extent on Svalbard was likely similar to present (Mangerud et al. 1998). Although disparities between terrestrial and marine records have resulted in considerable regional uncertainties regarding the timing, extent, and configuration of the Late Weichselian glaciation, it is recognized that, during the Last Glacial Maximum (LGM; ca. 20 kya), a coalesced ice sheet inundated the entire Svalbard archipelago and adjoining continental margins (**Figure 3.1**; Landvik et al. 1998; 2005).

Consensus regarding the westward extent of the LGM ice sheet was initially obscured by the complex, and occasionally contradictory nature of local terrestrial and marine records (Landvik et al. 2005 and Ingólfsson and Landvik 2013). Arguments for a limited ice extent on western Spitsbergen were founded on observations of undisturbed raised beach terraces recording higher than post-LGM marine limits as well as morphological and stratigraphic studies of cirque and fjord glaciers indicating that the LGM was slightly beyond present margins (Forman 1989; Landvik et al. 2005). In contrast to these conclusions, marine records



**Figure 3.1** Reconstruction of the limits of the Late Weichselian Svalbard-Barents Sea ice sheet at the LGM and during deglaciation. Ice stream locations are indicated by the white arrows. From Ingólfsson and Landvik (2013).



reveal till deposits underlying Holocene marine sediments, significant truncation (up to 150 m) of upper sedimentary bedrock, and terminal moraines on the western continental shelf – indicating grounded glacier cover (Svendsen et al. 1996; Landvik et al. 1998, 2005; Ottesen et al. 2005).

In an attempt to merge both terrestrial and marine records, Landvik et al. (2005) concluded that the western fjords and associated cross-shelf trough areas were filled with fast-flowing, erosive ice streams while the intermediate areas were overlain by glaciers with a lower erosional capacity. This conclusion permits the inclusion of previously incongruous terrestrial observations as spatial constraints on the regions of fast-moving ice. The realization that the deep-fjords and valleys of western Spitsbergen were occupied by erosive ice streams is of particular significance when considering the landscape development of Adventdalen as it suggests that ice sheets likely removed sedimentary evidence for previous glacial and interglacial periods.

### 3.1.2. *Deglaciation*

Following the LGM, the ice sheet retreated rapidly, calving in the deep water of fjords and troughs. The shelf area west of Spitsbergen was ice free by ca. 15 kya (Landvik et al. 1998). Radiocarbon dating of sediment cores indicates that the central Isfjorden area was deglaciated ca. 12.7 kya (Forwick and Vorren 2009). Sedimentary evidence from Billefjorden indicates that the inner branches of Isfjorden were deglaciated ca. 10 kya (Svendsen and Mangerud 1997; Lønne 2005). The Adventfjord area was also deglaciated at this time, permitting the development of a fjord-wide braidplain delta which began to prograde from the fjord head zone (Lønne and Nemec 2004; Lønne 2005).

Deglaciation occurred during a time of global eustatic sea-level rise (Fairbanks 1989). However, the rate of glacioisostatic rebound on Svalbard surpassed this rate and resulted in forced regression. This regression was likely associated with the onset of contemporary river-delta systems in the palaeofjords of western Spitsbergen.

### 3.1.3. *Post-LGM sea level changes*

Reconstructions of postglacial relative sea-level (RSL) changes are principally based on samples of radiocarbon dated organic material collected from raised marine deposits (ex. Salvigsen 1984 and Forman 1990). Pattern of RSL changes on western Spitsbergen show an exponentially-decaying emergence from deglaciation to present (Forman et al. 2004). RSL

has fallen during this period due to isostatic rebound rates which have outpaced concurrent eustatic sea-level rise.

In the Isfjorden area, post-LGM raised beach deposits occur up to 48 m a.s.l. in outer Isfjorden and increase to 90 m a.s.l. in inner Isfjorden (**Figure 3.2**; Salvigsen 1984; Forman 1990). The postglacial RSL development of Adventdalen is not as well known. Raised marine deposits dated to ca. 10 kya are located at 70 m a.s.l. in outer Adventdalen and 62 m a.s.l. ca. 16 km to the southeast in Adventdalen (Lønne and Nemec 2004).

#### 3.1.4. *Implications for permafrost development*

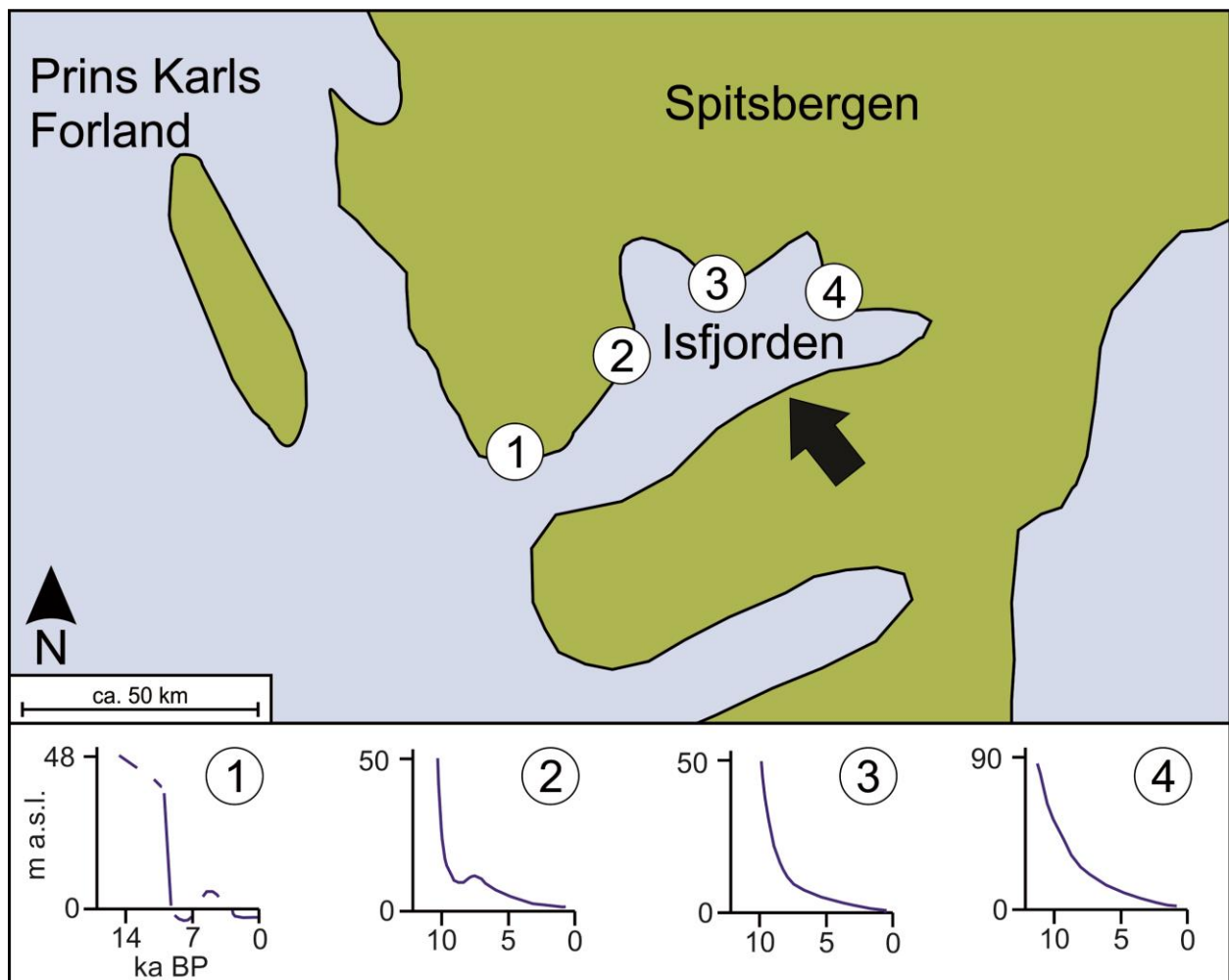
The conclusions presented above in association with geomorphic observations of glacial striae up to 200 m a.s.l. in central Spitsbergen indicate that warm-based glaciers were situated in valleys and fjords during the LGM (Humlum et al. 2003; Humlum 2005). Warm-based glaciers are those in which the basal temperature is above the pressure melting point, enabling sliding (Benn and Evans 2010). This observation has significant implications for permafrost conditions in valley bottoms as, during the presence of warm-based glaciers, permafrost degrades due to frictional heat generated by basal sliding and geothermal heat (Humlum 2005). Therefore, permafrost degradation under warm-based ice bodies occurs from both the bottom up and the top down. In contrast, under cold-based glaciers (basal temperatures below the pressure melting point) permafrost may be preserved (Humlum 2005).

Permafrost is unlikely to have established in submarine settings due to the relatively warm boundary conditions at the water-sediment interface (Osterkamp 2001). In polar regions, sub-sea permafrost is primarily found in shallow continental shelves which were exposed sub-aerially during glacial periods (French 2007). These permafrost bodies may be characterized as relic, warm, and degrading (Osterkamp 2001). Sub-sea permafrost is not known to occur in the study region at present (Yoshikawa and Nakamura 1996).

## **3.2. Climate and meteorology**

### 3.2.1. *Holocene palaeoclimate*

Three separate climatic phases have been recognized in the post-LGM and Holocene climate of western Spitsbergen through the examination of pollen assemblages in lake sediments (Birks 1991) as well as macrofossils and ice-rafted debris in marine sediments (Salvigsen et al. 1992; Salvigsen 2002; Hald et al. 2004). Following the LGM, climate gradually warmed,



**Figure 3.2** Relative sea level curves from the Isfjorden area. The arrow indicates the approximate location of the study area. Modified from Forman et al. (2004) and Ingólfsson & Landvik (2013).

reaching a maximum in the early Holocene (9 kya – 7.5 kya). Warm conditions persisted until ca. 5 kya (Humlum 2005). Glaciers on Spitsbergen during this period were less extensive than at present due to high summer temperatures (Svendsen and Mangerud 1997). Humlum (2005) notes, during the mid-Holocene, mean annual air temperatures ranged between 0 and -3 °C at sea level. Permafrost was likely discontinuous at low elevations during this time. Climatic conditions since 5 kya were cooler than during the early Holocene. Svendsen and Mangerud (1997) document the revival of glaciers from inner Isfjorden and at Kapp Linne from 4 kya. Decreasing diversity in terrestrial faunal communities, extinction of thermophilous molluscs from marine environments, and increased rates of sedimentation in glaciated catchments are additionally observed and attributed to climatic cooling during the mid-Holocene (Birks 1991; Salvigsen et al. 1992; Svendsen and Mangerud 1997). During the past century, mean annual air temperatures in Longyearbyen have increased by between 3°C and 4°C (Førland et al. 2011; Humlum 2005).

### 3.2.2. *Meteorology*

The study site in Adventdalen lies within the polar-tundra climate zone according to the Zoeppen-Geiger climate classification framework (Kottek et al. 2006). This area is dry and typified by long, cold winters and short, cool summers though it is considerably warmer than other locations at this latitude. Relatively warm mean annual air temperatures are attributed to two geographic factors. First, Svalbard is influenced by the warm Norwegian Current which flows north, along the western coast of Spitsbergen (Førland et al. 1997). The Norwegian current contributes to the reduction or absence of sea ice in the Longyearbyen area during winter. Second, Svalbard is located within the North Atlantic cyclone track (Hanssen-Bauer et al. 1990). This track is related to the location of the Siberian High, a cold anticyclone that forms over eastern Siberia during winter (Humlum et al. 2003). This system results in the advection of warm, moist air to the Svalbard region (Humlum et al. 2003).

The mean annual air temperature at the Svalbard Airport (ca. 7 km from the study site) is -4.6 °C (1981-2010; Førland et al. 2011). Approximately 191 mm (water equivalent) of precipitation falls annually at the Svalbard Airport of which ca. 60 % is deposited as snowfall during the snow season (Ekerstorfer and Christiansen 2011; Førland et al. 2011).

### 3.3. **Adventdalen region**

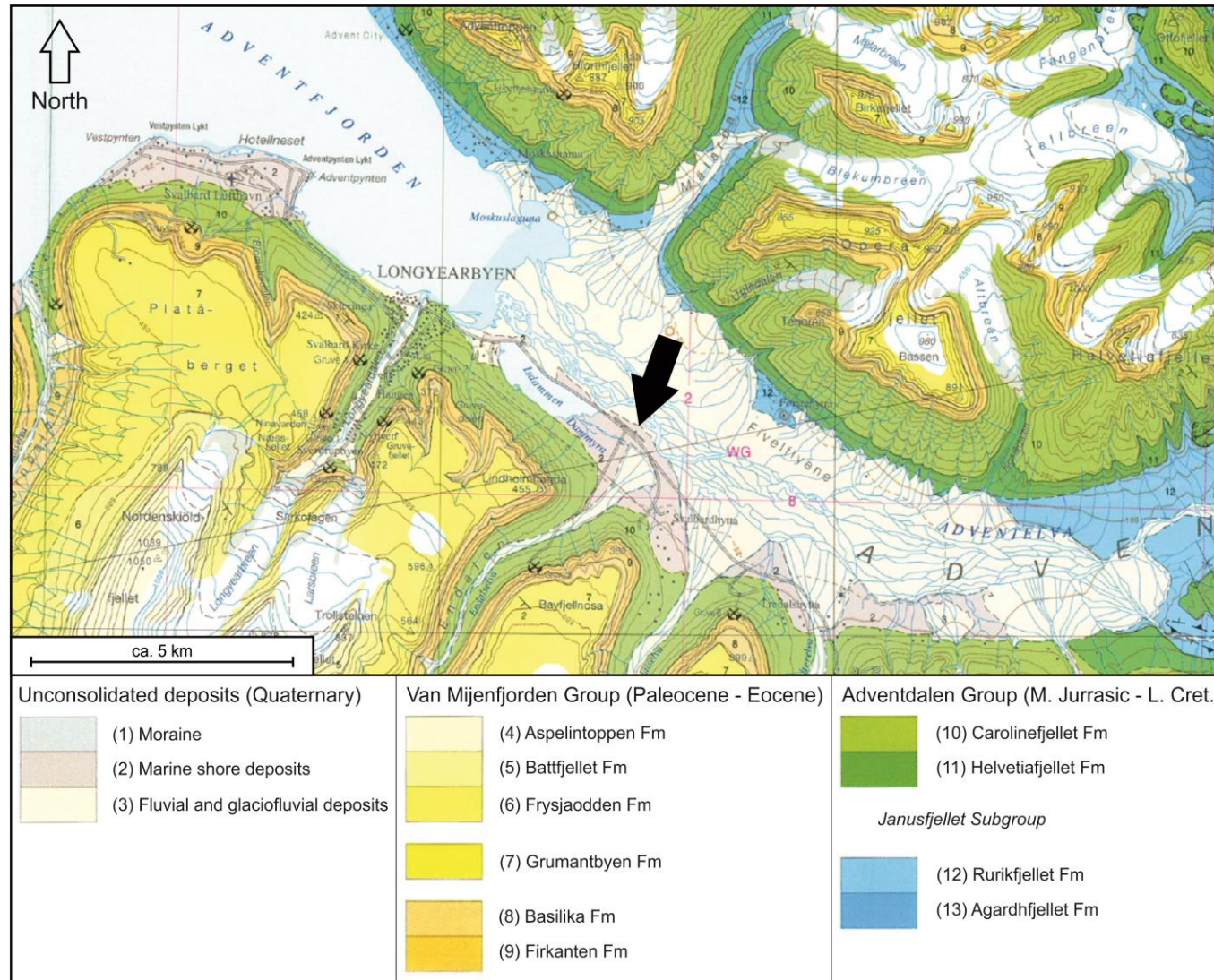
The study site is located on a terrace along the southern edge of Adventdalen near to the mouth of the Endalen valley and ca. 5 km from Longyearbyen (**Figure 1.1**). The terrace is

elevated approximately 5 m above the active river bed and consists of fluvial material deposited during a period when base level was higher than present. A patchy vegetation cover consisting of *Salix herbacea*, sedges, and mosses characterizes the ground surface (Bryant 1982). Surficial sediments at this site are predominantly composed of aeolian silts. This site has previously served as an unpaved runway for the former Longyearbyen airport. As a result, the surface material has been modified in some locations.

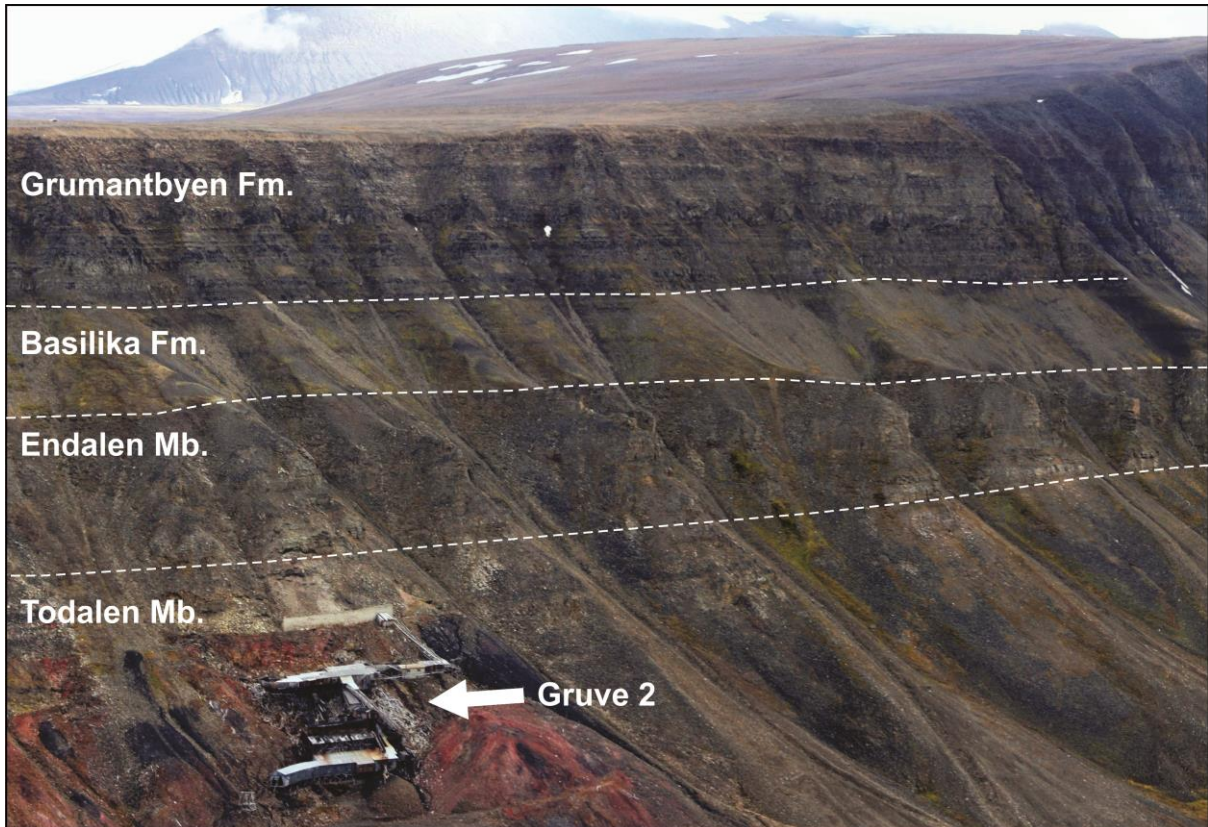
### 3.3.1. Geology

The study area is located within the Central Tertiary Basin of Spitsbergen, a regional synclinorium consisting primarily of clastic sedimentary rock (Steel et al. 1981). Adventdalen is carved into flat-lying, sedimentary rocks of Early Cretaceous (Aptian and Albian) to Tertiary (Paleocene and Eocene) age (**Figure 3.3**; Major et al. 2000). The Lower Cretaceous *Carolinefjellet Formation* was deposited in prodelta to distal-marine shelf environments and consists of alternating shales and sandstones (Dallmann et al. 2001). Dallmann et al. (2001) note, following a mid-Cretaceous uplift, no sediments were deposited on Svalbard until the early Tertiary.

Tertiary sediments of the Firkanten, Basilika, and Grumantbyen Formations present in the Adventdalen area (**Figure 3.3**; **Figure 3.4**). The *Firkanten Formation* is separated from the Carolinefjellet Formation by a low-angle unconformity and is subdivided into the Todalen and Endalen Members (Dallmann et al. 2001). The *Todalen Member* consists of several recurring shale-sandstone-coal successions of coastal marine to delta plain origin (Nagy 2005). Economically, the Todalen Member contains the most significant coal deposits of Svalbard. The *Endalen Member* consists of stacked sandstone intervals interpreted to be delta-front sheet sandstones (Dallmann et al. 2001; Nagy 2005). This is a cliff forming unit within the study area (**Figure 3.4**). The Endalen Member is transgressively overlain by shales and siltstones of the *Basilika Formation*, deposited during the late Paleocene under delta-influenced shelf conditions (Dallmann et al. 2001; Nagy 2005:163). The upper part of the Basilika Formation displays an upwards coarsening evolution into sandstones of the *Grumantbyen Formation*. This unit is interpreted to have been deposited as an inner to mid shelf sand barrier complex about the Paleocene-Eocene transition (Dallmann et al. 2001). The Grumantbyen Formation is relatively resistant to weathering and forms the top of mountains and plateaus in Adventdalen area (Major et al. 2000). The regional bedrock has a governing influence on the unconsolidated sediment composition and geomorphology in Adventdalen.



**Figure 3.3** Geological map of the Adventdalen Valley. The arrow indicates the location of the study site. Modified from Major et al. (2000).



**Figure 3.4** The abandoned coal mine “Gruve 2” on the western side of the Longyeardalen Valley. The mine’s entrance is located in the coal-bearing Todalen Mb. of the Firkanten Formation. The Todalen Mb. is overlain by the cliff-forming sandstones of the Endalen Mb. (Firkanten Fm.). The shales of the Basilika Fm. (mostly covered with scree) are succeeded by the dark sandstones of the Grumantbyen Fm..

### 3.3.2. *Quaternary geology and geomorphology*

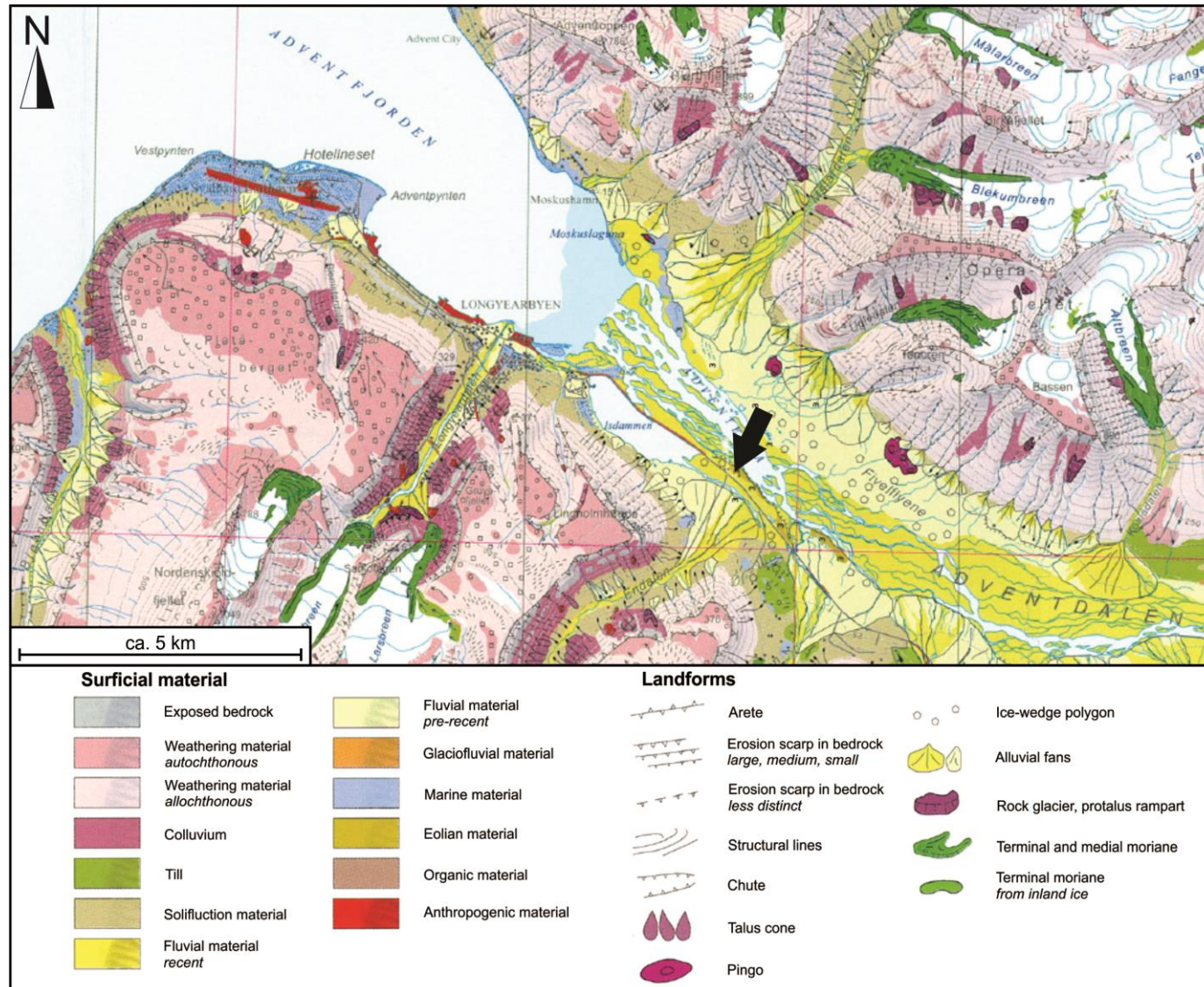
The large-scale geomorphology of the landscape such as plateaus and mountains are controlled by the bed orientation of the sedimentary rocks (Sørbel et al. 2001). The U-shaped profile of Adventdalen has been shaped during regional glaciations occurring during and prior to the Weichselian period (Mangerud et al. 1998). Landforms within the study area originate primarily from local glaciers, weathering, periglacial processes, and fluvial activity (**Figure 3.5**). Fluvial deposits, associated with Adventelva and its many tributaries, blanket the valley bottom. The margins of the active braided river system are often delineated by pre-recent river terraces extending up to ca. 10 m above the present river elevation. These fluvial terraces are frequently characterized by the presence of ice-wedge polygons and aeolian deposits, indicating stable sedimentary conditions (Bryant 1982; Christiansen 2005). The valley slopes are covered with allochthonous weathering deposits, colluvium, and alluvial fan sediments (Tolgensbakk et al. 2000). These deposits may be further characterized by the presence of debris-flow tracks, solifluction, and evidence of snow avalanche activity. Till, in the form of moraine deposits, occurs sporadically throughout the study area and likely relates to Holocene ice-bodies (Tolgensbakk et al. 2000).

### 3.3.3. *Permafrost*

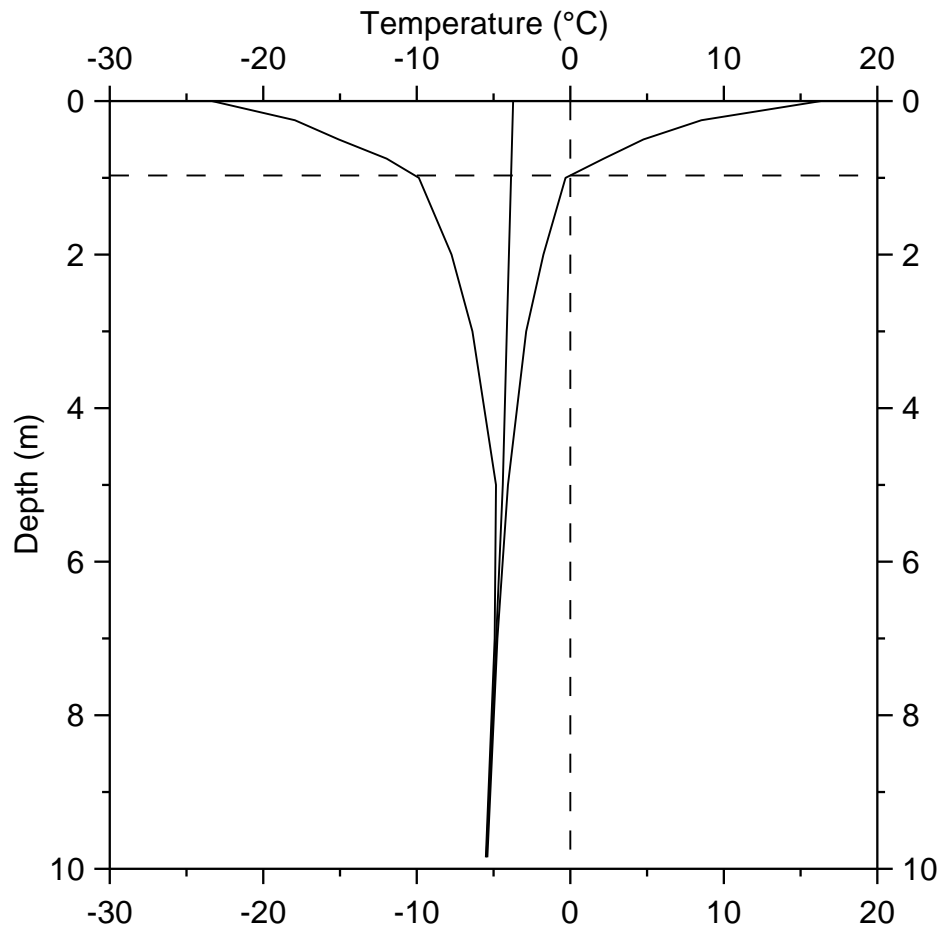
Svalbard is located within the continuous permafrost zone (Humlum et al. 2003). Perennially frozen ground is virtually ubiquitous under terrestrial areas not covered by glaciers (Humlum et al. 2003). In low-altitude areas, below the maximum Holocene sea level, permafrost is presumably of late-Holocene age as aggradation is only plausible following subaerial exposure of the ground surface (Humlum 2005). Because of the significant time required for thick permafrost bodies to come into equilibrium with present climate, these sites are also likely characterized by ongoing permafrost aggradation (Burn and Zhang 2009).

In Adventdalen, ground temperatures are recorded to a depth of ca. 10 m at the UNIS CO<sub>2</sub> well park. The monitoring location is within 100 m of the drill site and ground thermal conditions are taken to be representative. The annual mean ground temperature (taken at the depth of zero annual amplitude; 9.85 m) for the 2012-2013 hydrologic year (September 1<sup>st</sup> to August 31<sup>st</sup> of the subsequent year) is -5.5 °C. Ground temperature has risen by ca. 0.04 °C year<sup>-1</sup> since monitoring began in 2008. The thermal envelope for this site is presented in **Figure 3.6**. Active-layer thickness, reconstructed from the thermal regime, was ca. 97 cm in 2013 (**Figure 3.6**). Permafrost is estimated to be ca. 107 m thick in lower Adventdalen





**Figure 3.5** Quaternary geological and geomorphological map of the Adventdalen valley. The arrow points to the location of the study site. Modified from Tolgensbakk et al. (2000).



**Figure 3.6** Ground-temperature envelope from the study site. Constructed for the period between September 1<sup>st</sup>, 2012 and August 31<sup>st</sup>, 2013. Horizontal line denotes the interpolated depth of the active layer (ca. 0.97 m in 2013). (NORPERM 2014).

(Humlum 2005). A simple linear extrapolation suggests that ground temperatures within the cored interval (0 m – 60 m depth) likely range between ca. -5.5 °C and ca. -3.5 °C.

Permafrost has a controlling influence on environmental and geomorphological processes. Ground water in permafrost environments is limited to the seasonally unfrozen active-layer and unfrozen ground below permafrost. The occurrence of ground ice is directly related to the hydrology of permafrost regions (Mackay 1972). Additionally, permafrost environments are characterized by a unique suite of landforms not present in areas with perennial frost (French 2007). These include ice-wedges and pingos – both of which present in the study area.

### **3.4. Modern sedimentary environments**

Adventdalen is a glacial-formed valley characterized by steep walls and a valley-wide braided river system. A gilbert-type delta occurs at the interface between the Adventfjord and Adventelva river system. Since the early Holocene, this fjord-wide braidplain delta has prograded ca. 10 km to its present position (Johansen et al. 2003; Lønne and Nemeč 2004). The contemporary Adventfjord is 8.4 km in length, 3.4 km wide, and ca. 50 m deep, increasing to 100 m towards Isfjorden (Zajączkowski and Włodarska-Kowalczyk 2007; **Figure 1.1**). Sediment input to Adventfjord is primarily sourced from the braided river (Adventelva) at the fjord head. Additional, input is supplied by ice rafting, rivers, landslides, rockfalls, avalanche activity, and debris flows. It is anticipated that facies and sediment characteristics in the 60 m core reflect these processes as well as glacial and marine conditions that have occurred earlier in the Holocene.

Adventelva is frozen during the winter and does not supply fresh water or sediment to the fjord during this time. During the summer, a hypopycnal plume of brackish, sediment laden water extends up to 0.8 km into the fjord (Zajączkowski and Włodarska-Kowalczyk 2007). The water in Adventelva is principally derived from glacier and snow melt, precipitation, and groundwater flowing through the active layer. Zajączkowski and Włodarska-Kowalczyk (2007) report that, during the melt period, Adventelva flows with an average discharge of  $3.6 \text{ m}^3 \text{ s}^{-1}$  and transports ca.  $309 \text{ mg l}^{-1} (\pm 177)$  of solid material in suspension (Zajączkowski et al. 2004).

Along the long-axis of the Adventfjord/Adventdalen system the seaward transition in depositional environments is as follows: fluvial-dominated zone, tidal mudflat, steep delta slope (delta front), prodelta zone, and basin floor (**Figure 3.7**). Marine sediment cores have revealed that the sediments of the basin floor are underlain by till deposited during the late

Weichselian glaciation (Forwick and Vorren 2009). These environments and their associated deposits are briefly introduced here to provide a background for the range of sedimentary facies identified in the core under study. In a sense, the principles of uniformitarianism are applied to suggest that the suite of processes contributing to contemporary deltaic sedimentation have likely occurred in association with the Adventelva delta during its Holocene progradational history.

### **Delta plain and aeolian sedimentation**

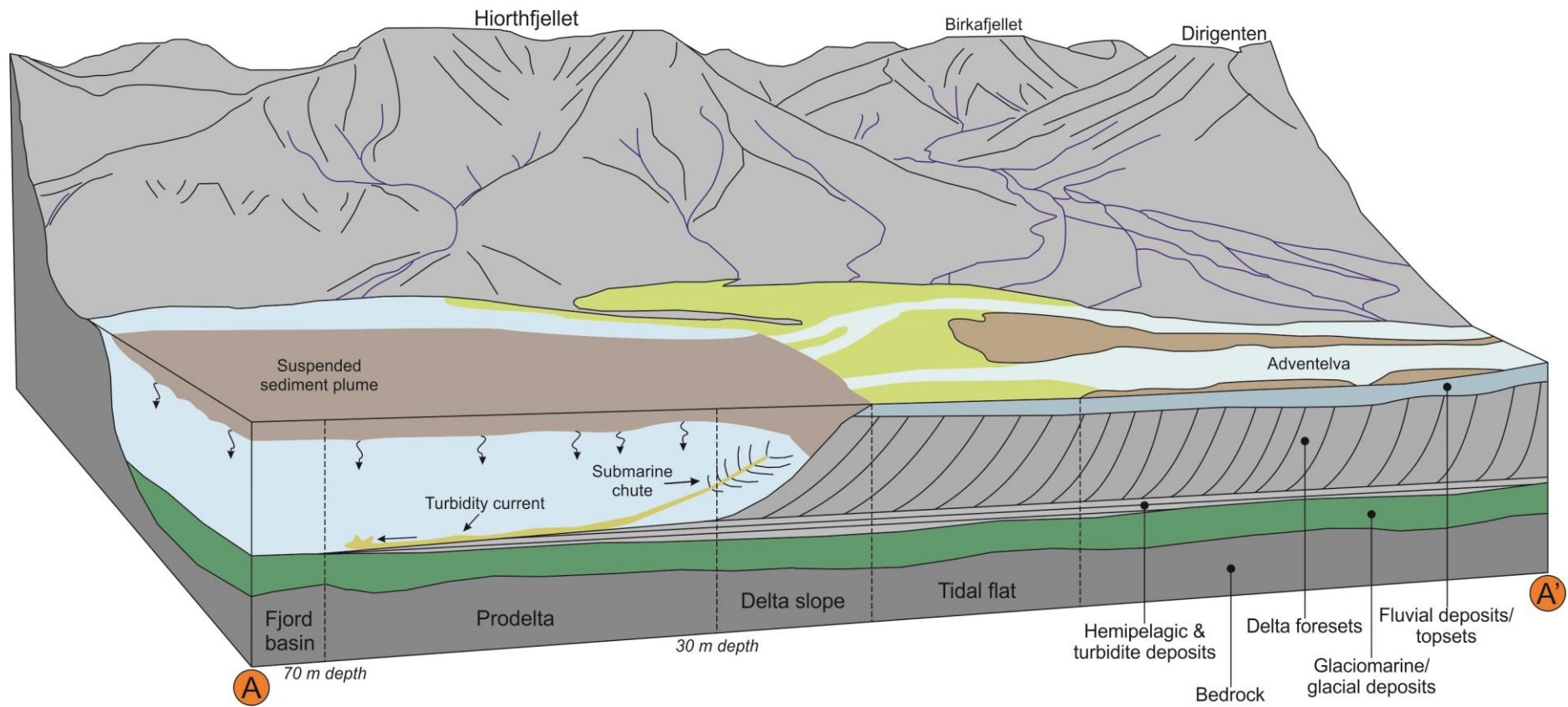
River currents from Adventelva decrease in strength and importance in a seaward direction. The delta plain may be subdivided into two regions: the upper-delta plain (discussed here), influenced primarily by fluvial processes, and the lower-delta plain (the tidal flat, discussed below), dominated by marine and tidal processes.

Sediment characteristics of Adventelva and the upper-delta plain have not been reported in previous studies. The braided, upper-delta plain is defined by the presence of distributary channels and inter-channel areas. The diversity of sedimentary environments has likely resulted in an array of deposits with different structural and textural attributes.

Aeolian sediments have accumulated atop the alluvial terraces which border Adventelva. These deposits result from the deflation of fluvial sediments in the valley bottom. This interpretation was based on the observation of frosted surfaces on quartz grains, a distinct grain size distribution, aeolian bedforms and deflation hollows in the source areas, and the observation of clouds of fine sediments in the valley (Bryant 1982). Aeolian sediments are described as poorly sorted, horizontally-laminated sandy silt (Bryant 1982).

### **Tidal flat**

A tidal flat is situated between the mouths of Adventelva and Longyearelva in the innermost part of Isfjorden (**Figure 1.1; Figure 3.7**). During low (ebb) tide, it is ca. 0.9 km wide and slopes gently (inclination of  $0.1^\circ$ ) towards the fjord (Zajączkowski and Włodarska-Kowalczyk 2007). The maximum tidal range is ca. 1.6 m – placing Adventfjord within a microtidal setting (Zajączkowski 2008; James and Dalrymple 2010). Sediments are characterized by rhythmic lamination resulting from tidally controlled suspension and deposition cycles. Monthly sedimentation rates of rhythmically laminated sequences are estimated to be ca.  $8 \text{ cm mo}^{-1}$  (Zajączkowski and Włodarska-Kowalczyk 2007). Occasionally tidal sediments are eroded by storms or ice scour. The tidal flat displays the lowest degrees of benthic faunal abundance and diversity in the deltaic environment (Włodarska-Kowalczyk et al. 2007).



**Figure 3.7** Primary sedimentary environments in contemporary Adventfjorden. Sedimentation and reworking dominated by: (1) the progradation of the fjord-head delta, (2) slope instability in the subaqueous delta front resulting in turbidity currents (Prior et al. 1981), (3) settlement of particles from hypopycnal, river-generated plumes, and (4) side-entry input from rivers and slope processes. Zone identification based on descriptions by Zajaczkowski and Włodarska-Kowalczyk (2007). Refer to **Figure 1.1** for the location of this cross-section.

### **Delta slope and prodelta**

The tidal flat progresses seaward into the steeply inclined ( $15^{\circ} - 19^{\circ}$ ) slope of the delta front. Zajączkowski and Włodarska-Kowalczyk (2007) note the highest concentration of suspended sediment occurs at this break in slope (ca.  $911.3 \text{ mg l}^{-1}$  during the summer). Freshwater, terrigenous sediment input, and high turbidity impact the benthic fauna resulting in a reduction in diversity and abundance (Włodarska-Kowalczyk et al. 2007). Turbidity decreases with distance from the river mouth and corresponds with an increase in diversity and abundance in the benthic faunal assemblage (Włodarska-Kowalczyk et al. 2007). The delta slope terminates at ca. 30 m water depth, transitioning into the prodelta depositional environment (**Figure 3.7**). The prodelta grades into the basin floor deposits by 70 m water depth (slope inclination  $7^{\circ} - 8^{\circ}$ ; Zajączkowski and Włodarska-Kowalczyk 2007; Zajączkowski 2008).

Within the water column, peaks in suspended material are observed indicating interflow (Zajączkowski and Włodarska-Kowalczyk 2007). Sediment transport on the delta slope and into the prodelta setting is dominated by gravity-driven processes (primarily grain flows, turbidity currents, and slumps) though laminated sediments, attributed to suspension settling, do occur (Prior et al. 1981; Zajączkowski and Włodarska-Kowalczyk 2007). Grain size in both subenvironments ranges between coarse silt and fine sand. Sand-rich deposits are interpreted to have been deposited by turbidity currents (Zajączkowski and Włodarska-Kowalczyk 2007). Clay is largely absent from these deposits indicating either that it is transported further into the basin or that it was only present in small amounts to begin with. Sediments range from poorly to very poorly sorted and typically display symmetrical to positive skewness. Modern sedimentation rates calculated from caesium ( $^{137}\text{Cs}$ ) spikes, associated with atmospheric testing of nuclear weapons, indicated a sedimentation rate of ca.  $18.7 \text{ m ka}^{-1}$  in the prodelta (sample from 60 m water depth; Zajączkowski et al. 2004).

The steeply sloping delta front is further characterized by the presence of chutes and subsidence areas, interpreted as evidence of sediment gravity flows (Prior et al. 1981). Zajączkowski and Włodarska-Kowalczyk (2007) measured six seaward directed near-bottom currents in a 25 hour period in summer 2002. These currents were accompanied by increases in suspended sediments from  $29.4 \text{ mg l}^{-1}$  to ca.  $174.7 \text{ mg l}^{-1}$ . Elevated concentrations of suspended sediment were additionally observed in the hours following these events. Distal extensions of these turbidity currents were detectable further out into the basin (Zajączkowski and Włodarska-Kowalczyk 2007).

### **Basin floor**

The central part of the fjord (basin floor) is flat and slopes gently towards Isfjorden (inclination of  $1^\circ$ ; Zajączkowski 2008). Sediments are characterized as homogenous, bioturbated muds (Zajączkowski and Włodarska-Kowalczyk 2007). Bioturbation traces are interpreted to reflect the activity of polychaetes (Włodarska-Kowalczyk et al. 2007). Large, angular pebbles are found in these deposits and attributed to ice-rafting processes. Zajączkowski and Włodarska-Kowalczyk (2007) report deposits associated with turbidity currents are not observed. Instead, deposition reflects low-energy suspension settling in an environment where the rate of biogenic activity exceeds sedimentation. Sedimentation rates in the basin range from  $8.7 \text{ m ka}^{-1}$  to  $0.7 \text{ m ka}^{-1}$ , decreasing towards Isfjorden (Zajączkowski et al. 2004). The usually distinct spikes in  $^{137}\text{Cs}$  have been altered by biogenic mixing of this sediment and these sedimentation rates should be interpreted with caution (Zajączkowski and Włodarska-Kowalczyk 2007).

## CHAPTER 4 MATERIALS AND METHODS

### 4.1. Core retrieval

This study is based on the analysis of a 60 m ice-bonded sediment core from the UNIS CO<sub>2</sub> well park (9 m.a.s.l., 78°12'N, 15°49'E). The core was retrieved over a 24-hour period beginning on September 3<sup>rd</sup>, 2012. The inner diameter of the core is 6.4 cm and sections were retrieved in 1.5 m lengths. Drilling was conducted using an industrial-scale drill rig fitted with a triple-core barrel system (**Figure 4.1a**). The triple-core barrel system limited the exposure of the core material with the drilling fluid by encasing the sample within a plastic tube during drilling (**Figure 4.1b**). This process resulted in a retrieval rate of ca. 80 %; 48.1 m of the possible 60 m of sediment was recovered. Unrecovered portions were distributed across the span of the core and were associated with sand-rich deposits susceptible to mechanical disintegration. It is believed that all depositional environments are accounted for in the recovered sediments.

Following retrieval, core sections were labelled and placed in a temporary cold storage unit on site. Periodically, samples were transferred from the temporary storage to permanent cold storage at the University Center in Svalbard. Here samples were kept at ca. -12 °C for approximately four months until they could be processed (**Figure 4.1c**).

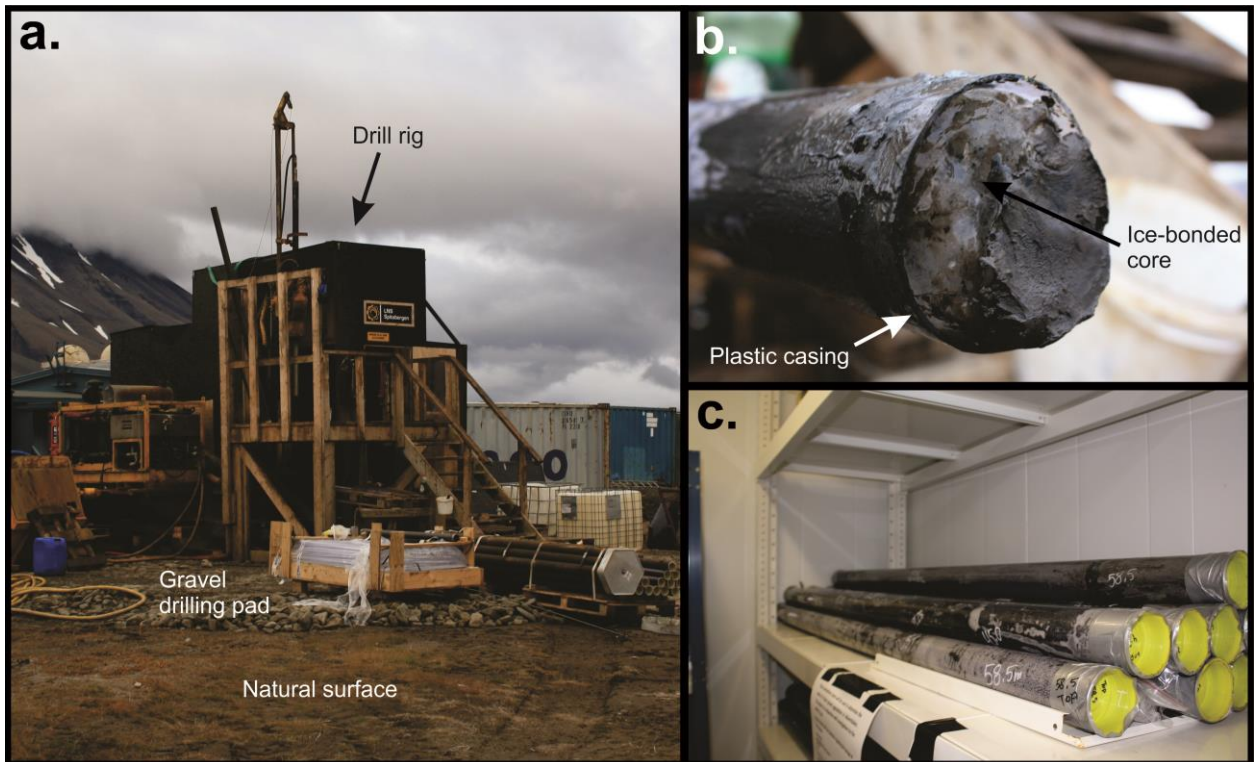
### 4.2. Analysis of core samples

Core sections were analyzed in a freezing laboratory with an ambient temperature of ca. -8 °C. The plastic casing was removed and the 1.5 m segments were split evenly into four subsections (each ca. 38 cm in length) to ease processing with the existing equipment. Next, each subsection was split lengthwise using a masonry table saw fitted with a diamond cutting blade. One half of each core was kept as a frozen archive while the other was utilized in the procedures introduced below. Disturbance material resulting from the cutting procedure was carefully removed from the core surface by repeated scraping with a razor blade. All exposed half cores were then photographed and described in detail. Samples were sealed in labeled bags to limit desiccation during storage. This process represents a significant investment of time, and accounts for approximately 10 weeks of the project. The entire collection of core photographs is provided in the **digital appendix G**.

#### 4.2.1. *Sedimentary log*

Classification of core sediments follows the grainsize classifications presented in **Table 4.1**. A comprehensive sedimentary log (scale 1:10) was created from laboratory observation of the





**Figure 4.1** a) Drill rig on site, September 3<sup>rd</sup> 2012. Note the presence of the artificial drill pad (ca. 0.4 m thick at the borehole location) overlaying the natural surface. b) Recovery of frozen sediment. c) Samples in cold storage at UNIS.

**Table 4.1** Modified Wentworth grain size classification system (Friedman and Sanders 1978).

<b>Wentworth classification</b>	<b>Phi units (<math>\phi</math>)*</b>	<b>Approximate size range (mm or <math>\mu\text{m}</math>)*</b>
Gravel	-1 to -6	64 to 2 mm
Very coarse sand	0 to -1	2 to 1
Coarse sand	1 to 0	1 mm to 500 $\mu\text{m}$
Medium sand	2 to 1	500 to 250
Fine sand	3 to 2	250 to 125
Very fine sand	4 to 3	125 to 63
Silt	9 to 4	63 to 2
Clay	>9	<2

\* The relationship between phi units and the metric scale is:  $\phi = -\log_2 D$ , where D is equal to the grain diameter in millimeters.

frozen half cores in addition to photographs. These logs were subsequently digitized using CorelDRAW (version X6). An overview log is provided in **Appendix A**.

#### 4.2.2. *Facies, facies associations, bioturbation, and trace fossils*

Facies are identified in the cored sediments on the basis of lithology, sediment texture, primary structures, bed contacts, stratigraphic relationships, and fossil content. Within each facies, lithology may vary slightly though each is believed to represent a unique depositional process. These facies are grouped together into facies associations, representing different depositional environments or subenvironments.

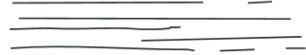





A bioturbation index (BI) classification was developed after Taylor and Goldring (1993) and is presented in **Table 4.2**. Six grades are identified based on the clarity of primary sedimentary structures and burrow abundance (Taylor and Goldring 1993). A BI value of 0 is used where bioturbation is absent. Where biogenic structures are subordinate to physical structures a BI value of 1 or 2 is indicated. Higher degrees of bioturbation (BI values of 3 and 4) are characterized by an increase in biogenic activity such that bedding boundaries are disturbed and may be difficult to discern. Complete bioturbation (BI = 5) represents the total, biogenic homogenization of the sediment. It is important to note that, in the core, bedding boundaries may also be obscured by soft-sediment deformation and the development of segregated-ice lenses.

Observed trace fossils were identified and described (refer to **Appendix C** for a detailed discussion). Identification was conducted in accordance with a number of introductory textbooks, principally Bromley (1996) and Knaust and Bromley (2012).

#### 4.2.3. *Grain size determination and statistical parameters*

152 samples were selected to account for the vertical variation in sediment characteristics. These samples are a subsample of those utilized in the assessment of gravimetric moisture content (presented below). A sieve with a mesh size of 2 mm (-1  $\phi$ ) was used to remove coarse material where present. The remaining fraction (< 2 mm) was analyzed with a laser diffraction particle size analyzer (Beckman Coulter LS 13 320) in order to separate sand, silt, and clay. The manufacture states a working range of 0.017 – 2000  $\mu\text{m}$  (Beckman Coulter 2011). Samples were run a minimum of two times each to establish reproducible results. Analysis was conducted in accordance with standard procedures defined by Solem et al. (1996). Sand is used to describe particles with a diameter between 2 mm and 63  $\mu\text{m}$  (-1  $\phi$  to

**Table 4.2** Bioturbation index (BI). Each grade is defined by the clarity of primary sedimentary features and burrow abundance.

Grade (BI value)	Percent bioturbated*	Classification*	Visual representation <sup>†</sup>
0	0	Absence of bioturbation, primary sedimentary fabric clearly visible.	
1	1-30	Sparse to low bioturbation. Primary sedimentary structures are distinct, low density of traces and/or escape structures.	
2	31-60	Moderate bioturbation, boundaries are sharp, traces are discrete and rarely overlap.	
3	36-90	High bioturbation, bedding boundaries are indistinct, high trace diversity with overlap common.	
4	91-99	Abundant bioturbation, bedding is completely disturbed though may be barely visible.	
5	100	Complete bioturbation, total homogenization of sediment by repeated biogenic overprinting.	

\* Percentage bioturbation values and descriptions are modified from Taylor and Goldring (1993: 142).

<sup>†</sup> Visual representation modified from MacEachern et al. (2005). Note, in some intervals, disruption of bed boundaries may occur due to soft-sediment deformation and water-escape processes and may not be a product of bioturbation exclusively.

4  $\phi$ ). Silt sized particles are those within the range of 63  $\mu\text{m}$  and 2  $\mu\text{m}$  (4  $\phi$  to 9 $\phi$ ). Clay particles are 2  $\mu\text{m}$  and smaller ( $> 9 \phi$ ). Grains larger than 2 mm ( $< -1 \phi$ ) were excluded from calculations due to the influence of single large grains on data bias (in accordance with Forwick and Vorren 2009).

From the perspective of laboratory efficiency, laser diffraction size analysis is superior to traditional sieve or pipette methods. Using the laser sizing technique, a single sample can be processed in approximately 30 minutes and results show a high degree of reproducibility. However, like most analytical technique this method has its limitations. Weaknesses of laser diffraction size analysis include: limits of detection (subpopulations of larger particles accounting for up to 3% of the sample volume may go undetected; Kelly and Kazanjian 2006), inability to distinguish between dispersed particles and agglomerates, and shape dependent results (assumption of spherical particle symmetry; Kelly and Kazanjian 2006). For a discussion of the general principles and limitations of laser diffraction size analysis the reader is referred to Jilavenkatesa et al. (2001).

Konert and Vandenberghe (1997) note, in comparison to pipette and sieve methods, laser diffraction results deviate in two respects. First, with the exception of particles  $> 2 \mu\text{m}$ , there is a general coarsening in mean grain size by ca. 0.25  $\phi$  when using laser diffraction methods. Second, the platy, nonspherical, form of clay particles results in the underestimation of clay content using the laser measurements. Knoert and Vandenberghe (1997) suggest that the 8  $\mu\text{m}$  grain size, defined by laser diffraction, corresponds to the 2  $\mu\text{m}$  grain size when using the pipette method. The results of grain size determinations in this investigation have not been adjusted to reflect these observations.

Grain size statistics were calculated using the GRADISTAT program (Blott and Pye 2001). Calculated parameters include: mean, median, standard deviation (surrogate for sorting), skewness (measure of symmetry), and the first percentile (C; a measure of the maximum transport competency) of each sample. Statistics were calculated using equations proposed by Folk and Ward (1957) and methods suggested by Passega (1957, 1964). The results of grain size determinations are included in **Appendix D**.

#### 4.2.4. *Excess ice content and gravimetric moisture content*

Laboratory investigations to determine excess ice content and gravimetric moisture content were conducted on 270 samples in order to determine moisture and excess ice content. Each sample was a 1-2 cm thick slice of the half core. Samples were selected to account for vertical heterogeneity in the deposits. Frozen samples were transferred into graduated

beakers, weighed, and allowed to thaw. Where excess ice was present, the volumes of saturated sediment and supernatant water were recorded in order to determine excess ice content,  $I_c$  (%), of each sample using the following formula:

$$[ 1 ] \quad I_c = \frac{(W_v \times 1.09)}{S_v + (W_v \times 1.09)} \times 100$$

Where  $W_v$  is the volume (ml) of supernatant water, multiplied by 1.09 to estimate the equivalent volume of ice; and  $S_v$  is the volume (ml) of saturated sediment (after Kokelj and Burn 2005).

Each sample was then transferred into a 40 ml plastic container and weighed to establish the wet sample weight. Samples were then refrozen and transferred to a freeze-drying machine in order to dehydrate. This method was preferred over oven drying at 105 °C as both organic material and clay minerals are altered by exposure to high temperatures. Following desiccation, the weight of the dried sediment was recorded in order to quantify gravimetric moisture content,  $W_g$  (%), as follows:

$$[ 2 ] \quad W_g = \frac{S_w - S_d}{S_d} \times 100$$

where,  $S_w$  and  $S_d$  refer to the wet and dry weights of the samples, respectively.

#### 4.2.5. *Cryostratigraphy and cryostructures*

Cryostructures (patterns formed by ice development in frozen ground) were defined using a classification modified from North American and Russian frameworks (Murton and French 1994; French and Shur 2010). The classification system used in this study is presented in **Table 4.3**. All cryostructures are easily distinguishable with the naked eye.

#### 4.2.6. *Chronology (OSL and AMS <sup>14</sup>C)*

To develop a detailed chronology of the core, 42 samples were selected for Optically Stimulated Luminescence (OSL) dating and 2 samples for Accelerator Mass Spectrometry (AMS)-radiocarbon dating. The radiocarbon dates are intended to provide an independent age assessment of the OSL results. Sampling of material for OSL dating was conducted under subdued orange light conditions. This experimental method requires quartz or potassium feldspar grains which been exposed to ultra violet light prior to deposition. Readers are referred to Krbetschek et al. (2002) and Puthusserry et al. (2006) for a detailed description of the OSL dating technique and discussion regarding the application and limitations of luminescence dating to arctic sediments.

The analysis of OSL samples was conducted by the Nordic Laboratory for Luminescence dating (Aarhus University, Denmark). Samples for AMS  $^{14}\text{C}$  were selected from organic rich clasts – material was terrestrial in origin. The evaluation of AMS  $^{14}\text{C}$  samples was conducted by the AMS  $^{14}\text{C}$  Dating Center (Aarhus University, Denmark). For a general discussion of this method the reader is referred to Jull (2007). Given the relatively short half-life of the  $^{14}\text{C}$  isotope (5568 yrs), radiocarbon dating is not reliable beyond ca. 40 kya (Björck and Wohlfarth 2001). Given the age of the sediments under study the application of this method is appropriate.

**Table 4.3** Classification of cryostructures porous (often termed structureless), layered, and micro-lenticular cryostructures result from epigenetic freezing while lenticular structures result from syngenetic permafrost development.

Cryostructure		Ice	Occurrence as or within
Porous		<i>In situ</i> freezing of pore water	Pore ice in deposits with varying textural properties.
Layered		Segregated or intrusive	Ice layers (0.5 – 3 cm thick) bounded by sediment containing pore ice. Occasionally inclined dykes but commonly horizontal, occurring between dissimilar sedimentary units.
Lenticular	Micro-lenticular	Segregated	Small ice lenses (< 0.5 mm thick) in fine silts or clay deposits.
	Lenticular	Segregated	Ice lenses (> 0.5 mm thick) in silt



## CHAPTER 5 RESULTS: SEDIMENTOLOGY

### 5.1. Facies and Facies Associations

The deposits have been divided into 27 facies, ranging from diamictons (facies 1 and 2), through silts and sands (facies 3 to 24), to silts and sands rich in plant material (facies 25 and 26). Facies were identified on the basis of lithology, sediment texture, primary structures, bed contacts, stratigraphic relationships, and fossil content. Individual facies represent different modes of deposition and post-depositional processes. Additionally, a disturbance facies (facies D) was identified and is interpreted to reflect deposits resulting from the drilling procedure and not from natural sedimentary processes. The distribution of these facies is presented in **Figure 5.1**. A detailed distribution is given in association with a complete sedimentary log in **Appendix A**. Images of select facies are presented in **Figure 5.2**, images of all remaining facies may be found in **Appendix B**.

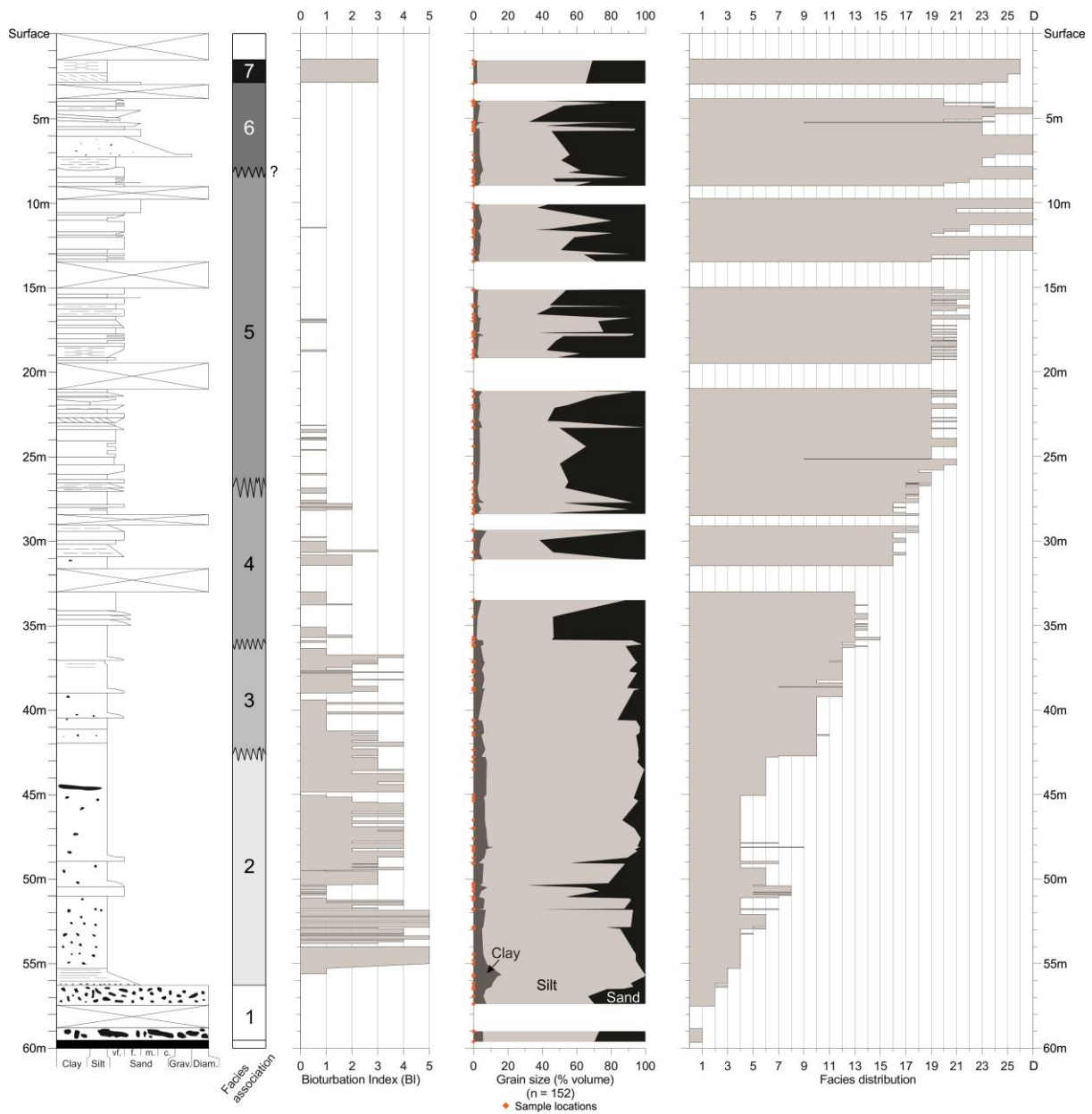
Seven facies associations (FA1 – FA7) are resolved, each consisting of a number of component facies. Each facies association reflects a unique depositional environment or segment of the deltaic, valley-fill system (**Figure 5.1**). A summary of the 27 component facies is presented in **Table 5.1**.

#### **Facies association 1 (FA1)**

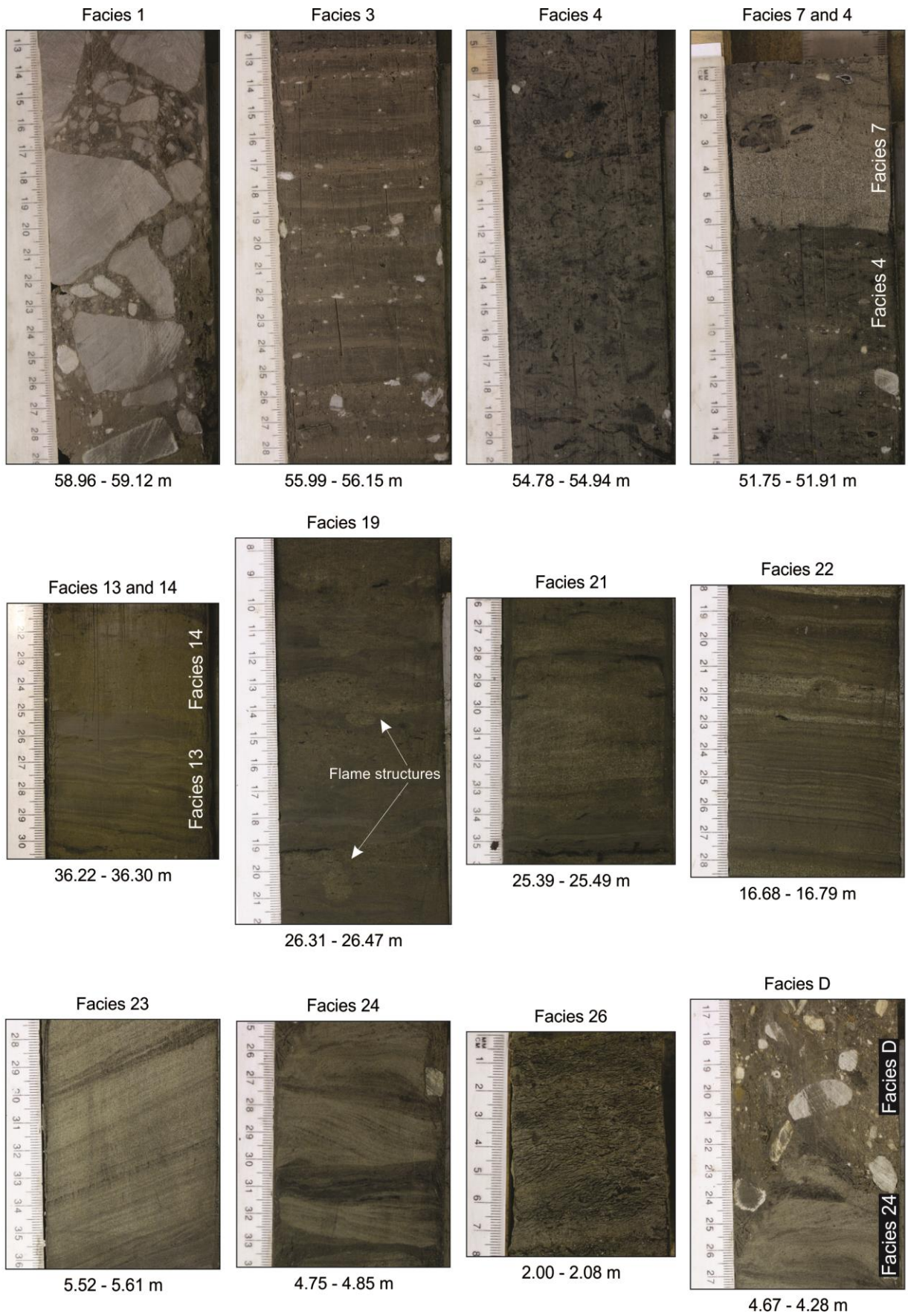
This facies association is ca. 3.5 m thick and occupies the lower most position in the core (59.67 m – 56.40 m depth; **Figure 5.1**). FA1 consists of two beds of diamicton (facies 1 and 2; **Figure 5.1**). The lower boundary is erosional and cut into Cretaceous bedrock (Carolinefjellet Fm). The bedrock underlying FA1 is fractured, possibly as a result of pressure release associated with glacial unloading or freeze-thaw processes beneath a glacier (Benn and Evans 2010). These structureless diamictons contain abundant outsized clasts but no mollusc shell fragments or evidence of bioturbation. The upper boundary, to FA2, is sharp and represents an abrupt change in depositional conditions.

#### **Facies association 2 (FA2)**

This facies association is ca. 13.6 m thick and occurs between 56.40 m and 42.80 m depth (**Figure 5.1**). FA2 is comprised of laminated silts (facies 3; **Figure 5.2**) which fine upwards into bioturbated silts and weakly laminated silt and sand deposits (facies 4 and 5; **Figure 5.2**). The sediments contain abundant shell fragments and occasionally *in situ* paired mollusc shells. Facies 5, 7, and 9, also present in FA2, representing departures from the background sedimentation. The presence of this diverse array of facies suggests that this environment is



**Figure 5.1** Simplified sedimentary log with facies and facies association distributions (detailed log in **Appendix A**). The intensity of biogenic activity decreases upwards in relation to coarsening and shallowing of the deposits. The grain size distribution is included to provide context for the location of facies and facies associations and will be discussed in reference to **Figure 5.3**. Note that crossed out boxes indicate the location of unretrieved intervals.



**Figure 5.2** Images of select core facies. For images of remaining facies refer to **Appendix B**.

**Table 5.1** Detailed description of the sedimentary facies in the Adventdalen 60 m core. The distribution of each facies in the core is documented in **Figure 5.1**. Images of select facies (boldface) are presented in **Figure 5.2**, images of additional facies are presented in **Appendix B**. The precise location and distribution of these facies is presented in **Appendix A**. The interpretation of these deposits will be discussed in **Chapter 7**.

<b>Facies</b>	<b>Lithology</b>	<b>Structures, bedding characteristics, and description</b>	<b>Fossils*</b>	<b>Bioturbation index</b>	<b>Interpretation</b>
F1. <b>Diamicton</b>	Muddy to sandy matrix supported diamicton with clast supported portions.	Consolidated, structureless unit, ca. 1-2 m thick. Grains are predominantly angular. Erosional lower boundary overlaying bedrock. Upper boundary not recovered.	Absent	0	Lodgement till deposited beneath a palaeo-ice stream (Benn & Evans 2010; Forwick & Vorren 2009).
F2. Diamicton	Sandy matrix supported diamicton. Clasts are smaller than in facies 1.	Structureless unit ca. 1 m thick. Lower boundary not recovered. Sharp, conformable upper boundary.	Absent	0	Glaciomarine diamicton associated with deglaciation. Alternatively, deposition by debris flow in a proglacial setting (Benn & Evans 2010).
<b>F3. Laminated silt</b>	Coarse (dark brown) to medium (light brown) silt. Outsized clasts up to pebble size.	Thin (2 – 5 mm) alternations of silt sized lamina. Pebble sized clasts occur and are most frequently associated with coarser (lighter) laminae. Black laminae occur near the top of this facies.	Absent	0-1 <i>increases upwards</i>	Deposition by sediment fallout from glacial suspension plumes (Ó Cofaigh & Dowdeswell 2001). Outsize clasts deposited by ice rafting processes (Benn & Evans 2010). Black laminae may result from the decay of organic material produced below sea-ice cover during the spring (Cowan et al. 1999).
<b>F4. Bioturbated silt</b>	Bioturbated dark silt with outsized clasts.	Completely biogenic homogenization of the sediment. Amount of outsized clasts is less than in F3. Dark mottles initially appear on cut surfaces but change to grey with prolonged exposure. Shell fragments and paired shells are present. Sharp to transitional boundaries.	Common	1-5 <i>typically 4-5</i>	Deposited in a distal glaciomarine environment by suspension fallout. With increasing distance from the sediment source, sedimentation rates decline and an accompanying increase in bioturbation results in the production of homogenous, bioturbated mud (Jaeger & Nittrouer 1999; Ó Cofaigh & Dowdeswell 2001).
F5. Massive pebbly sand	Pebbly sand.	Structureless units 2-5 cm thick with sharp upper and lower boundaries.	Absent	0	Deposited by melt out or roll dumping from icebergs or sea ice (Reading 1996; Benn & Evans 2010).
F6. Weakly-laminated silt and sand	Very fine sand and silt. Occasional sand beds are slightly coarser (medium sand).	Bioturbated sediment, bedding boundaries are sharp to indistinct. Sharp to transitional boundaries between adjacent facies.	Common	1-5 <i>typically 2-4</i>	Deposited from suspension fallout from sediment plumes. Occasional inclusion of fine to very fine sand may be due to deposition by distal turbidites (Reading 1996).
<b>F7. Graded sand and silt</b>	Moderately sorted fine grained sand and silt.	Weak lamination occasionally presents otherwise structureless (A division of the Bouma sequence). Sharp, erosive lower boundary with sole markings, flame structures, and other evidence of loading. Diffuse upper boundary.	Absent	0-2 <i>higher near top of beds</i>	Deposition from high density turbidity currents and associated hypopycnal suspension plumes (James & Dalrymple 2010).
F8. Interbedded sand and silt	Fine to medium sand and silt with low clay content.	Beds are 1- 10 cm thick, diffusely laminated and normally graded. Bed boundaries are typically sharp.	Rare	1	Deposition of sand by small turbidity currents. Fine-grained deposits are derived from suspended sediments (Ó Cofaigh & Dowdeswell 2001).
F9. Massive mud	Dark mud characterized by the presence of segregated ice lenses.	Structureless unit. Sharp upper and lower boundaries.	Present	0	Deposition in a low energy environment, possibly away from active tributary channels and submarine chutes (Zajączkowski & Włodarska-Kowalczyk 2007). Alternatively, rapid sedimentation from hyperpycnal fluid mud (Bhattacharya & MacEachern 2009).
F10. Laminated silt	Poorly sorted silt	Laminated to weakly-laminated depending on the degree of bioturbation. Individual laminae are typically thin (1-10 mm) and normally graded.	Absent	1-4	Deposition from hyperpycnal fluid muds from density currents (Bhattacharya & MacEachern 2009). Vertical variation in bioturbation intensity may be associated with

		Bioturbation intensity greatest along bedding surfaces.			quiescent periods between floods where salinity and low sedimentation rates favour burrowing.
F11. Graded silt	Poorly sorted silt.	Normal grading is common. Erosive or sharp lower boundaries with limited evidence of loading. Sharp or gradational upper boundaries.	Absent	0-1	Deposition from dilute hyperpycnal underflows formed by density currents or by collapsing hypopycnal plumes (James & Dalrymple 2010).
F12. Bioturbated silt	Bioturbated light-brown silt with occasional outsized clasts.	Predominantly structureless unit with a high degree of bioturbation and trace occurrences. Some deformation structures associated with water escape and soft-sediment deformation. Gradational contact to underlying facies. Sharp upper boundary.	Absent	1-3	Sediment deposited predominantly by suspension settling from hypopycnal plumes (James & Dalrymple 2010).
<b>F13. Weakly laminated silt and sand</b>	Fine to very-fine-grained sand and silt.	Weakly laminated beds (5-10 cm thick) disrupted by soft-sediment deformation. Lower boundaries are sharp and non-erosive while upper boundaries are typified by the presence of water-escape structures.	Absent	0-1	Deposition from suspension settling from hypopycnal plumes and hyperpycnal fluid muds. The presence of deformation and absence of bioturbation may indicate that F13 is associated with higher sedimentation rates in proximity to the active river.
<b>F14. Massive sand</b>	Fine to medium-grained sand.	Structureless to faintly laminated beds 5 – 10 cm thick. Water-escape structures are present at loaded bases. Upper boundaries are sharp.	Absent	0	Deposited from turbulent hyperpycnal plumes (Zajączkowski & Włodarska-Kowalczyk 2007).
F15. Weakly laminated sand	Poorly sorted fine-grained sand.	Distinct to diffuse planar parallel-laminated beds up to 20 cm thick. Massive to upwards fining trends observed. Lower boundaries are sharp and erosional. Gradational upper boundary to bounding facies.	Absent	1	Deposition from turbidity currents and suspension fall out from hypopycnal plumes (James & Dalrymple 2010).
F16. Moderately bioturbated sand and silt	Bioturbated sand and silt.	Indistinct bedding boundaries due to bioturbation and soft-sediment deformation. Where overlain by F15 upper boundaries are sharp otherwise gradational boundaries between bounding facies are most common.	Absent	2	Deposition from suspension settling from hypopycnal plumes. The presence of bioturbation indicates a relatively low sedimentation rate permitting the establishment of benthic organisms (James & Dalrymple 2010).
F17. Thinly bedded sand	Poorly sorted fine to medium-grained sand.	Planar-parallel, normally graded bed. Beds up to 30 cm thick. Laminations become less distinct towards the top of the bed. Lower boundaries are typically sharp and erosive. Upper boundaries are gradational.	Absent	0	Deposition from turbidity currents as indicated by erosive lower boundaries. Laminations may result from multiple, successive turbidity currents of short duration (Reading 1996; Zajączkowski & Włodarska-Kowalczyk 2007).
F18. Weakly laminated sand and silt	Poorly sorted silt and fine to very fine-grained sand.	Interbedded sand and silt. Silt deposits typically laminated but, when overlain by sand, lamination is obscured by water-escape structures. Transitions to bounding facies are sharp or gradational.	Absent	0	Deposition from hyperpycnal plumes. Sand deposited from hyperpycnal plumes.
<b>F19. Sand and silt with water-escape structures</b>	Poorly sorted silt and fine to very fine-grained sand.	Interbedded sand and silt. Boundaries where sand beds overlay muds are marked by water-escape structures including ball-and-pillows and dish structures. Upper and lower boundaries are sharp or gradational.	Absent	1 (vertical burrows)	Rapid deposition by suspension settling from hypopycnal plumes. High sedimentation rates result in the formation of over-pressurized muds leading to soft-sediment deformation (James & Dalrymple 2010).
F20. Massive sand	Poorly sorted fine to medium-grained sand.	Structureless units up to 120 cm thick. Transitions to bounding facies are commonly sharp.	Absent	0	Deposition by rapid suspension fallout from hypopycnal plumes (James & Dalrymple 2010) or from gravitational failures along the walls of submarine chutes (Prior et al.

						1981; Reading 1996).
<b>F21. Ripple laminated sand</b>	Poorly sorted fine-grained sand.	Unspecified ripple lamination.	Absent	0		Deposition by unidirectional traction currents, associated with turbidity currents (Garcia-Garcia et al. 2011).
<b>F22. Laminated sand and silt</b>	Fine-grained sand and silt.	Rhythmic (?) couplets of fine grained sand and silt. Individual laminae display normal grading with sharp contacts to bounding laminae. Possible reactivation surfaces associated with some sand-rich laminae.	Absent	0		Deposition in a tide-influenced environment where sand laminae are deposited during periods of tidal current activity while silt laminae are deposited during slack tide.
<b>F23. Subhorizontally laminated sand and silt</b>	Poorly sorted fine-grained sand and silt.	Upwards coarsening subhorizontal laminations with systematic thickening and thinning of laminae. Dip decreases to near horizontal at the top of each unit where ripple lamination (?) may be observed. Water escape structures occur. Bed contacts are typically sharp.	Absent	0		Deposition by tractional currents as part of a prograding unit. Likely represents the migration of dunes or point bars. Systematic thickening and thinning indicates tidal influence (James & Dalrymple 2010). In some cases, 11-12 sand layers may be counted between silt layers.
<b>F24. Ripple laminated sand</b>	Heterolithic deposits composed of sand and silt.	Climbing ripple, laminated sands with mud drapes on the leeward side.	Absent	0		Formed under unidirectional flow by concurrent deposition from traction and suspension and indicates high sedimentation rates (Ashley et al. 1982). Frequently occur in fluvial and deltaic overbank, turbiditic, and glacial outwash deposits. May also occur in tidal environments (Tessier 1993).
F25. Thinly interbedded sand and silt with roots	Fine to very fine sand and silt with <i>in situ</i> plant remains.	Sub-horizontal planar parallel-stratified beds 1 cm to 5 cm thick. Sharp bed contacts partially obscured by the development of segregated ice lenses.	Absent	3 <i>roots</i>		Deposition of sand from sheet floods on the Endalen alluvial fan surface. Silt sized particles deposited by aeolian processes (Bryant 1982).
<b>F26. Massive silt with roots</b>	Fine grained sand and silt with <i>in situ</i> plant remains.	Structureless unit characterized by the presence of roots, plant material, and segregated ice lenses. Boundaries are not observed due to sample loss surrounding this interval.	Absent	3 <i>roots</i>		Growth of terrestrial plants during concurrent deposition of sand and silt by aeolian processes (Bryant 1982).
<b>FD. Disturbance material</b>	Well to moderately sorted gravel and sand.	Structureless, commonly characterized by upwards fining from gravel to sand. Lower boundaries are sharp and erosive. These contacts are further characterized by erosion of the underlying core resulting in a convex geometry. FD is only observed at the top of the 1.5 m core sections. Similar deposits are never observed at the bottom of preceding sections.	Absent	0		Deposition by suspension settling in the drill hole. During drilling, deposits from the unfrozen active layer and gravel drill pad were mobilized by the drilling fluid. These sediments progressively settled out of the water column until there were removed entirely.
* Refers to calcareous microfossils (paired shells and reworked shell fragments).						

typified by variable energy and depositional processes. The upper boundary towards FA3 is gradational and is characterized by the absence of calcareous macrofossils.

### **Facies association 3 (FA3)**

This facies association is ca. 6.4 m in thickness, occurring between 42.80 m and 36.40 m depth (**Figure 5.1**). FA3 consists of laminated or bedded sand and silt (facies 10 and 11) and bioturbated deposits (facies 12). When not influenced by bioturbation, silt and sand beds are sharp based and display normal or inverse grading. However, most beds show some degree of bioturbation ranging from occasional burrows to near complete homogenization. Sand-rich facies generally become thicker with decreasing depth. The upper transition to FA4 is gradational and is characterized by a reduction in bioturbation and an increase in sand content.

### **Facies association 4 (FA4)**

This facies association is 9.65 m thick and is observed between 36.40 m and 26.75 m depth (**Figure 5.1**). FA4 is comprised of weakly-laminated sand and silt (facies 13, 15, and 18; **Figure 5.2**), structureless sand (facies 14; **Figure 5.2**), bioturbated sand and silt (facies 16), and laminated sand deposits (facies 17). FA4 is characterized by an overall upwards coarsening trend with a corresponding increase in sand content (**Figure 5.1**). FA4 is distinguished from FA3 on the basis of grain size and bioturbation intensity. The transition to the upper bounding facies (FA5) is gradational.

### **Facies association 5 (FA5)**

This facies association is ca. 18.9 m in thickness, accounting for the interval between ca. 26.75 m and ca. 7.87 m in the core (**Figure 5.1**). FA5 consists of sands and silts with water escape structures (facies 19), massive sands (facies 20), ripple cross-laminated sands (facies 21), and planar-parallel laminated sand and silt deposits (facies 22). The individual beds range in inclination from horizontal to slightly subhorizontal (maximum inclination of ca. 12°). Bioturbation is limited to a few zones and appears to be associated with fine grained, organic-rich (?) deposits. The upper transition to FA6 is not visible due to disturbance during drilling.

### **Facies association 6 (FA6)**

The facies association is ca. 4.9 m in thickness and is observed between ca. 7.78 m and 2.90 m in the cored interval (**Figure 5.1**). FA6 consists of laminated sand (facies 23), ripple-cross laminated sand (facies 24), and minor occurrences of massive sand deposits (facies 20).

Evidence of tidal influence is common particularly in facies 23 and facies 24 and includes rhythmites and mud drapes on the leeside of climbing ripples. Internal erosion surfaces are associated with Facies 23. Erosional boundaries are defined by thin coarse sand lag deposits. The upper boundary to FA7 is sharp and conformable.

### **Facies association 7 (FA7)**

This facies association is 1.4 m thick and occurs between 2.90 m and 1.50 m depth (**Figure 5.1**). FA7 consists of sub-horizontal beds of sand and silt (facies 25) and massive silt (facies 26). Both facies are further characterized by the presence of segregated ice lenses, roots, and plant material. The effects of ice segregation may serve to disrupt laminations which would have otherwise been visible. The upper boundary was not recovered due to sample loss. Regional observations suggest that FA7 reflects processes occurring in the modern environment.

## **5.2. Grain size distribution and statistical parameters**

### *5.2.1. Grain size distribution*

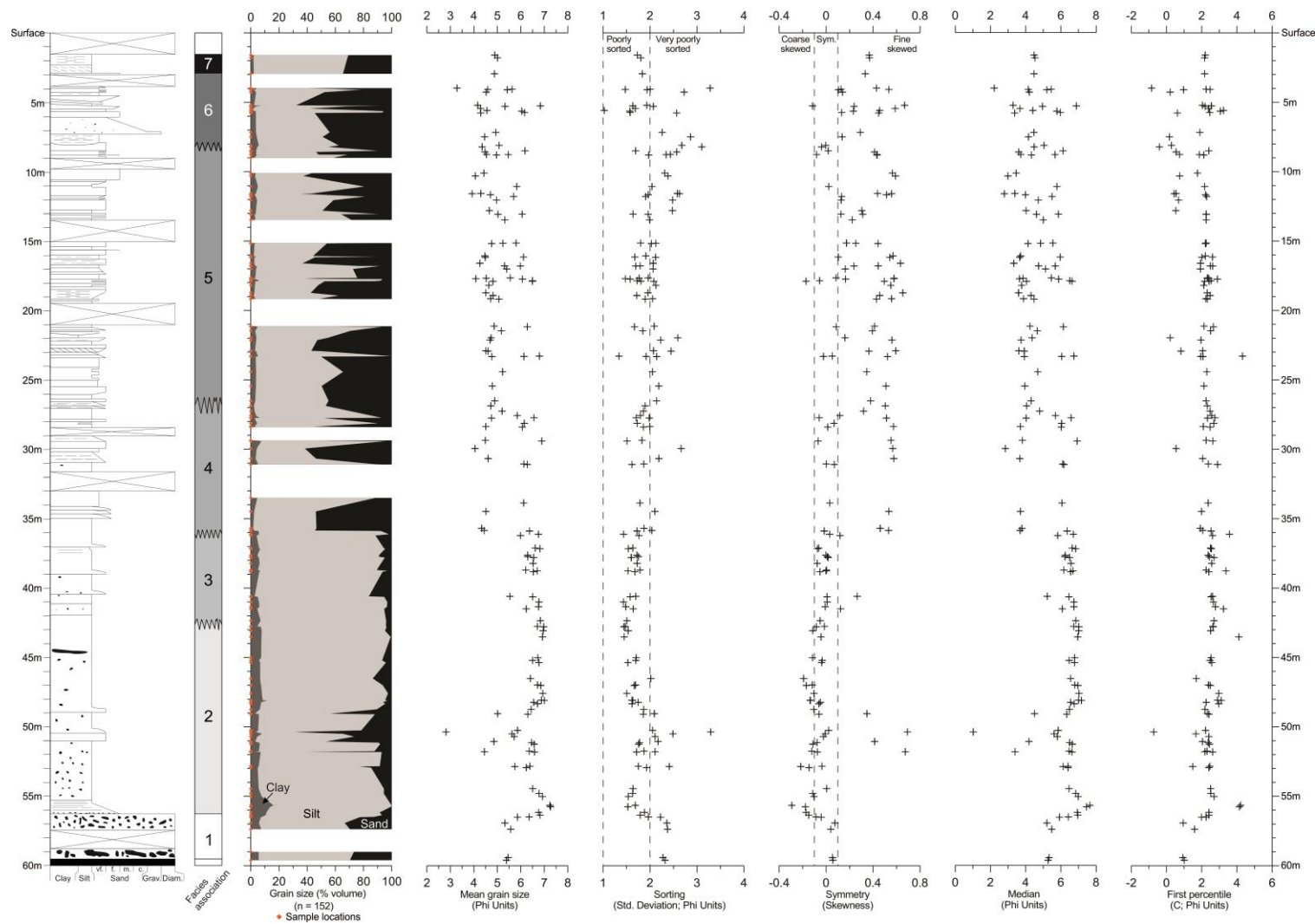
The vertical distribution of grain size parameters indicates that silt is the dominant particle size in the cored sediments, though sand increases in dominance towards the ground surface (**Figure 5.3**). Clay sized particles are present in all samples and range between 1 % and 16% of the total sample volume. Pebble sized clasts are observed in 29 of the 152 grain size samples. Pebble and gravel sized particles form a significant proportion of FA1, accounting for up to 40 % of the dry sample weight (**Appendix D**). The remaining observations are distributed sporadically across the core, comprising of between 1 % and 40% of the samples, where present. Generally, core sediments are characterized by an upwards coarsening succession, a hallmark of prograding deltaic deposits (James and Dalrymple 2010).

### *5.2.2. Grain size statistical parameters*

Statistical parameters derived from grain size distributions include the mean, median, standard deviation (a surrogate for sorting), skewness (a measure of the preferential spread of each sample), and the first percentile (a metric of the maximum competency of the transporting medium; Passega 1964). These parameters can be used to infer the evolution of sedimentary environments (McLaren and Bowles 1984; Zhang et al. 2009).

As noted above, mean grain size increases towards the top of the core. Additionally, the mean grain size amplitude is commonly higher in the upper facies associations (FA4 – FA6; **Figure 5.3**). Sorting decreases upwards as sediments transition from predominantly poorly sorted, to poorly and very poorly sorted (**Figure 5.3**). These observations indicate that the





**Figure 5.3** Distribution of grain size parameters including sedimentary composition, mean grain size, sorting, symmetry, median, and the first percentile. Poorly sorted sediments are those with a standard deviation between 1.00 and 2.00 and very poorly sorted between 2.00 and 4.00. Symmetrical distributions are those with a skewness between -0.1 and 0.1; fine (positively) skewed sediments  $>0.1$ ; coarse (negatively) skewed sediments  $<-0.1$  (Folk and Ward 1957; Blott and Pye 2001).

upper facies associations are likely characterized by a greater diversity of depositional environments than those below.

Positive skewness has been renamed ‘fine skewed’ indicating an excess of fine particles. Similarly, negative skewness has been renamed ‘coarse skewed’ as this signifies a tail of coarser particles (after Blott and Pye 2001). As seen in **Figure 5.3**, two populations exist with respect to this parameter. Deposits below ca. 36 m depth are typically coarse (negatively) skewed or symmetrical while sediments from the upper 36 m are characteristically finely skewed.

The median (M) and first percentile (C) of each samples have been included as these parameters are used to reconstruct C-M diagrams (Passega 1957, 1964; **Figure 5.3**). The vertical distribution of M follows a pattern similar to that described for the mean grain size. In finely-skewed samples the median is coarser than the mean value while the opposite is true for coarsely-skewed deposits. C is intended to provide an approximation of the competency of the transport agent (Passega and Byramjee 1969). C shows little variation throughout most of the cored interval perhaps indicating the absence of coarser sediments in the source area. An increase in the range of C-values is nevertheless observed in the upper portions of FA5 and FA6. Together, C and M can be used to infer transport and depositional mechanisms, permitting the evaluation of the hydraulic conditions under which sediments were deposited (Passega 1957). This will be addressed in Chapter Seven.

### **5.3. Bioturbation and trace fossil characteristics**

#### *5.3.1. Bioturbation*

Bioturbation is generally defined as displacement within sediments and soils resulting from the activity of organisms and plants (Taylor and Goldring 1993). There is significant variability in the degree of biogenetic activity present in the component facies (**Table 5.1**). Some intervals are characterized by complete bioturbation resulting in homogenization of the sediment such that no primary structures are visible (BI = 4-5). In contrast, other units display no evidence of biogenic activity (BI = 0). Generally, the degree of bioturbation decreases towards the top of the core.

Evidence of biogenic activity is absent in FA1. The highest bioturbation intensities are observed in FA2 where BI values range from 0 to 5 but are typically between 3 and 5 (**Figure 5.1**). In FA2, low degrees of bioturbation are associated with coarser deposits (ex. facies 7) and may represent periods of elevated sedimentation associated with turbidity currents or

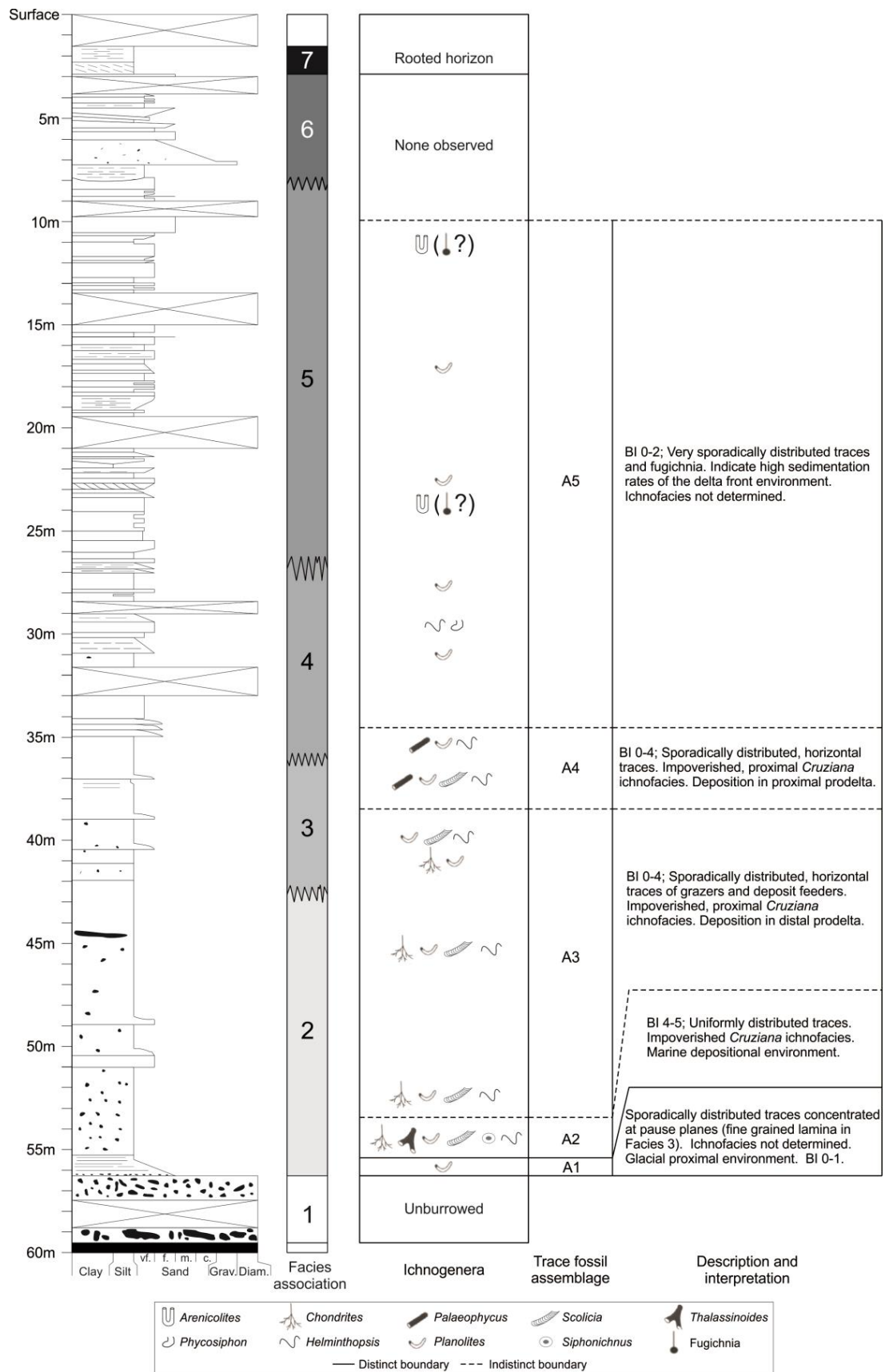
other types of sediment gravity flows. FA3 is typified by high degrees of biogenic activity (BI typically between 3 and 5).

With the exception of FA7, the remainder of the cored interval (FA4, FA5, and FA6) is characterized by a low degree of biogenic activity (BI = 0-2; **Figure 5.1**). Where present, traces display low diversity and high abundance. This may reflect increasing sedimentation rates, deteriorating environmental conditions, and a resultant decline in infaunal biomass and diversity. Within FA7, bioturbation is the result of the activity of plants and their associated root systems. Determining the degree to which sediment deformation is the result of biogenic activity is problematic as this interval is also characterized by intrasedimental ice, which further perturbs bedding boundaries.

### 5.3.2. *Trace fossils*

Sedimentological analysis is the primary tool used to distinguish between different depositional environments and subenvironments. However, many sedimentary processes are not particularly sensitive to the depositional environment. In contrast, organisms are strongly controlled by environmental variables. For this reason, the analysis of trace fossil characteristics provides an excellent additional method to aid in the reconstruction of depositional settings. Though the application of ichnology to improve palaeoenvironmental interpretation of Late Quaternary glacial environments is in its infancy, marginal-marine and deltaic environments represent, perhaps, the most successful areas of ichnological research. A brief introduction to ichnology and a detailed description and interpretation of the core ichnogenera is the focus of **Appendix C** and only the key findings will be reported here. Eight trace fossils are identified and are used to construct five trace fossil associations (**Figure 5.4**). Ichnogenera represent feeding and grazing ethologies. Suspension feeding is precluded by high water turbidity induced by hypopycnal flow in the river-dominated depositional environment (Włodarska-Kowalczyk et al. 2007).

Towards the top of the core a reduction in trace fossil diversity corresponds to the upwards coarsening and swallowing sedimentary succession. Trace fossil inclination changes from predominantly horizontal to mixed horizontal and vertical traces along this gradient. FA2 displays a uniform to sporadic distribution of trace fossils oriented parallel to the bed planes. FA3 to FA5 are characterized by the sporadic colonization of fine grained sediments; trace fossils are highly facies controlled in this interval. No trace fossils are observed in FA1 or FA6. FA7 is dominated by the presence of roots and plant material but evidence of faunal activity is absent.



**Figure 5.4** Simplified sedimentological log with trace fossil assemblages. The intensity of biogenic activity decreases upwards in relation to coarsening and shallowing of the deposits. The trace fossil assemblages illustrate a glacial proximal – open fjord basin – delta transition. See **Appendix C** for details regarding core ichnology.

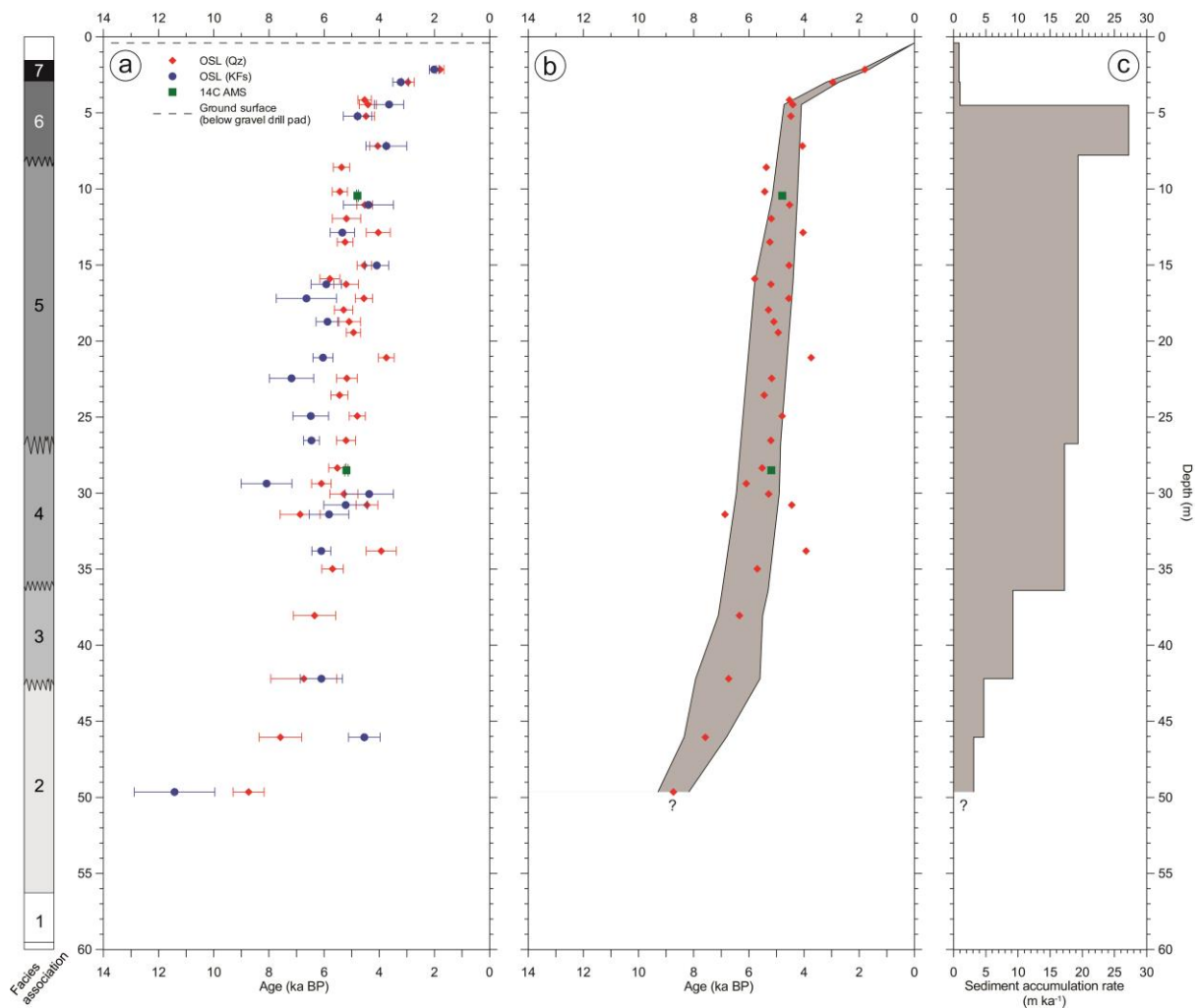
#### 5.4. Age and sedimentation rates

Of the 42 samples selected for OSL analysis, 35 yielded usable results. These results, in addition to two AMS  $^{14}\text{C}$  dates, are illustrated in **Figure 5.5a**. An age-depth curve is estimated from comparison of the OSL ages, determined from quartz mineral grains, and radiocarbon dates (**Figure 5.5b**). The OSL ages, determined from feldspar grains, vary significantly and are considered to be a less likely alternative. The addition of these samples is primarily to assess the bleaching of the quartz grains. For this reason, the feldspar OSL dates are not included in the age assessment of these deposits. The sediment accumulation rate (**Figure 5.5c**) for each facies association is estimated using the age-depth curve in **Figure 5.5b**. These rates do not account for the effects of sediment compaction since deposition. Dating results are listed in **Appendix E** and imply a Holocene age for all dated intervals.

The depositional age of FA1 could not be determined using the OSL method as sediments were not sufficiently well bleached. This suggests that these deposits have likely never been exposed to ultraviolet light at the surface. The lowermost date was obtained from 49.65 m depth and indicates a depositional age of 8.7 kya, corresponding to the early Holocene period. FA2 was deposited prior to 6.8 kya. Sedimentation rates reconstructed for this interval display an upwards increase from  $3.1 \text{ m ka}^{-1}$  to  $4.7 \text{ m ka}^{-1}$  near the top of the unit. The deposition of FA3 is restricted to between ca. 6.8 kya and 6.1 kya (**Figure 5.5b**). A sedimentation rate of  $9.1 \text{ m ka}^{-1}$  is resolved for this interval (**Figure 5.5c**).

The results of age determination indicate a narrow age range in which FA4 and FA5 have been deposited. Considering the errors in the data, the deposition of these sediments is constrained to between ca. 4.6 kya and ca. 6.1 kya. High rates of sediment accumulation are implied by the overlapping ranges of individual OSL dates in this interval (**Figure 5.5a**). Interpreted sedimentation rates for FA5 and FA4 are  $19.3 \text{ m ka}^{-1}$  and  $17.2 \text{ m ka}^{-1}$ , respectively (**Figure 5.5c**). These rates may be subject to substantial uncertainty. For example, if sedimentation rates are calculated from only the two radiocarbon results (10.4 m and 28.5 m depth), an accumulation rate of ca.  $45.7 \text{ m ka}^{-1}$  is resolved.

FA6 was deposited in the interval between 4.6 and 3.0 kya. Two distinct sedimentation rates are observed in the slope of **Figure 5.5b** and reconstructed in **Figure 5.5c**. In the lower interval of FA6 (7.87 m to 4.50 m), the resolved sedimentation rate is  $27.2 \text{ m ka}^{-1}$ . In the upper interval (4.50 m to 2.90 m) the sediment accumulation rate is ca.  $1.0 \text{ m ka}^{-1}$ . This likely reflects the presence of internal unconformities resulting from erosion in this setting. FA7 is extended beyond the top of the core at 1.5 m to the ground surface at ca. 0.4 m depth (due to the presence of a constructed gravel drill pad approximately 0.4 m in thickness).



**Figure 5.5** Core chronostratigraphy. a) Age-depth plot containing all viable ages from OSL and AMS  $^{14}\text{C}$  analysis. b) Accumulation curve interpreted from the results of the quartz OSL method and AMS  $^{14}\text{C}$ . The slope of the curve represents the sediment accumulation rate. c) Sediment accumulation rates for the facies associations, determined from the mean slope in b. Multiple sedimentation rates are noted where possible.

These sediments are estimated to range in age, from between 3.0 kya to the present. Facies analysis, discussed above, in association with observations of the present environment, indicate that a similar suite of depositional processes operate today as did 3.0 kya. Sediment accumulation rates for FA7 are estimated to be  $0.9 \text{ m ka}^{-1}$ , the lowest observed in the core.

## 5.5. Summary

This chapter has examined the sedimentary characteristics a 60 m core from lower Adventdalen. The following points summarize the results presented above:

- (1) Seven facies associations are defined from 27 facies. Facies associations transition upwards from a diamict facies association (FA1) to an intensely bioturbated interval characterized by the presence of shell fragments and oversized clasts (FA2). Subsequently, an upwards coarsening and shallowing succession from FA3 to FA6 records the progradation of the Adventelva delta. Finally, silty deposits, rich in terrestrial organic material, form the upper most facies association, FA7. FA7 is believed to represent the contemporary depositional environment at the study site.
- (2) Grain size supports a general upwards coarsening and shallowing of these deposits. With respect to statistical parameters, deposits display a transition from poorly sorted, fine grained deposits to poorly or very-poorly sorted, sand-rich deposits towards the top of the core. Coarse-skewed to symmetrical distributions are typical of fine grained deposits below 36 m depth while the overlying interval is predominantly fine-skewed.
- (3) An upwards reduction in biturbation corresponds to coarsening and shallowing of these deposits. Trace fossils exhibit a concurrent reduction in diversity and abundance.
- (4) Dating results suggest a Holocene age for deposits above 49.6 m (the location of the lowermost date). Three general trends in sediment accumulation rates are noted. First, FA2-FA2 exhibit progressively increasing sedimentation rate with depth (from  $3.1 \text{ m ka}^{-1}$  to  $9.1 \text{ m ka}^{-1}$ ). Subsequently, FA4, FA5, and FA6 were deposited in the interval between 6.1 kya and 4.6 kya, enabling the reconstruction of sediment accumulation rates between  $17.2 \text{ m ka}^{-1}$  and  $27.2 \text{ m ka}^{-1}$ . Finally, FA7 was deposited after 3.0 kya and is characterized by slower sedimentation ( $0.9 \text{ m ka}^{-1}$ ).

## CHAPTER 6 RESULTS: GROUND ICE AND CRYOSTRATIGRAPHY

### 6.1. Gravimetric moisture content and excess ice content

270 samples were collected to determine the vertical distribution of gravimetric moisture (ice) content and excess ice content. All gravimetric moisture content and excess ice content values are provided in **Appendix F**. **Figure 6.1** illustrates the results of gravimetric moisture content determination. Generally, values lie between 20% and 40%, indicating the dominance of ice-poor permafrost in these deposits. Concerning gravimetric moisture content, these sediments are divisible into two zones: an ice-rich upper layer (corresponding to FA7; gravimetric moisture content > 50%) underlain by ice-poor permafrost (FA1 – FA6; gravimetric moisture content < 50% **Figure 6.2**). In the near-surface, ice-rich sediments, gravimetric moisture contents ranges between 49.4 and 160.3 % (mean value of 97.2 %). The remaining sediment is comparatively deficient with respect to ice and values range between 6.9 % and 53.2 % (mean value of 28.2 %). No correlation is detected between gravimetric moisture content and the grain size characteristics presented in Chapter Five.

As noted previously, all sediments are ice bonded, but contained little to no excess ice. Apart from ca. 20 ice layers (discussed below), only 5 samples exhibited excess ice (**Figure 6.2**). Given the high ice contents noted in connection with FA7, it may be expected that a greater number of samples would have contained supernatant water upon thawing. The relationship between these two parameters is likely confounded by the presence of organic material in the near surface sediment. Similar observations have been made in the western Canadian arctic where the absence of excess ice is attributed to organic-rich soils with low bulk densities (Morse et al. 2009).

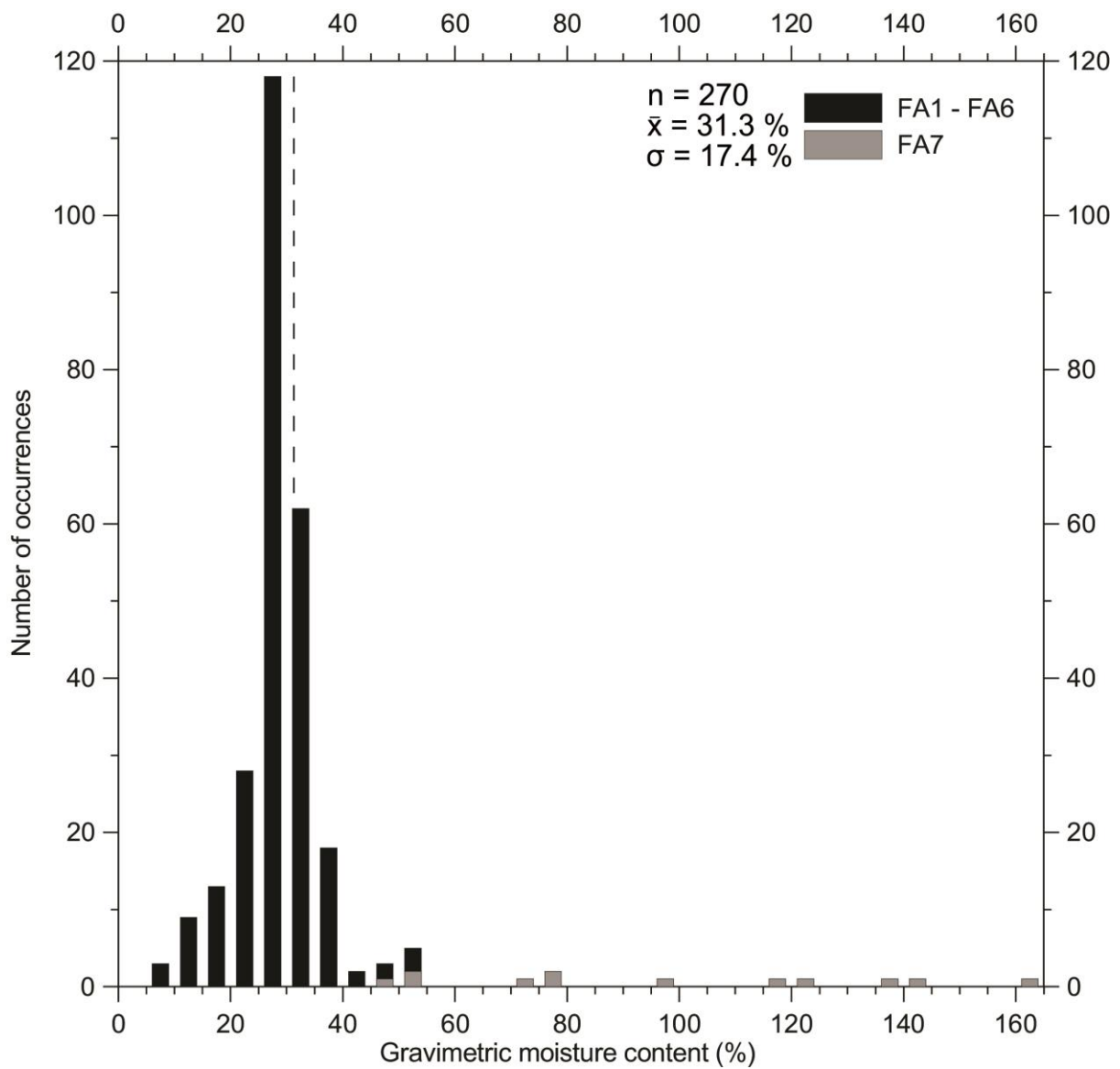
### 6.2. Cryostratigraphy of the Adventdalen core

Four unique cryostructures are distinguished on the basis of morphological traits and gravimetric moisture content: (1) porous cryostructure – Po; (2) layered cryostructure – La; micro-lenticular cryostructure – mLe; and (4) lenticular cryostructure – Le. The first three of these cryostructures are associated with the development of epigenetic permafrost. Only the lenticular cryostructure is regarded as being connected with syngenetic permafrost aggradation. The distribution of cryostructures in the core is included in **Figure 6.2**. Images of these ice types are presented in **Figure 6.3**.

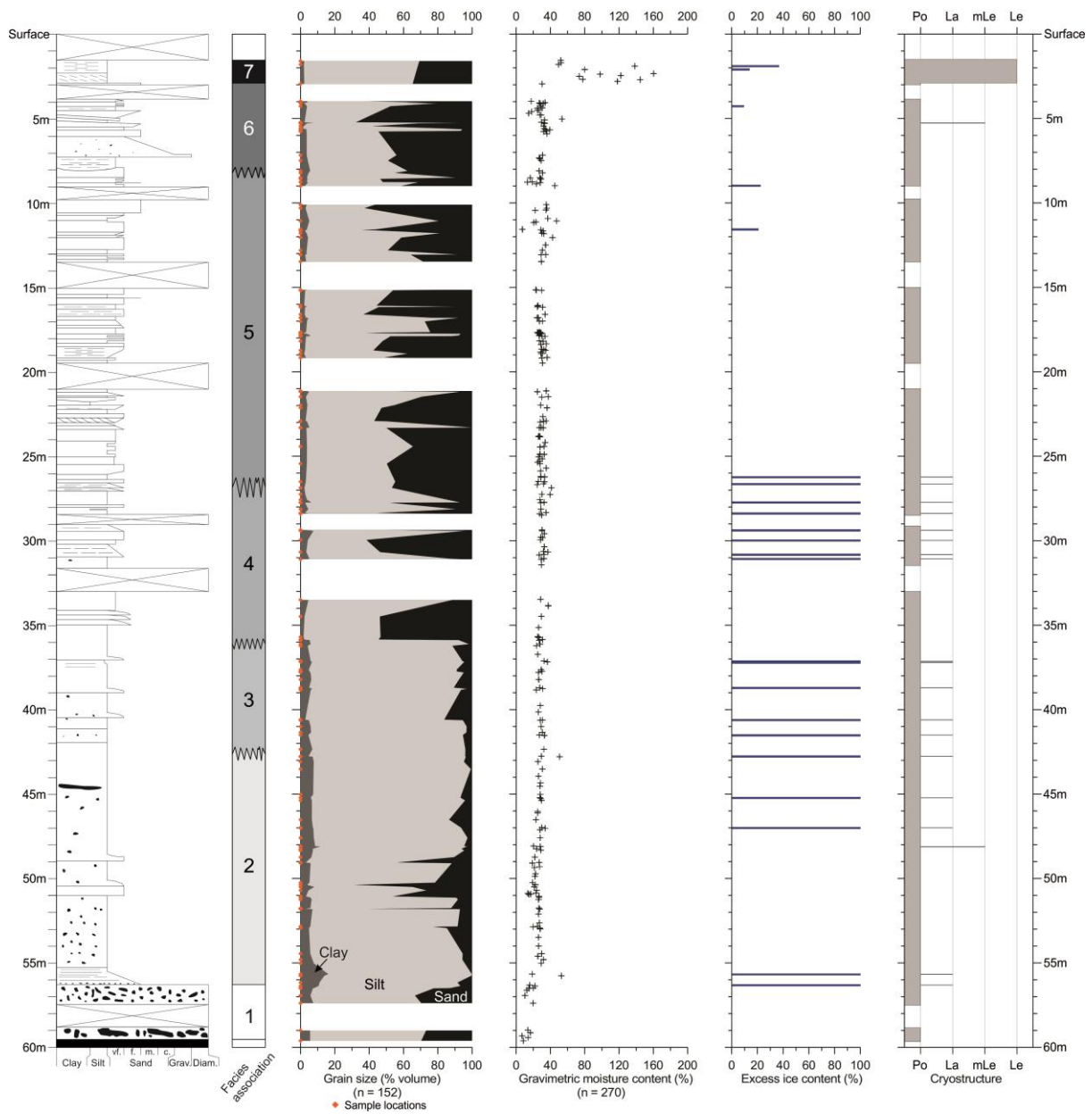
#### **Porous cryostructure – Po**

In deposits characterized by the porous cryostructure, ice is present within the pore space of





**Figure 6.1** Frequency distribution of gravimetric moisture content. The average gravimetric moisture content of all 270 samples was 31.3 % (vertical dashed line).



**Figure 6.2** Vertical distribution of geocryological parameters discussed in text. Note excess ice contents of 100 % are estimates for ice layers (La cryostructure). Grain size parameters are included for reference. No correlation is observable between textural and geocryological properties.

the sediment matrix and is not visible to the naked eye (**Figure 6.3**). The porous cryostructure is the most pervasive ice type in these deposits and exists within all sediment types and facies associations (**Figure 6.2**). In deposits with lenticular cryostructures, pore ice exists in the sediments between individual lenses. The gravimetric moisture content of sediments characterized by porous cryostructures typically ranges between 20 % and 35%. Lower values are noted in the clast-rich facies of FA1. The observation of pore ice in fine-grained, frost susceptible sediments suggests that much of the permafrost in the core deposits is epigenetic.

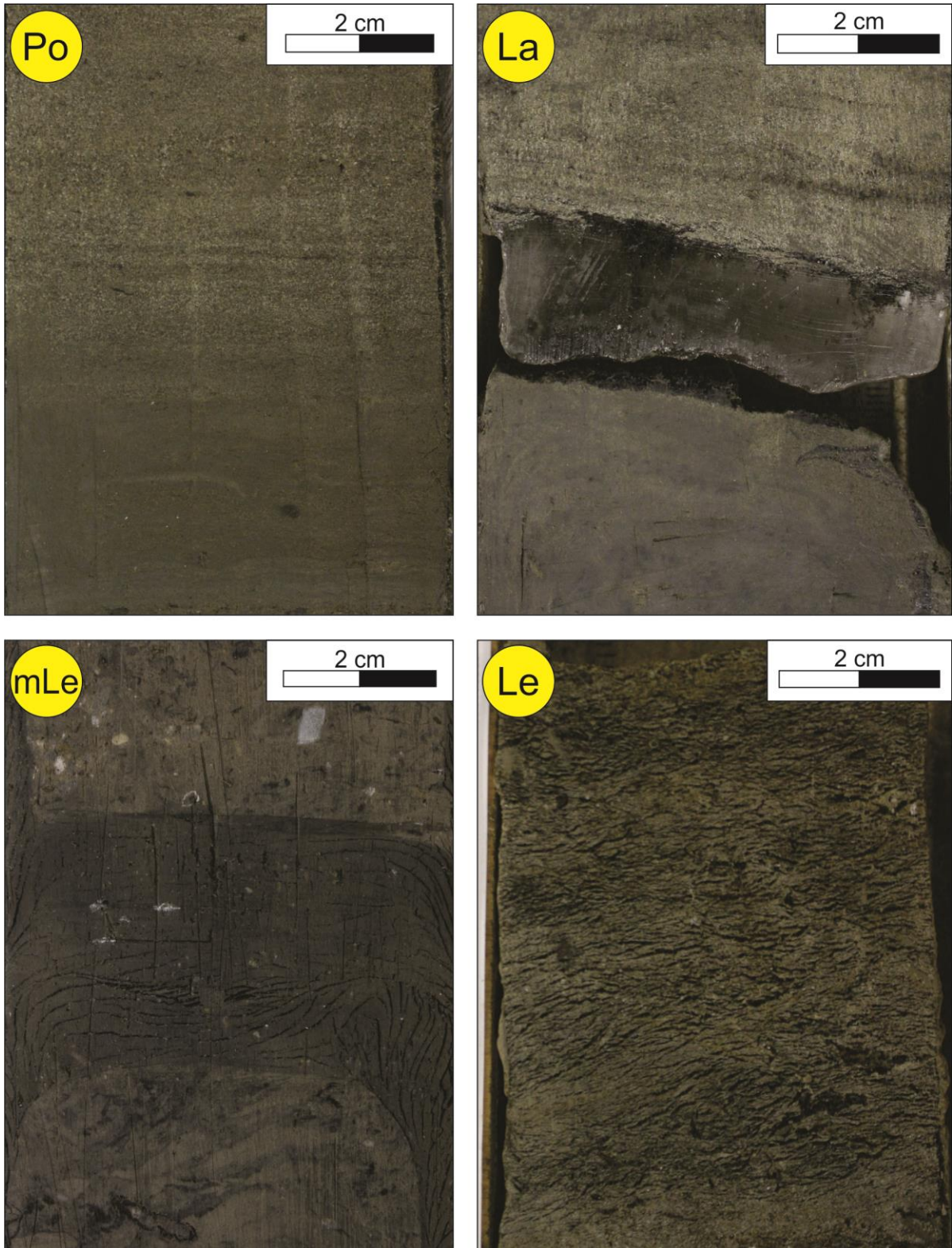
#### **Layered cryostructure – La**

The layered cryostructure is characterized by discrete ice layers occurring periodically between the 25 m and 60 m depth intervals in the core (**Figure 6.2**). Layers range in thickness from ca. 0.5 cm to 3 cm. The ice does not contain sediment and is frequently smaller in diameter than the rest of the core (**Figure 6.3**). These two observations are used to eliminate the possibility that the ice layers formed from the refreezing of sediment laden fluid used during drilling. The reduction in diameter is attributed to thermal erosion during drilling. Layers were not melted in this investigation as they will be used in additional studies that require them to be in a frozen state. The gravimetric moisture content of these layers is anticipated to approach infinity and is not included in **Figure 6.2**. Excess ice content is estimated to be 100 % as particulate matter was not observable in the ice.

Typically, ice layers are horizontal and occur at bed transitions. However, more often than not, bed transitions are characterized by the absence of ice layers. The sediment bounding these ice layers were analyzed to identify variations in texture. In all cases, the overlying sediment is coarser (greater mean grain size) than the underlying sediment – often differences are minimal. Ice layers are tentatively classified as intrusive ice, formed by pore-water expulsion during the freezing of overlying deposits.

#### **Micro-lenticular cryostructure – mLe**

The micro-lenticular cryostructure is typified by thin, elongate lenses of ice in silt deposits. Lenses are wavy and less than 1 mm in thickness; length ranges up to ca. 2 cm (**Figure 6.3**). The orientation ranges from horizontal in the center of the core to vertical near the edge of the core. The vertical orientation indicates that this sediment was subjected to thawing during drilling and subsequent refreezing. This ice type has two occurrences in the sediments under study (**Figure 6.2**). Associated gravimetric moisture contents were ca. 30 %; excess ice was not present.



**Figure 6.3** Cryostructures identified in the core. Po: porous cryostructure containing pore ice. La: layered cryostructure of segregated or intrusive origin. mLe: microlenticular cryostructure observed twice in fine silt deposits and attributed to segregation. Le: lenticular cryostructure associated with coarse silt in FA7; segregation origin (aggradational ice).

### **Lenticular cryostructure – Le**

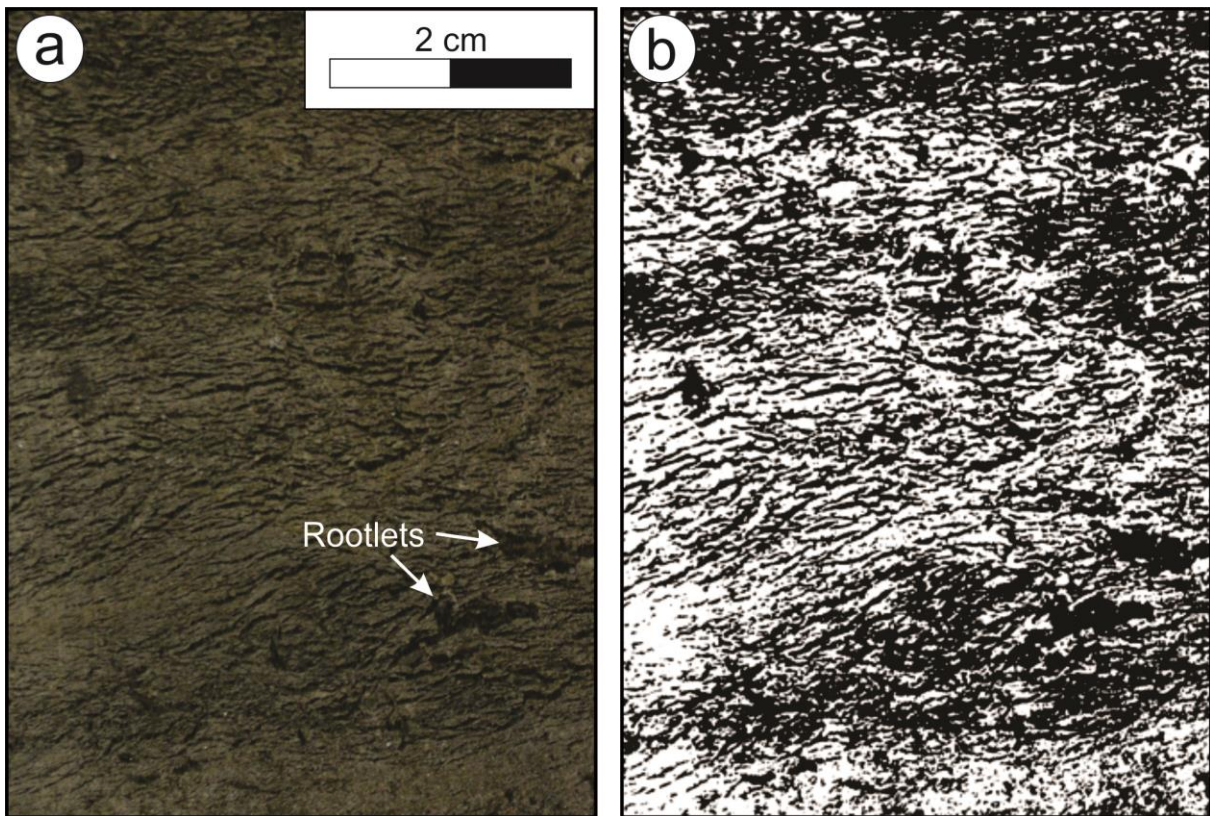
Lenticular cryostructures are associated, exclusively, with the sandy silt deposits of FA7 (1.5 m – 2.9 m depths). The thickness of discrete ice lenses is ca. 1 mm; length varies up to ca. 1 cm (**Figure 6.3**). Lenses are horizontal to sub-horizontal in inclination and exhibit a shard-like morphology (**Figure 6.4**). Gravimetric ice contents range between ca. 50 % and ca. 160 %. Excess ice is observed in two samples (**Figure 6.2**).

### **6.3. Summary**

The cored deposits are divisible into two zones with respect to the geocryological characteristics presented above:

- (1) The uppermost facies association, FA7, is characterized by segregated, lenticular ice and high gravimetric moisture contents. FA7 marks the occurrence of syngenetic permafrost in the core.
- (2) The remainder of the deposits (FA1 – FA6) are typified by the porous cryostructure, punctuated by micro-lenticular or layered ice. With the exception of ice layers, this region is ice poor. Permafrost in these deposits is epigenetic, indicating that permafrost aggradation post-dated deposition.

The occurrence of both epigenetic and syngenetic permafrost permits the classification of these deposits as polygenetic, concerning permafrost.



**Figure 6.4** Lenticular cryostructures at ca. 2.5 m depth (**Figure 6.3- Le**). a) Unaltered photo of the core. b) Transformed photo showing ice (black; shard-like morphology) and sediment (white). Roots and other organic material appear black as well but are distinguishable based on morphology.

## CHAPTER 7 DISCUSSION

Fjord is a genetic term used to describe a marine estuary which has been excavated by grounded glacier ice (Syvitski and Shaw 1995). The Adventfjord-valley system is the product of glacier and interglacial cycles during the Quaternary period (Mangerud et al. 1998). The large-scale geomorphology reflects the advance and retreat of ice and changes in relative sea level during this period. Due to high degrees of positive accommodation, fjords serve as efficient sediment traps. High sedimentation rates are associated with isostatic uplift and glacier activity in hinterland regions. These factors contribute to a suite of depositional processes, occurring in unstable environments recently exposed by deglaciation.

This chapter has been subdivided into three sections. Section one presents the interpretation of the facies associations introduced in Chapter Five. A general discussion of select elements of core sedimentology follows in section two. Specifically, section two considers the correlation of glacial and glaciomarine facies with other investigations in Isfjorden, the origin of oversized clasts, and methods of deciphering depositional processes from grain size parameters. Lastly, section three contains a discussion of the geocryological results introduced in Chapter Six.

### 7.1. Facies associations

#### FA1 – Glacial facies association

FA1 is composed of two component facies (facies 1 and 2; **Table 5.1**). Facies 1 is a consolidated, very-poorly sorted, structureless, matrix supported diamicton with clast supported portions. Grains  $< -1 \phi$  are almost exclusively angular. On the basis of high clast content, over-consolidation, location in the core, and the erosive transition to underlying bedrock, Facies 1 is interpreted to be a basal till (Benn and Evans 2010).

Facies 2 is a structureless, matrix supported diamicton, overlying facies 1. The boundary between these two facies was not recovered. In comparison to facies 1, facies 2 is less compact and characterized by a lower concentration of smaller oversized clasts. Given characteristics such as diamict texture, clast abundance, and stratigraphic position, Facies 2 is likely an ice-proximal glaciomarine deposit. The precise interpretation is less certain and two possibilities are proposed.

The first, and preferred, explanation is that these deposits originated from the rain-out of iceberg rafted debris and suspended fine grained sediments. Resultant deposits are typically massive, matrix supported diamictons with dropstones (Ó Cofaigh et al. 1999). Alternatively, Facies 2 may have been deposited by subaqueous glacigenic debris flows. However, this

hypothesis would be supported by an erosive lower contact to Facies 1 (Ó Cofaigh et al. 1999). This determination is not possible as the lower transition to facies 1 was not recovered. Additionally, evidence of crude bedding and the presence of rip-up clasts commonly characterize cohesive, glacial debris flow deposits (Ó Cofaigh et al. 1999). Such features were not observed in Facies 2.

A glacial origin for FA1 is supported by the inability to resolve OSL dates from these deposits. Sediments originating at the base of, or within glacial ice are unlikely to have been exposed to ultraviolet light. Further, the significant water depth, turbidity, and high sedimentation rate during deglaciation excludes the possibility that deposits were exposed to light following deposition (Puthusserry et al. 2006). Together, these two facies form the glacial facies association, FA1, and are interpreted to reflect conditions during and immediately following glaciation.

#### **FA2 – Glacimarine facies association**

FA2 consists of seven component facies (F3-F9; **Table 5.1**). This facies association is characterized by the presence of calcareous macrofossils (bivalve and gastropod shells) and abundant outsized clasts. A sharp, conformable transition is observed between FA2 and the underlying diamicton of FA1. At the bottom of FA2, Facies 3 consists of horizontally laminated coarse and fine silt. Sediments contain dropstones, associated with coarse lamina, and drape underlying deposits. Interlaminations vary in grain size and thickness. Both grain size and the thickness of individual lamina decrease towards the top of this facies. Bioturbation is largely absent with the exception of a few isolated horizontal burrows (*planolites*) near the top of the facies. The thickness of individual lamina, grain size, and clast abundance decreases upwards as this facies fines into Facies 4. On the basis of clast content, stratification, and low bioturbation Facies 3 is interpreted as an ice-proximal glaciomarine deposit (Ó Cofaigh and Dowdeswell 2001).

Facies 3 was deposited during deglaciation as an ice front retreated eastwards in Avenfjorden. Sediment was supplied from suspension settling of buoyant plumes emanating from glacial meltwater conduits. Lamination reflects cyclical sedimentation, possibly the product of fluctuations in meltwater discharge or tidal control of turbid plumes (Cowan and Powell 1990; Cowan et al. 1999). The vertical variation in particle size and lamina thickness records a transition from an ice-proximal to distal setting. The term *cyclopel* has previously been introduced by Mackiewicz et al. (1984) to describe laminated silt lithofacies produced by deposition from turbid plumes in glaciomarine environments. Outsized clasts, interpreted

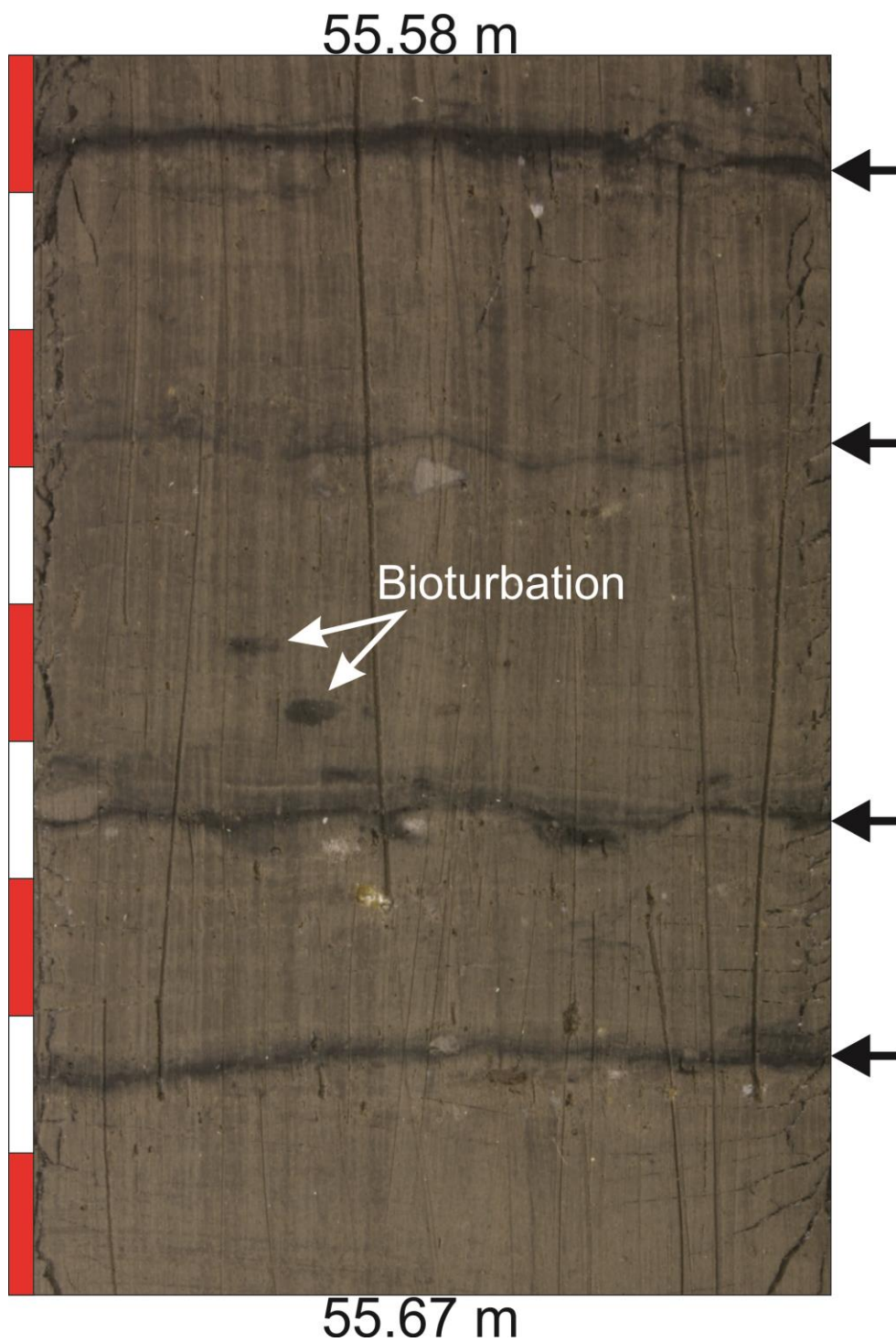


to be ice rafted-debris (IRD; either by icebergs or sea ice), are distributed throughout Facies 3. IRD appears to occur in greatest abundance in association with coarser laminae. This may reflect higher calving rates during period of meltwater discharge or the mobility of ice floes following spring breakup (Ó Cofaigh and Dowdeswell 2001).

Black mud laminae (up to 2 mm thick) occur in the upper portion of facies 3 (**Figure 7.1**). Similar laminae have been observed in Kongsfjorden and are suggested to occur annually (Elverhøi et al. 1980). The black, monosulphidic layers, identified by Elverhøi et al. (1980), were attributed to the high production rates of organic matter during the spring, while Kongsfjorden was still covered by sea ice. Cowan et al. (1999) note, in order to produce such distinct layers, plankton blooms must contribute organic material to the basin floor prior to the onset of the melt season in order for deposits to remain undiluted by siliciclastic sediment. In Alaskan fjords, similar black mud laminae have been used to define the early-spring period (Cowan et al. 1999).

Sedimentation rates were likely high during the deposition of Facies 3 as evidenced by the relative absence of bioturbation. Despite the lack of dating results for this interval, the presence of annual layers permits the estimation of sediment accumulation rates. Without accounting for the effects of sediment compaction, the four annual varves identified in **Figure 7.1** suggest that the sedimentation rate during this short interval was ca. 2 cm yr<sup>-1</sup>. This is slightly lower than contemporary rates from ice-proximal environments in Svalbard marine settings where values upwards of ca. 10 cm yr<sup>-1</sup> have been reported (Elverhøi et al. 1980; Ó Cofaigh and Dowdeswell 2001). With increasing distance from the glacier front, sedimentation rates decline and Facies 3 grades into the homogenous, bioturbated deposits of facies 4.

Facies 4 is comprised of massive, bioturbated dark silts with outsized clasts (IRD). Fragments of gastropod and bivalve shells are present. Fresh surfaces are black in colour but change to grey with prolonged exposure to air. Facies 4 displays the highest degree of bioturbation and hosts the most diverse suite of trace fossils in the core. On the basis of bioturbation intensity, trace fossil characteristics, and the presence of IRD and marine macrofossils, this facies is interpreted as having been deposited in a glaciomarine environment (Ó Cofaigh and Dowdeswell 2001; Forwick and Vorren 2009). Fine-grained sediments were principally supplied by fallout from hypopycnal suspension plumes (Syvitski and Shaw 1995).



**Figure 7.1** Image of four black mud laminae (monosulphidic layers?; marked by the black arrows) from Facies 3. Patches of monosulphide are due to bioturbation. The vertical scale bar in centimeters. Depths denote location in the core.

The remainder of FA2 consists of fine-grained sediments accumulated from suspension fallout (Facies 6) and sand-rich deposits (Facies 7 and Facies 8). The deposits of Facies 7 and 8 are attributed to slumping and reworking by turbidity currents on side-wall slopes. Sediment input may have additionally originated from the side-entry valley, Endalen. However, the precise origin of these deposits is unknown. Facies 7 represents single turbidites separated by fine-grained deposits of Facies 4 or 6. A turbidite interpretation is supported by scoured bases characterized by water-escape structures and absence of bioturbation (Reading 1996). The deposits of Facies 7 are generally weakly laminated and normally graded. Facies 8 records amalgamated deposits formed by low-density turbidites. Individual turbidites are occasionally separated by thin beds of silt, attributed to suspension fallout from hypopycnal plumes.

The deposits of FA2 display large variations with respect to mean grain size and sorting parameters (**Figure 7.2**). This is attributed to two main factors. First, the component facies of FA2 represent a spectrum of depositional processes ranging from suspension settling to turbidity currents. Each process varies in the way in which individual grains are entrained and deposited so distinct populations with respect to statistical parameters should be expected (McLaren and Bowels 1985). Second, ice rafting is known to occur in this environment as evidenced by the presence of IRD and gravel-rich beds. Changes in the concentration of ice-rafted sediment delivered to this environment may have implications for sorting and mean grain size. Indeed, with the exception of Facies 3, sorting appears to increase towards the top of FA2 (**Figure 5.3**). This may reflect a reduction in ice rafting during this interval.

Dating results indicate that FA2 was deposited during the early Holocene (prior to ca. 6.8 kya). This coincides with a period of rapidly declining RSL during glacio-isostatic uplift (Lønne and Nemec 2004). Emergence during a decline in base level increased the accessibility of glaciogenic and marine sediments to reworking by fluvial and slope processes (Ballantyne 2002b). In addition, the presence of temperate glaciers in Adventdalen cirques during the early Holocene likely resulted in enhanced glacial sediment input (Lønne and Nemec 2004). It is suggested that the amalgamated turbidites of Facies 8 reflect slope instabilities and side-entry input following base level decline. The reduced extent of cirque glaciers and ameliorated RSL decline moving into the middle Holocene permitted the reestablishment of quiescent conditions conducive to the development of Facies 4 and 6.

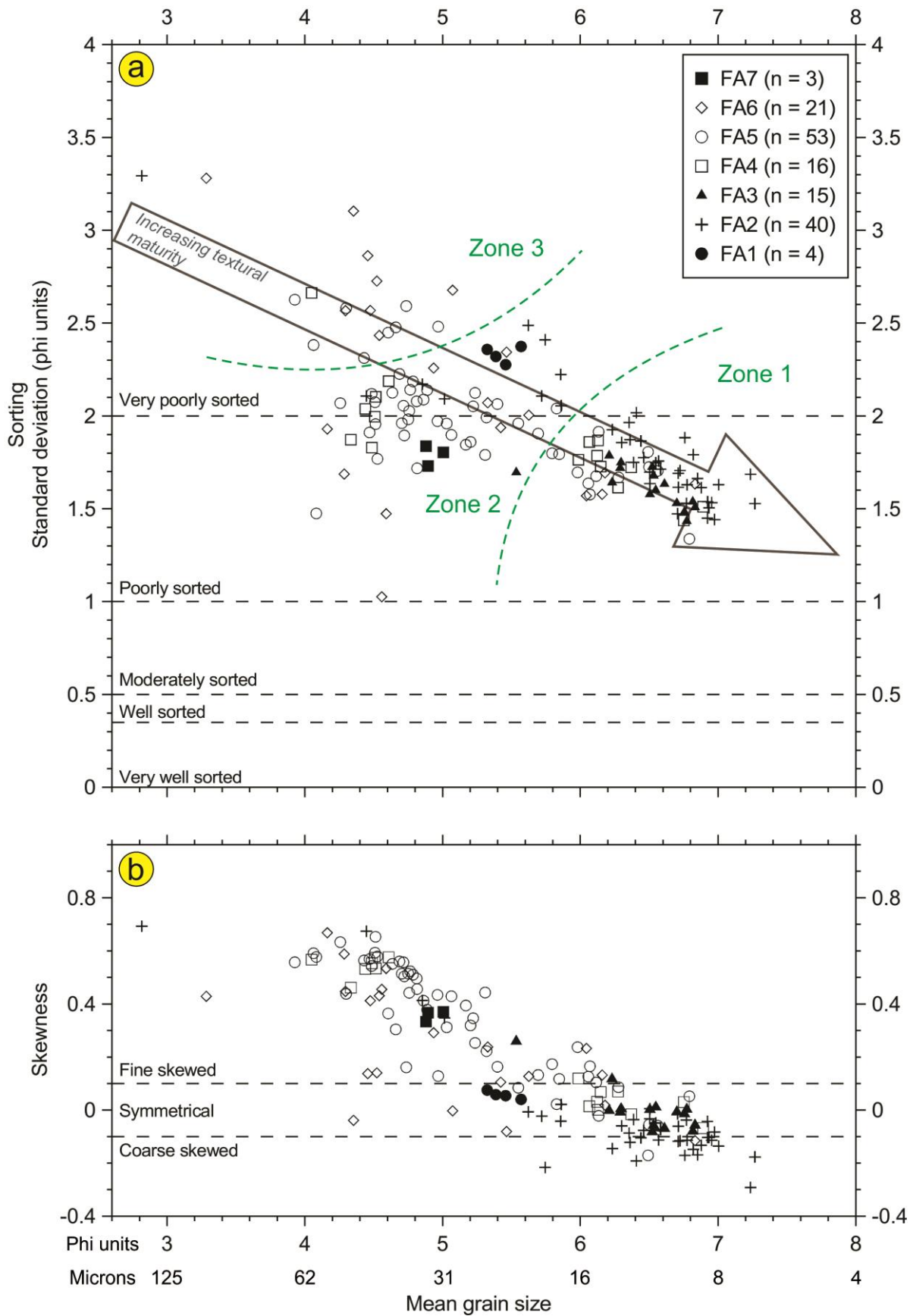
### **FA3 – Prodelta facies association**

FA3 consists of laminated or bedded sand and silt (Facies 10 and 11) and bioturbated silt (Facies 12). This facies association occurs above FA2 and is interpreted to record the transition to a prodeltaic depositional environment. The sediments of the component facies were deposited from dilute hyperpycnal plumes and suspension settling from hypopycnal plumes (**Table 5.1**). Outsized clasts are scattered throughout FA3 and attributed to ice-rafting processes (Forwick and Vorren 2009). Dating results indicate that this environment characterized the study site between 6.8 kya and 6.1 kya.

The absence of shell material, sporadic distribution of trace fossils, and variable bioturbation intensity indicates fluctuating environmental conditions during the deposition of FA3. Deposition from hyperpycnal plumes may relate to periods of elevated fluvial discharge, resuspension of sediments at the sea floor by wave or tidal processes, or slope failure on the distal delta front (Bhattacharya and MacEachern 2009). During these events, high sedimentation rates and reduced salinity stressed benthic faunal communities resulting in a decrease in biogenic structures (Syvitski et al. 1989). Fine-grained, bioturbated deposits likely originated from suspension. This may have been accentuated during winter periods when the river is not active or by sea-ice cover.

Sediments within FA3 are primarily fine grained, poorly sorted, and symmetrical with respect to skewness (**Figure 7.2**). Despite being poorly sorted, as defined by Folk and Ward (1957), these deposits display among the highest degree of sorting in the core. Folk (1966) notes strongly skewed samples are typically associated with zones of environmental mixing. The symmetry of these deposits and limited variation with respect to sorting and mean grain size suggests a limited number of depositional processes in this environment. Based on the component facies of FA3, suspension settling, punctuated by dilute turbidity currents are believed to be the primary depositional agents in the prodelta environment.

This interpretation is supported by observations from the contemporary environment. At ca. 60 m water depth (the prodelta environment), Zajączkowski and Włodarska-Kowalczyk (2007) record low velocity currents associated with increased suspended sediment concentrations. These are interpreted to be distal expressions of turbidity currents originating on the delta front (Zajączkowski and Włodarska-Kowalczyk 2007). Additionally, grain size distributions at 60 m depth are similar to those determined for FA3. Zajączkowski and Włodarska-Kowalczyk (2007) report symmetrically skewed and poorly sorted silts with a



**Figure 7.2** Bivariate plots displaying the relationship between (a) mean grain size and sorting and (b) mean and skewness for sediment samples. Zonation discussed in text.

maximum sand content of 20%. As in the contemporary environment, the prodeltaic sediments of FA3 indicate low energy conditions with a limited amount of transport by bottom currents (Zajączkowski and Włodarska-Kowalczyk 2007).

#### **FA4 – Delta-front transition facies association**

FA4 is composed of six component facies (F13 – F18; **Table 5.1**) and is interpreted to be a transitional facies association between prodelta and delta front environments. Bioturbation is generally low (BI 0-3) and sporadically distributed. Sediments in FA4 are significantly coarser than in FA3 (**Figure 5.3**). Deposits principally reflect two depositional processes: sediment fall out from suspension plumes and turbidity currents. Suspension deposits and turbidites are reflected by the two distinct grain size populations observed in **Figure 7.2**. Fine-grained suspension deposits cluster with samples from FA2 and FA3 within zone 1 while sand-rich turbidites generally group within zone 2 of **Figure 7.2a**.

The steep slopes and rapid progradation of the Adventelva delta resulted in instabilities and the development of submarine slides and slumps (Prior et al. 1981; McCann and Kostaschuk 1987). Slope failures result in the generation of turbidity currents and debris flows. Turbidity currents are an effective mechanism to transport sandy deltaic deposits into the basin and have been used to explain depositional patterns in Norwegian and western Canadian fjords (Holtedahl 1965; McCann and Kostaschuk 1987). Additionally, hyperpycnal plumes may result from density differences between the estuarine basin water and sediment-laden fluvial input during periods of river activity (Felix et al. 2006). The presence of turbidites in FA4 is evidence by the massive to normally graded deposits of F14, F15, and F17 which are separated by a sharp or erosive boundary from underlying deposits. Such boundaries are commonly characterized by soft-sediment deformation structures indicating high sedimentation rates (James and Dalrymple 2010).

In contrast, silt and fine-grained sand deposits of F13, F16, and F18 reflect calm conditions dominated by suspension settling. Low intensities of bioturbation (though the highest in this facies association) are associated with these deposits. Deposition likely occurred either away from active chutes on the delta front or during winter periods when Adventelva did not supply sediments to the delta. F18 contains weak lamination and evidence of soft sediment deformation signifying higher sedimentation rates (Reading 1996). A comparable succession has been observed in Holocene deltaic deposits from Eastern Greenland (Hansen 2004).

### **FA5 – Delta front facies association**

FA5 consists of four component facies (F19 – F22) and is interpreted to have been deposited during delta progradation between 4.6 kya and 6.1 kya (**Figure 5.5**). Deposits primarily result from river-derived hyperpycnal underflow, resedimentation by gravitational failure, and suspension settling (**Table 5.1**). Facies variations are attributed to changes in river discharge, migrating fluvial distributary channels, and slope instabilities along the sides of submarine chutes (Hansen 2004; Prior et al. 1981). Soft-sediment deformation commonly characterizes bedding boundaries. Such features include convolute lamination, dish structures, and ball-and-pillow structures. James and Dalrymple (2010) note soft-sediment deformation is characteristic of rapid sedimentation in delta front environments. Indeed, a high average sedimentation rate of  $19.3 \text{ m ka}^{-1}$  is reconstructed for this interval (**Figure 5.5**).

FA5 is characterized by minimal bioturbation (BI typically 0) and low trace fossil diversity. The combination of high sedimentation rates and brackish estuarine waters resulted in impoverished benthic macrofauna such that primary sedimentary structures have remained intact. Where present, trace fossils occur in association with dark, organic-rich layers. The distribution of bioturbation and trace fossils is likely controlled by the availability of benthic food, sedimentation rates, salinity, and possibly oxygen conditions (Bann and Fielding 2004). Vertically oriented trace fossils and *Fugichnia* are typically characteristic of environments with high or variable sedimentation rates (Bromley 1996). The presence of *Phycosiphon* may indicate periods of dysoxic conditions in the sediments (Rodríguez Tovar et al. 2014).

The amelioration of density differences between sea and river water in estuarine environments enhance the ability of a river to generate turbidity currents (Felix et al. 2006). Detrital clasts, containing terrestrial plant fragments, are abundant in layers with unidirectional ripples (F21). These observations suggest direct river input as hyperpycnal underflows (James and Dalrymple 2010). Grain size parameters for these deposits are similar to those of turbidity currents discussed in association with FA4; these deposits group within zone 2 of **Figure 7.2a**.

Massive sand beds (F20) were likely deposited from slumping in submarine chutes on the delta front (Reading 1996). Non-turbulent sediment gravity flows contribute to progradation in other Arctic, fjord head deltas (eg. Hansen 2004). Such chutes characterize the contemporary Adventelva delta front (Prior et al. 1981; Zajączkowski and Włodarska-Kowalczyk 2007) and similar features were presumably present during the progradational history of this system. The presence of slight age inversions, seen within the OSL dates of

**Figure 5.5**, support this interpretation as it suggests that reworking occurred following initial deposition on the delta slope (Krbetschek et al. 2002). Resultant deposits are very-poorly sorted and among the coarsest observed in the core, clustering within zone 3 of **Figure 7.2a**.

Facies 19 and Facies 22 reflect deposition by suspension settling from hyperpycnal plumes. These facies are heterolithic and contain abundant evidence of soft-sediment deformation. Flame, dish, and ball-and-pillow structures characterize bed boundaries, particularly in instances where sand overlays silt. These structures result from the formation of over-pressure in deltaic muds when buried by denser sands (James and Dalrymple 2010). Mud-couplets, present in Facies 22, were deposited by suspension settling and provide direct evidence of tidal forces (Reading 1996). Samples from these facies have similar grain size characteristics to the suspension deposits described in FA2 and FA3. As seen in **Figure 7.2a**, these deposits cluster within zone 1. Zajączkowski and Włodarska-Kowalczyk (2007) report alternating layers of coarse-silt and sand in the contemporary delta-front environment. Peaks of sand were interpreted to indicate turbidity flows. Samples from the modern delta front were further characterized as poorly to very-poorly sorted with fine to symmetrical skewness, similar to samples analyzed from FA5 in this study (**Figure 7.2b**).

Delta classifications are based on the dominant formation processes and consider three end members: river-, wave-, or tide-dominated (Galloway 1975; Reading 1996). The absence of wave-formed structures attests to the insignificance of wave processes in the protected fjord environment. On the basis of the facies present in the delta-front environment, it is suggested that the Adventelva delta be classified as a mixed-influence, river and tide dominated delta with tidal processes being of subordinate to fluvial inputs.

#### **FA6 – Delta-plain facies association**

FA6 is composed of four facies (F20, F23, F24, and FD; **Table 5.1**) which are interpreted to have been deposited within delta distributary channels and on interdistributary areas. This environment characterized the study site between 4.6 and 3.0 kya. The presence of disturbance material (Facies D) in these deposits limits the interpretation of depositional processes. Facies are generally characterized as heterolithic, indicating the influence of tidal forces in this environment. Tidal sedimentary structures include rhythmites (F23) and mud drapes on the leeward side of climbing ripples (F24; James and Dalrymple 2010). These deposits result from oscillations in current strength associated with ebb and flood cycles (Reineck and Wunderlich 1968). The grain size characteristics of samples from FA6 display a large



variation with respect to mean grain size and sorting, indicating a range of depositional environments (**Figure 7.2**).

The lower most deposits in FA6 consist of planar parallel laminated fine to medium sand with thin silt lamina. The relative coarseness of these deposits and presence of horizontal lamination indicates that this unit formed within the upper flow regime in a distributary channel (Reading 1996). The heterolithic nature of these deposits attests to the influence of tidal forces during deposition (James and Dalrymple 2010). This is overlain by F24 which consists of subhorizontally laminated, normally or inversely graded sand and silt deposits. Dip decreases towards the tops of individual occurrences and is occasionally capped by ripple lamination. F24 is interpreted to represent a progradational unit (either a distributary or point bar) occurring on the delta plain (Syvitski and Shaw 1995). Syvitski and Shaw (1995) report that energy decreases over these features resulting in a concomitant decrease in grain size (Syvitski and Shaw 1995). The proximal portions of distributary bars are characterized by the presence of an imbricated gravel lag which grades distally into ripples. This reflects the deceleration of river flow over the bar tops (Kostaschuk and McCann 1983; Syvitski and Shaw 1995). The stacking pattern of F24 may record the migration of distributary mouth bars during the progradation of the lower, intertidal delta plain (Syvitski and Farrow 1983). Climbing-ripple sets with mud drapes (F25) formed from rapid concurrent deposition from traction and suspension and indicate high sedimentation rates (Ashley et al. 1982). Climbing ripples are most frequently observed in fluvial or deltaic overbank areas. In FA6, these deposits likely formed in an interdistributary or levee environment (Tessier 1993).

#### **FA7 – Terrestrial facies association**

FA7 consists of two component facies (F26-F27). Both facies are characterized by the presence of segregated ice lenses and terrestrial plant material (**Table 5.1**). These factors contribute to the disruption of primary sedimentary structures. This is the only terrestrial sediments package observed in the core and is interpreted to represent the contemporary depositional environment. Deposits primarily consist of poorly-sorted, horizontally laminated, aeolian silts (Bryant 1982). Sand beds, present in F26, may have been deposited from sheet floods occurring in the distal portion of the alluvial fan situated at the mouth of Endalen (Reading 1996; Nichols and Fisher 2007). Alternatively, these sand deposits may have originated from the traction load of aeolian sediments (Kasse 2002).

Aeolian deposits are widespread on the alluvial terraces bordering contemporary Adventelva (Bryant 1982). These deposits contain abundant rootlets and plant material.

Bryant (1982) has investigated aeolian deposits in river exposures within 200 m of the drill location and reported a ca. 4 m thick package of horizontally laminated sandy silt, similar to Facies 27. Deformation of laminations is associated with the development of desiccation cracks. An aeolian origin was determined on the basis of field observations of active aeolian transport, deflation phenomena in the source areas, a distinct grain size distribution, and frosted surfaces with adhering fine particles on quartz grains (Bryant 1982).

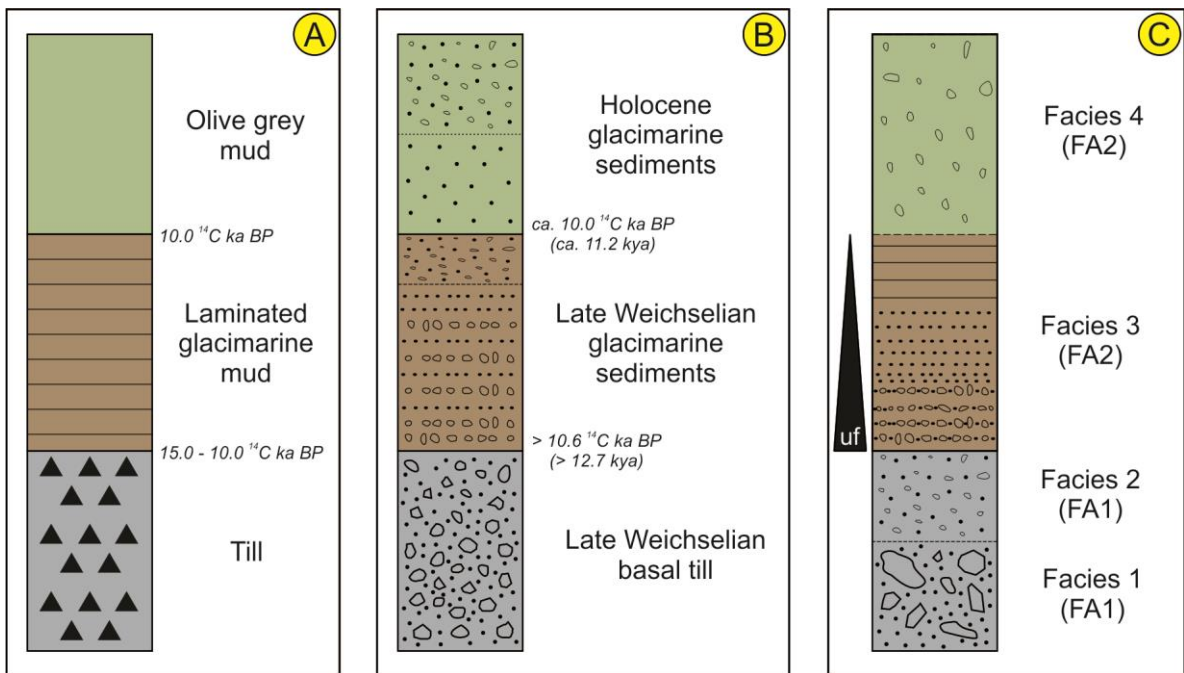
Horizontal lamination of aeolian sediments in periglacial environments has been attributed to several factors. Kasse (2002) suggest laminae result from variations in surface moisture. In this case, laminae form due to the adherence of grains to wet surfaces. Alternatively, lamination may form due to the reworking of aeolian sediments during spring melt (Pissart et al. 1978). Bryant (1982) concluded laminae in Adventdalen form as a result of vegetation and salt crust development at the ground surface. On the basis of lithology, location in the core, and proximity of the drill location to the sites investigated by Bryant (1982), FA7 is correlated with the aeolian deposits described in the river exposures along Adventelva.

## **7.2. General discussion**

### *7.2.1. Lithostratigraphic correlations*

Lithological data from investigations of Holocene marine sediments in central Isfjorden document three distinct sedimentary units (Elverhøi et al. 1995; Svendsen et al. 1992, 1996; Forwick and Vorren 2009, 2011). Overlying bedrock, a clast-rich diamicton is recognized as the lowermost Quaternary unit. This consolidated diamicton contains sub-angular clasts and is interpreted as till (Forwick and Vorren 2009). Extensive radiocarbon dating indicates these glacial sediments were deposited prior to 10 – 15 <sup>14</sup>C ka BP (**Figure 7.3a**; Elverhøi et al. 1995; Svendsen et al. 1996). Both Svendsen et al. (1996) and Forwick and Vorren (2009) further report the inclusion of shell fragments from the Kapp Ekholm interstadial, providing a maximum age for these deposits. Given these temporal constraints, this till is generally interpreted to have been deposited by an ice sheet during the late Weichselian glaciation (**Figure 7.3**). Marine seismic investigations indicate till occurs ubiquitously below post-glacial marine sediments in Isfjorden (Svendsen et al 1996; Forwick and Vorren 2011).

Laminated and bioturbated mud are subsequently recorded, overlaying Late Weichselian till (**Figure 7.3**; Elverhøi et al. 1995; Svendsen et al. 1996; Forwick and Vorren 2009). Laminated glaciomarine deposits are described as clast-bearing intercalated mud and sandy strata (Forwick and Vorren 2009), laminated pebbly mud (Elverhøi et al. 1995), or laminated



**Figure 7.3** Lithostratigraphic correlations with Isfjorden marine investigations. A) Stratigraphy modified after Elverhøi et al. (1995) and Svendsen et al. (1996). B) Lithostratigraphy for central Isfjorden based on Forwick and Vorren (2009). C) Lithostratigraphy from this investigation. Facies described in text. Dots indicate the presence of sand while unfilled shapes indicate gravel. Solid horizontal lines denote sharp boundaries. Dashed lines represent gradational boundaries. Figure after Forwick and Vorren (2009).

glaciomarine mud (Svendsen et al. 1996). These deposits generally fine upwards with a corresponding reduction in sandy strata. Dating of these intervals constrains deposition to between 12.7 kya and 11.2 kya (Forwick and Vorren 2009). Overlying laminated deposits, the upper most sedimentary unit in all marine sediment cores from Isfjorden consists of intensely bioturbated, olive-grey mud (Elverhøi et al. 1995; Svendsen et al. 1996; Forwick and Vorren 2009). Deposits contain drop stones and shell material. Dark mottles appear on fresh surfaces and are attributed to staining by monosulfides (Elverhøi et al. 1995; Svendsen et al. 1996). Dates from this interval indicate ages younger than 11.2 kya (Forwick and Vorren 2009).

The component facies of FA1 are the only primary glacial sediments recovered in the core under study. These deposits provide direct evidence of warm-based glacial overriding in the Adventdalen Valley. On the basis of stratigraphic position, lithology, and the apparently ubiquitous distribution of till under post-glacial marine sediments in the Isfjorden area, FA1 is correlated with till deposits recorded by Elverhøi et al. (1995), Svendsen et al. (1992, 1996), and Forwick and Vorren (2009, 2011). This implies FA1 was likely deposited during the late Weichselian glaciation. As the study area was inundated by erosive, fast-flowing ice streams during the LGM (Ingólfsson and Landvik 2013), sediments from earlier periods are believed to have been removed from Adventdalen (Elverhøi et al. 1995). Based on lithology and stratigraphic position the following correlations are made (**Figure 7.3**): Facies 3 and the interbedded ice proximal deposits, and the lowermost occurrence of Facies 4 with the homogenous, bioturbated marine muds. The inclusion of these correlations completes the chronostratigraphy of the cored interval by providing correlational evidence for the ages of deposits undated in this investigation.

#### 7.2.2. *Ice-rafted debris (IRD)*

Fluvial, aeolian, colluvial, littoral, and glacial sediments all serve as potential sources for IRD in the study area. The mechanisms for the incorporation of sediments into icebergs or floes are divided into active and passive processes (Gilbert 1990). Active processes refer to the freezing of sediments on to ice such as may occur in littoral or glacial settings. The grain size characteristics of sediments incorporated by active processes typically reflects the source deposits as little or no sorting occurs during incorporation. Conversely, passive ice rafting describes instances in which ice acts as the distributary agent for sediments deposited onto an existing ice surface (Gilbert 1990). In Adventdalen, aeolian, fluvial, littoral, and slope processes likely contribute debris to sea ice when present. Though kelp rafting of drop stones

is known to occur in Spitsbergen fjords (Alexanderson et al. 2010), no vegetation remnants were found attached to outsized clasts in this investigation.

Individual outsized clasts as well as beds of gravel (Facies 5), present throughout the core, are interpreted to be IRD. The presence of IRD in these sediments records the continuous activity of icebergs or floes during deposition in the Early Holocene. This may support the results of Forwick and Vorren (2009) who report evidence of the uninterrupted presence of tidewater glaciers in the Isfjorden area during the Holocene. This is in contrast to the conclusions of Svendsen and Mangerud (1997) who found no evidence for tidewater glacier activity during the early and middle Holocene in inner-Isfjorden (Billefjorden). However, the distinction between iceberg-rafted and sea-ice rafted debris is not made in this investigation and it remains possible that IRD reflects the activity of sea ice rather than icebergs. Conclusions in this regard are therefore limited.

Differentiation between iceberg-rafted and sea-ice rafted debris typically relies on the analysis of grain size parameters and particle characteristics (Gilbert 1990). Grain size may be used to infer the type of transport. Gilbert (1990) note large particles (i.e. boulders) are more likely to be derived from glacier ice. Sorting parameters may also provide insight as iceberg rafted debris is more likely to be poorly sorted given its glacial origin (Gilbert 1990). Forwick and Vorren (2009) have distinguished between IRD sources in Holocene sediments in Isfjorden on the basis of grain shape. In this instance, high concentrations of angular grains were interpreted to represent iceberg rafting (Forwick and Vorren 2009). This is permitted by the notion that deposits originating from littoral or fluvial settings are rounded by the processes occurring in these respective environments. Therefore, sediments dropped or dumped from sea ice are anticipated to contain fewer angular grains (Forwick and Vorren 2009). However, as noted by Gilbert (1990), the pervasiveness of frost weathering processes and short transport distances, characteristic of fjords and arctic environments, make such determinations difficult. Similarly, the presence of striated clasts likely indicates a glacial origin although the absence of striations does not preclude iceberg rafting (Gilbert 1990).

Spitsbergen exhibits strong provincialization with respect to bedrock characteristics (Dallmann 1999). Gilbert (1990) note, sea ice is likely to deposit sediments closer to the point of origin as rafts are smaller, melt quickly, and are easily disrupted by wind and waves. Therefore the presence of clasts derived from foreign bedrock provinces may signify ice rafting. This is problematic as transport of reworked glacial sediments onto sea ice may also yield the same result. Though the distinction between iceberg and sea-ice rafted debris does

not have any direct implications for the present investigation, the differentiation may contribute to the understanding of Holocene glacial conditions in the region of study.

### 7.2.3. Grain size distributions

#### **Comparison of textural parameters**

Progressive changes in grain size distributions along transport pathways have been recognized in many environments and applied to infer the transport history of sedimentary deposits (McLaren 1981; McLaren and Bowels 1985). Le Roux and Rojas (2007) note grain size trends are a natural result of sediment transport processes and relate to the influence of selective sorting and abrasion. Due to these factors, grain size generally decreases along the transport pathway. In order to interpret the transport and depositional history of the deposits under study, the relationships between statistical parameters is considered. This includes mean grain size vs. standard deviation (**Figure 7.2a**) and mean grain size vs. skewness (**Figure 7.2b**).

The mean grain size of the 152 sediment samples analyzed in this investigation varies between  $2.9\phi$  and  $7.2\phi$  (**Figure 7.2**). Mean grain size depends on the calibre of available sediments and the energy of the transport agent (Glaister and Nelson 1975). Sorting values of these samples differs between poorly sorted and very-poorly sorted. Deposits with a mean grain size of less than  $6\phi$  are generally better sorted than those coarser than  $6\phi$  (**Figure 7.2a**). Sorting is a function of source material, the nature of the sedimentary process, and the persistence of energy conditions conducive to transport (Glaister and Nelson 1975). Skewness ranges between coarse skewed and fine skewed (**Figure 7.2b**). Most samples are characterized by some degree of skewness. Folk (1966) notes that strongly skewed samples are often associated with zones of environmental mixing.

The bivariate plots presented in **Figure 7.2** illustrate two main points. First, the significant amount of overlap and scatter limits reliable identification of facies associations from a single sample. Second, results cluster with respect to depositional processes. Three zones are identified in **Figure 7.2a**. Zone 1 principally contains deposits which have originated from suspension fall out. These sediments are fine-grained and better sorted than remaining samples reflecting the influence of selective sorting and abrasion along the transport pathway (Glaister and Nelson 1974; Le Roux and Rojas 2007). With the exception of FA1 and FA7, all facies associations contain deposits of this nature. In the glaciomarine (FA2) and deltaic (FA3-FA5) facies associations, samples within zone 2 primarily reflect turbidity current activity. This is supported by sedimentological observations described above in connection

with each facies association. Given the heterolithic nature of FA6, the occurrence of samples within this interval may indicate a mixture of tidal suspension and bedload deposits (Reading 1996). Zone 3 consists of very poorly sorted, coarse deposits. In general, these samples are believed to have originated from slumps within tidal channels (FA6) or submarine chutes (FA4 and FA5; Prior et al. 1981).

Skewness shares a strong positive correlation with mean grain size (**Figure 7.2b**) and generally increases towards the top of the core (**Figure 5.3**). The increase in skewness observed from FA2 to FA3 may be attributed to a dilution of the IRD signal. With increasing proximity to the delta front, IRD deposits become progressively diluted as fluvial derived sediments increase in dominance. FA4, FA5, and FA6 typically display positive skewness indicating the presence of a fine-grained tail (**Figure 7.2b**). This may be due to flocculation of fine grained particles deposited in a marine environment or, in some instances, due to the difficulties associated with sampling heterolithic sediments (Syvitski and Shaw 1995). However, McLaren and Bowels (1985) note, when sediments are eroded, the probability of the entrainment of an individual grain shares a negative correlation with grain size. This results in sediments in transport which are finer and more negatively skewed than the source area. Sediments remaining in the source area thereby become coarser and more positively skewed (McLaren and Bowles 1985). If sediments present within the temporally adjacent members of FA4, FA5, and FA6 are interpreted to represent the source for sediments in FA2 and FA3, then this process may provide satisfactory explanation for the observed trends in the symmetry parameter without considering external sediment sources (eg. IRD) or chemical processes (eg. flocculation).

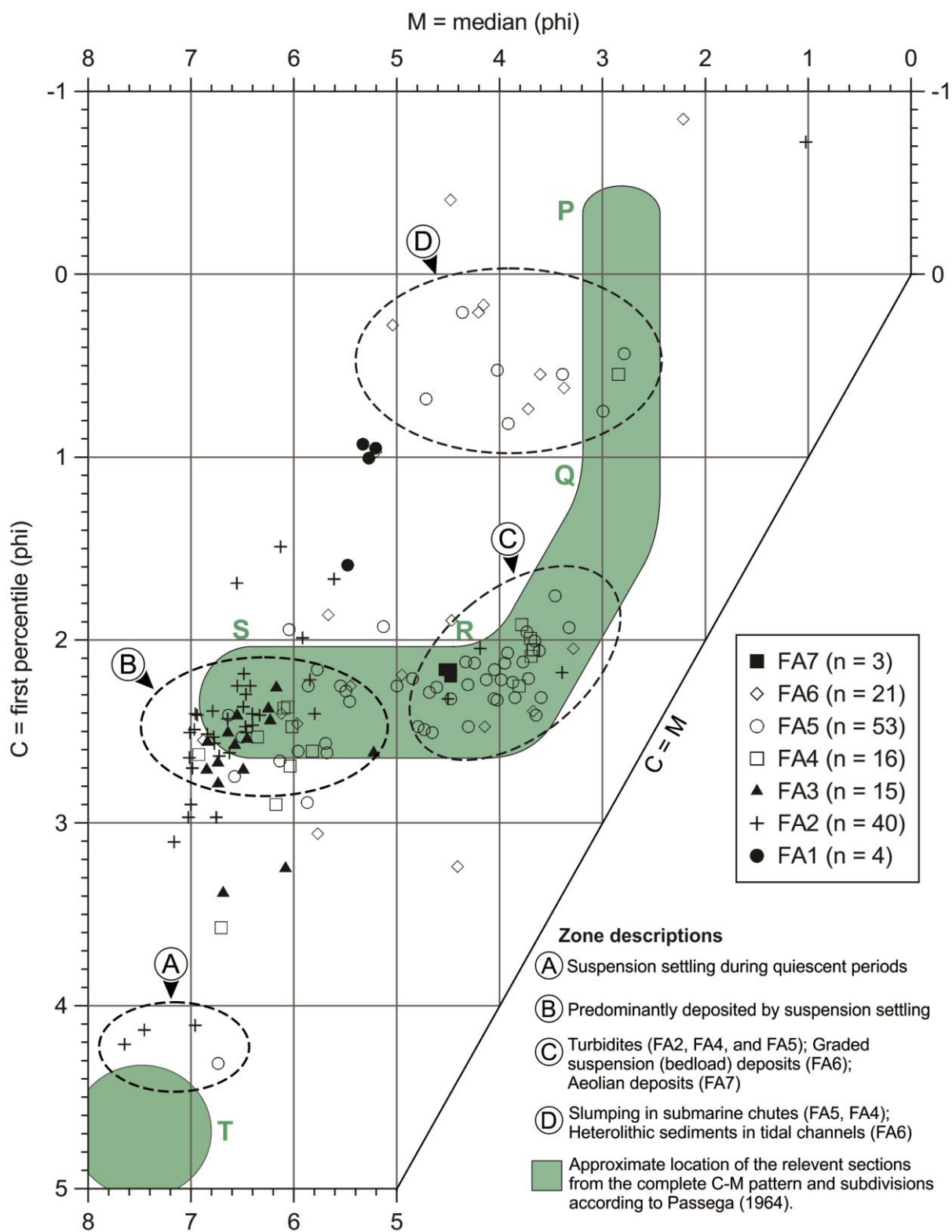
#### **Application of the C-M diagram**

The C-M diagram was first proposed by Passega (1957, 1964) to infer depositional processes from grain size characteristics. C refers to the value of the first percentile<sup>3</sup> and is representative of the maximum competency of the transporting medium (Passega 1957; Mycielska-Dowgiałło and Ludwikowska-Kędzia 2011). M is the median grain size of the distribution. Passega and Byramjee (1969) note C and M closely relate to transport and depositional mechanisms, permitting the evaluation of the hydraulic conditions under which sediments were deposited.

A C-M diagram, constructed for the deposits under study, is presented in **Figure 7.4**. Four

---

<sup>3</sup> C is the grain size at which 1% of the distribution is coarser (Passega 1957).



**Figure 7.4** C-M diagram (after Passega 1957, 1964) generated for the samples investigated in this study.



zones (A-D) are identified and interpreted to represent unique suites of transport processes. Zone A (**Figure 7.4**) encompasses deposits derived from suspension settling in calm conditions (Passega and Byramjee 1969). The characteristics of the sediments in region A are slightly coarser than Passega's (1964) 'T' classification which is reserved for deposits derived from pelagic sedimentation (Passega and Byramjee 1969). Deposits present within Zone B in **Figure 7.4** have principally resulted from suspension settling from hypopycnal plumes (Passega 1964). Zone B corresponds with the RS (uniform suspension) interval of the complete C-M pattern (**Figure 7.4**; Passega 1957). Zone C of **Figure 7.4** represents graded suspension deposits (Passega 1964). In the glaciomarine and deltaic facies associations (FA2, FA4, and FA5) these deposits are most likely turbidites (Passega and Byramjee 1969). This is supported by observed sedimentary structures. In these facies associations, erosive boundaries, load casts, and cross-bedding are common. Aeolian deposits (FA7) are also present within this interval. This may suggest that these sediments formed primarily from the deposition of saltating grains. The distribution of Zone C corresponds to the QR interval of the complete C-M diagram (Passega 1957). Passega and Byramjee (1969) note this pattern is characteristic of turbidites.

Deposits within Zone D (**Figure 7.4**) form a pattern similar to slump deposits, described by Passega (1957) in submarine canyons off the coast of California. Submarine chutes are known to characterize the contemporary delta front environment in Adventfjorden (Prior et al. 1981). It is suggested that samples within Zone D from FA4 and FA5 reflect slump deposits formed along the walls of these chutes during progradation. Zone D corresponds, approximately, to the PQ interval of the complete C-M pattern (Passega and Byramjee 1969). The pattern of the samples taken from FA6 is similar to bedload samples from the Mississippi River (Passega 1957). For this reason it is proposed that FA6 samples in this zone may represent bedload deposits in tidal or fluvial channels on the delta plain. Low M values are likely attributable to the addition of fine-grained suspension deposits by tidal processes.

As observed in **Figure 7.4**, many samples lay outside of four identified zones. Samples between Zone A and Zone B are likely derived from suspension settling under an intermediate energy regimes. The presence of IRD has probably resulted in the over-estimation of C for many samples. This is particularly true in FA2 and FA3 where gravel-sized ice-rafted clasts are abundant. Additionally, the exclusion of grains  $> -1\phi$  leads to the under-estimation of C where such grains were present. The degree to which these factors have influenced the C-M pattern of the cored deposit has not been considered here but would likely strengthen resultant conclusions. Nevertheless, the clear distribution and groupings of

results and the close relationship to the complete C-M pattern presented in **Figure 7.4** permit the identification of the dominant sedimentary processes during the progradation of the Adventelva delta.

Analysis of grain-size parameters (bivariate plots - **Figure 7.2**; C-M diagram – **Figure 7.4**) strengthens the identification of the main transport and depositional processes determined from sedimentological observations. The deposits of the lowermost aquatic facies associations (FA2 and FA3) are dominated by uniform fallout from hypopycnal suspension plumes. Turbidites, identified on the basis of sedimentary structures, are supported by the C-M pattern of FA2. The deltaic facies associations (FA4 and FA5) are composed of a combination of deposits derived from suspension settling, turbidity currents, and slumping in submarine chutes. The C-M image constructed for FA6 indicates elements of bedload deposits (rolling or saltating grains) as well as those derived from suspension settling. The interpretation of FA1 and FA7 using the C-M diagram is problematic as most studies using this method focus on aquatic deposits. FA1, consisting of primary glacial deposits, expectedly lies outside of the complete C-M pattern identified by Passega (1964) as little to no sorting occurs in this depositional environment (Benn and Evans 2010). As mentioned above, the location of FA7 deposits within the graded suspension interval may suggest deposition of saltating aeolian grains (Passega and Byramjee 1969).

### **7.3. Permafrost in lower Adventdalen**

#### *7.3.1. Permafrost in saline sediments*

Frozen saline sedimentary deposits characterize large areas of Arctic coast lines subjected to antecedent marine incursion (Hivon and Segó 1993). Alternatively, continental ‘salinization’ of permafrost affected sediments occurs in evaporation dominated hydrological regimes, permitting the accumulation of sulphate and carbonate ions (Brouchkov 2002). Frozen saline deposits have significant geotechnical implications due to the presence of unfrozen water and significant freezing point depressions. Lenses of saline brines present in permafrost sediments are termed cryopegs (Streletskaia 1998). Though permafrost by definition, cryopegs remain unfrozen due to high concentrations of solutes in the pore water.

Though all cored intervals appeared frozen at the ambient laboratory temperature of -8 °C, ground temperatures at the study site are slightly warmer (ca. -5.5 °C to -3.5 °C). Additionally, fine grained marine and deltaic sediments have been compacted during the deposition of succeeding sedimentary units. Many fine grained samples remain indurated following thawing and drying. Determination of the occurrence of unfrozen water by

empirical evidence is therefore problematic. Cryopegs are believed to occur in the study area as other investigations, drilling through the Quaternary deposits at the CO<sub>2</sub> well park, have reported blowouts attributed to the presence of unfrozen, pressurized mud (Alvar Braathen, 2013, Personal Correspondence).

### 7.3.2. *Formation of ice layers in epigenetic permafrost*

Isolated layers of ice occur sporadically within epigenetic permafrost below ca. 26 m depth. These layers typically occur at bedding plains and range in thickness from 0.5 cm to 3 cm. Grain size analysis of samples bounding eleven ice layers indicates that, in all instances, sediments overlying the ice layers are coarser than the underlying deposits. Horizontal ice layers of this nature are not believed to have been previously described in permafrost literature. Sill ice, so termed as it resembles ingenious intrusions, is morphologically similar to the ice layers described in this investigation and also occurs along bedding plains (Mackay 1972). However, sill ice bodies are of significantly greater vertical extent, ranging up to 13 m in thickness. Sill ice originates from the upwards injection of ground water towards the lower limit of permafrost (French 2007). In most instances, deposits below such ice bodies are coarser than the overlying material (Mackay and Dallimore 1992). These observations likely indicate a different formative process to that which resulted in the ice layers observed in the Adventdalen deposits.

A tentative explanation for the formation of the ice layers identified in this investigation is presented here. During permafrost aggradation, as the freezing front descended from the ground surface, the volume expansion associated with the freezing of pore water in saturated sands resulted in expulsion of excess water away from the freezing front<sup>4</sup>. Hydraulic conductivity is likely greater in the coarser, overlying deposits than in those below ice layers (Brady and Weil 2008). In instances where a sand-rich bed is underlain by fine-grained deposits, expelled water accumulates above fine grained sediments due to a reduction in permeability. Where the rate of downward permafrost aggradation exceeds the hydraulic conductivity of the underlying sediment, an ice layer developed. Pore-water expulsion generally results in the uplift of the ground surface (Williams and Smith 1989; Mackay and Dallimore 1992). However, given the substantial thickness of the overlying sediments, it seems more likely that the formation of ice layers contributed to the compaction of unfrozen,

---

<sup>4</sup> Pore-water expulsion from freezing, saturated sands in permafrost environments is well known (Williams and Smith 1989; Mackay and Dallimore 1992). Mackay and Dallimore (1992:1243) note that the volume of pore water that can be expelled from freezing sand will be less than or equal to the 9% volume expansion of pore water upon freezing.

underlying sediments. This explanation suggests that ice layers develop synchronously with permafrost aggradation.

A pore-water expulsion hypothesis remains problematic as it is unknown why ice layers do not characterize all sand-silt bed transitions. As noted above, marine deposits are commonly characterized by the presence of unfrozen water due to high solute concentrations (Streletskaia 1998). Indeed, ice layers may result from unfrozen water migration in saline sediments following permafrost development. A comparison of the oxygen and hydrogen isotopic ratios of the ice layers with the surrounding pore ice may provide an indication of a common or dissimilar water source (Mackay and Dallimore 1992).

### *7.3.3. Timing and nature of permafrost aggradation*

The aggradation of permafrost in lower Adventdalen coincides with the transition from FA6 to FA7 ca. 3.0 kya. This conclusion is supported by four independent approaches, two of which are the product of this investigation. Evidence includes: (1) the transition from subaquatic to terrestrial sedimentation documented in the core under study; (2) the restriction of aggradational ice to the upper 2.9 m in these deposits; (3) Holocene climate reconstructions indicating that early Holocene temperatures were likely not conducive to the development of continuous permafrost at sea level (Humlum et al. 2003); and (4) studies investigating the ages of diagnostic permafrost landforms (Svensson 1971; Yoshikawa and Nakamura 1996; Jeppesen 2001; Budantseva et al. 2012).

#### *Argument 1: Implausibility of submarine permafrost aggradation*

Generally, permafrost does not form at the sea bed (Williams and Smith 1989). Observations of subsea permafrost in the circum-Arctic region are primarily associated with regions that were exposed subaerially during the LGM (Rachold et al. 2007). These areas were subsequently inundated during post-glacial sea level rise. Such permafrost bodies are considered relic in that they are not aggrading under prevailing environmental conditions.

Isostatic rebound following the late Weichselian glacial maximum on Svalbard has resulted in a general upheaving of the landscape and most Holocene relative sea level curves display an emergence pattern (Foreman et al. 2004; Ingólfsson and Landvik 2013). This generally precludes the possibility that permafrost may have formed subaerially at some point during the Holocene and then, subsequently, been submerged. Subsea permafrost is not known to exist in the Adventdalen area. Yoshikawa and Nakamura (1996) note seismic soundings and electrical resistivity investigations indicate the absence of permafrost in the near-shore environment around Adventfjord.

The sedimentary analysis of this core has reconstructed a transition from glacial (FA1) to subaquatic (FA2-FA6) to terrestrial sedimentation (FA7). With the exception of FA7, all facies associations were deposited in environments in which permafrost aggradation is improbable. The transition from FA6 to FA7 therefore records the shift to conditions favourable to permafrost development. This development occurred ca. 3.0 kya and is interpreted as the earliest possible timing of permafrost aggradation at the study site.

*Argument 2: Presence and distribution of aggradational ice*

Permafrost in these deposits is polygenetic. Below FA7 (2.9 m depth), ice-poor, epigenetic permafrost extends to the base of the core. Syngenetic permafrost characterizes interval between 2.9 m and the base of the active layer (ca. 1 m depth). In this investigation it was determined that lenticular cryostructures with dense ice lenses were the most reliable diagnostic feature of syngenetic permafrost. Rhythmically organized, lenticular cryostructures appear to be a universal characteristic of syngenetic permafrost in fine-grained deposits (Shur et al. 2004; French and Shur 2010). The lenticular cryostructure is only present in FA7 and is interpreted as aggradational ice. As mentioned previously, the presence of this ice-rich zone is attributed to the incorporation of ice lenses previously present at the base of the active layer into permafrost (Mackay 1972). Aeolian sedimentation has resulted in surface aggradation. Assuming a relatively consistent active-layer thickness during the past 3 kya, as the ground surface increased in elevation, the top of permafrost rose upwards at a rate proportional to that of sediment accumulation. The restriction of syngenetic permafrost to this interval supports the hypothesis of permafrost aggradation following the transition from FA6 to FA7.

*Argument 3: Holocene climate variations*

Climate during the early Holocene (prior to ca. 5 kya) was warmer than present. Warmer conditions are reflected in changes in lacustrine pollen assemblages (Birks 1991), the presence of thermophilous molluscs in marine deposits (Salvigsen et al. 1992), and reduction in glacier ice evidenced in IRD concentrations (Svendsen and Mangerud 1997). Humlum (2005: 121) indicates, during this period, mean annual air temperatures at sea level ranges between 0 °C and -3 °C. As a result, permafrost at sea level was likely absent or discontinuous, during the early Holocene.

*Argument 4: Ages of permafrost landforms*

Several investigations have been conducted in the Adventdalen region to determine the age of ice wedges and pingos. These landforms are diagnostic of permafrost and do not occur in non-permafrost environments (French 2007). The Longyear Pingo is situated on the northern

flank of Adventdalen, opposite to the drill site for this investigation. Drift wood, present in the up-thrust marine sediments, has been dated to ca. 2.65 kya BP (Svensson 1971). Though this date provides only an indication of the timing of regression at this locale, it is further interpreted to represent a maximum age for the establishment of permafrost (Yoshikawa and Nakamura 1996).

Investigations of excavated ice wedges conducted have yielded similar ages. Radiocarbon dating of organic material incorporated into wedge ice produced ages of ca. 2.9 kya (Jeppesen 2001). This suggests ice wedges in lower Adventdalen are likely late Holocene features. These conclusions support the hypothesis that permafrost in lower Adventdalen aggraded no earlier than ca. 3.0 kya.

#### *7.3.4. Implications for permafrost aggradation in Spitsbergen valley deposits*

Permafrost in lower Adventdalen is a late Holocene phenomenon, linked to the subaerial exposure of the land surface during isostatic uplift and delta progradation. This conclusion indicates that permafrost below the upper marine limit in valleys throughout Svalbard is likely of Holocene age with the exact timing being closely associated with landscape emergence following marine regression.

## CHAPTER 8 SUMMARY AND CONCLUSIONS

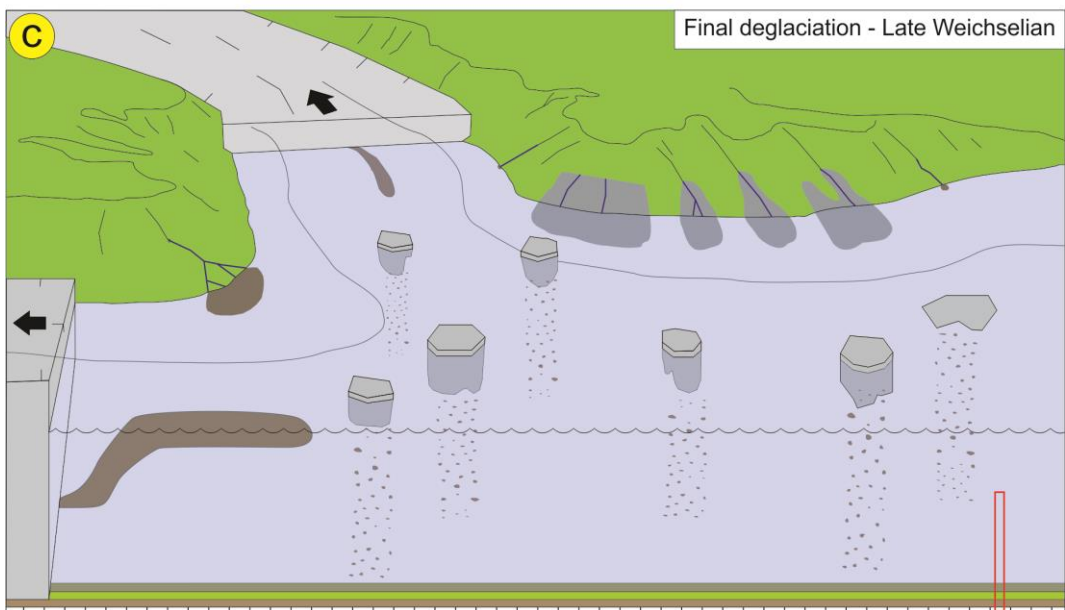
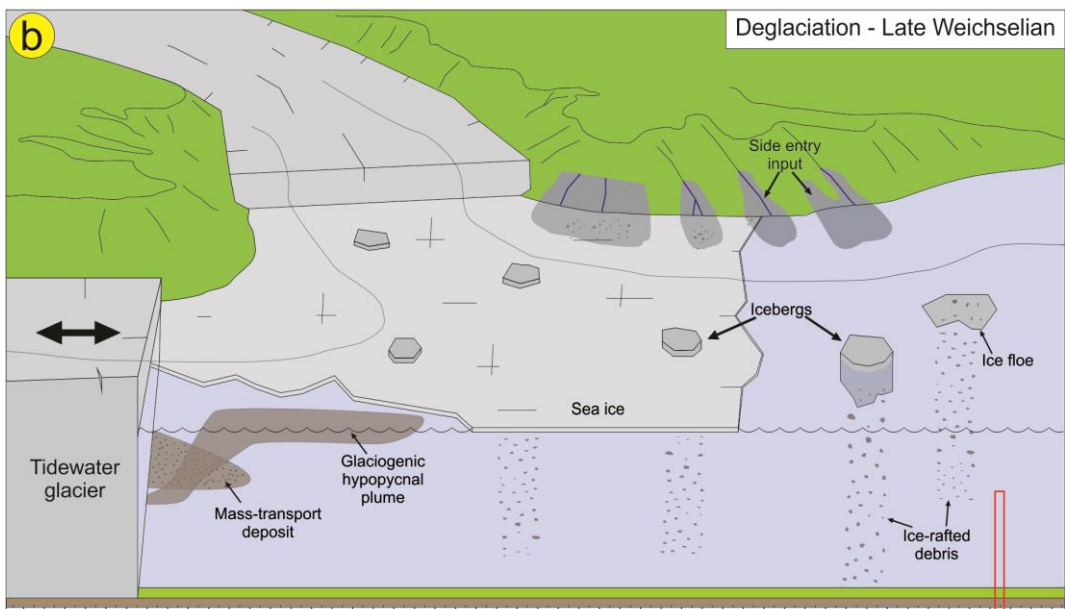
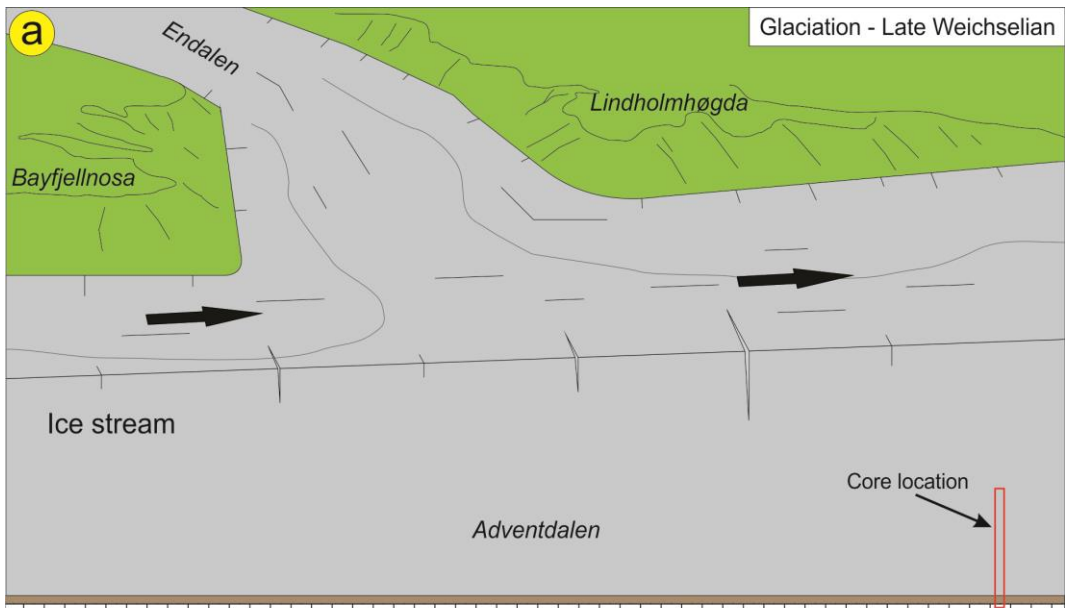
### 8.1. Summary: sedimentary and permafrost development of the Adventdalen Valley

This thesis has characterized the late Quaternary sediment of lower Adventdalen and examined the relationship between sedimentological processes and permafrost aggradation in the valley bottom. Data was gathered from a 60 m ice-bonded permafrost core taken from the UNIS CO<sub>2</sub> Project Well Park, five kilometers east of Longyearbyen. Results were used to determine the depositional and landscape development following the Late Weichselian glaciation and to establish the timing of permafrost aggradation at the study site. The principle findings of this investigation are summarized below in a four-stage landscape development model (**Figure 8.1**). The approximate distribution of these depositional environments in the simplified sedimentological log used throughout this thesis is illustrated in **Figure 8.2**. Given similar geomorphologies and landscape histories, this model is likely representative of the sedimentological and permafrost development of other side-entry fjord valleys along western Spitsbergen.

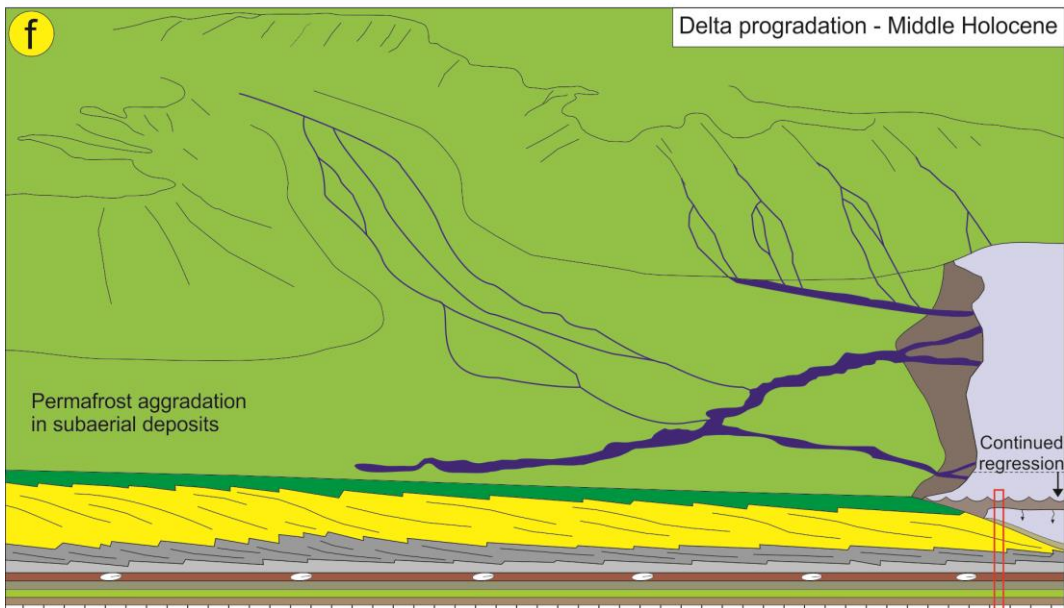
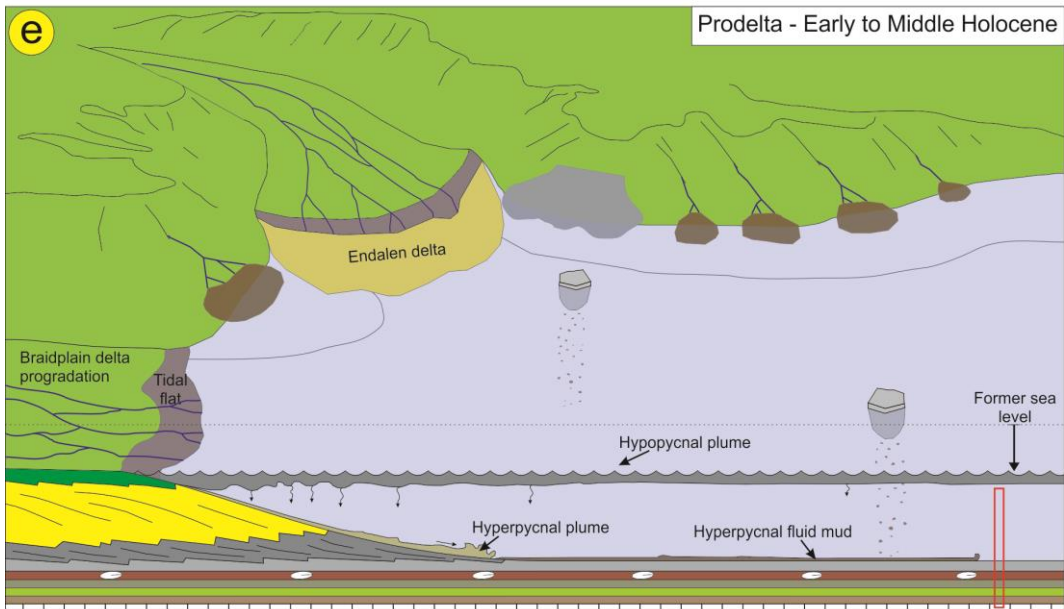
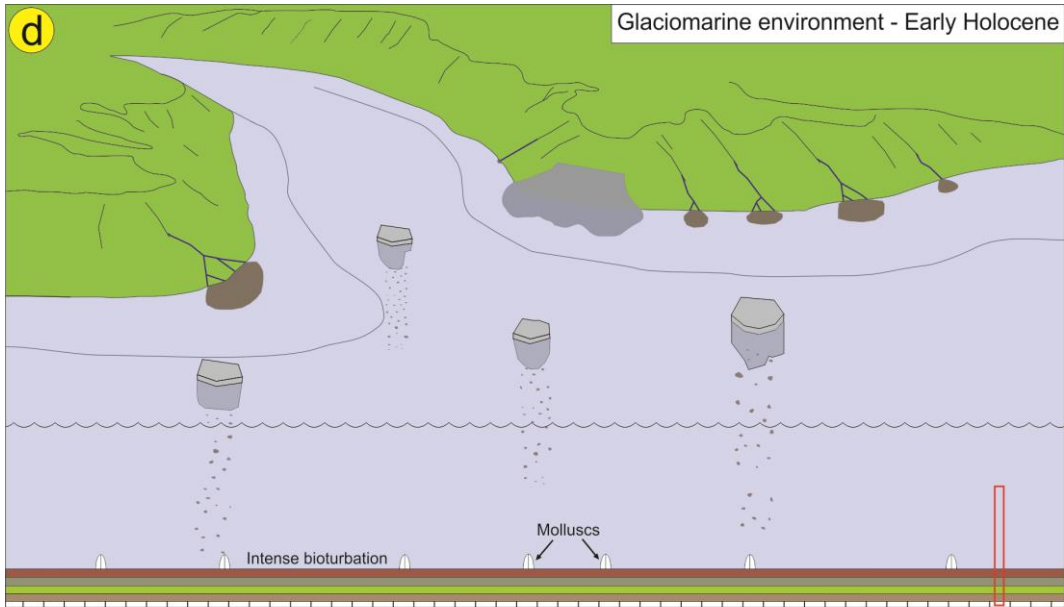
#### *Stage 1: Glaciation and deglaciation (late Weichselian)*

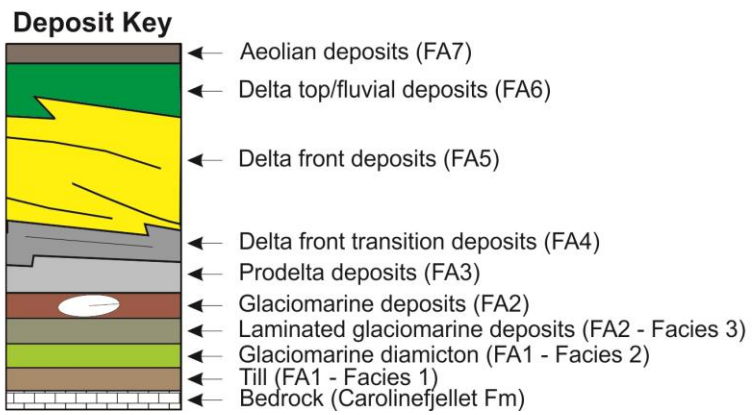
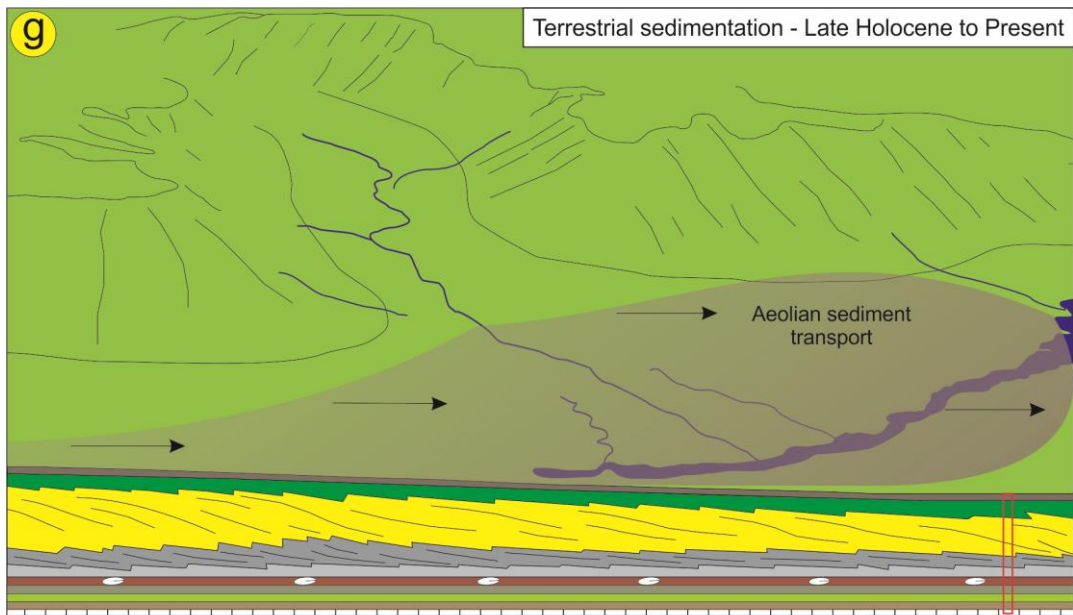
During the late Weichselian glaciation, a warm-based glacier, situated in Adventdalen, eroded and transported significant quantities of unconsolidated sediments towards the continental shelf edge (Elverhøi et al. 1995). If present, permafrost in the bottom of Adventdalen degraded due to frictional heat generated by basal sliding and trapping of geothermal heat (Humlum 2005). The glacier in Adventdalen served as a tributary to the Isfjorden ice stream, draining the Late Weichselian Svalbard-Barents Sea Ice Sheet (Forwick and Vorren 2009; Ingólfsson and Landvik 2013). This event is recorded by the presence of a basal till overlying bedrock (**Figure 8.1a**).

During deglaciation, glacial drainage systems transported sediment and meltwater to the ice margin, depositing heterogeneous glaciomarine deposits. In front of the glacier, high efflux of meltwater and sediment in combination with intense ice rafting resulted in the deposition of a massive, glaciomarine diamicton (**Figure 8.1b**). During the final stages of deglaciation, as the glacier retreated eastwards, laminated glaciomarine sediments record variations in the intensity of hypopycnal plumes emanating from glacial conduits. With increasing distance from the ice front, these laminated deposits fine and thin upwards into bioturbated glaciomarine muds (**Figure 8.1c**). Following deglaciation, fjords were rapidly inundated by the sea. The level of maximum transgression was between 70 m and 62 m above present sea level (Lønne and Nemec 2004) and is attributed to glacioisostatic depression of the lithosphere.

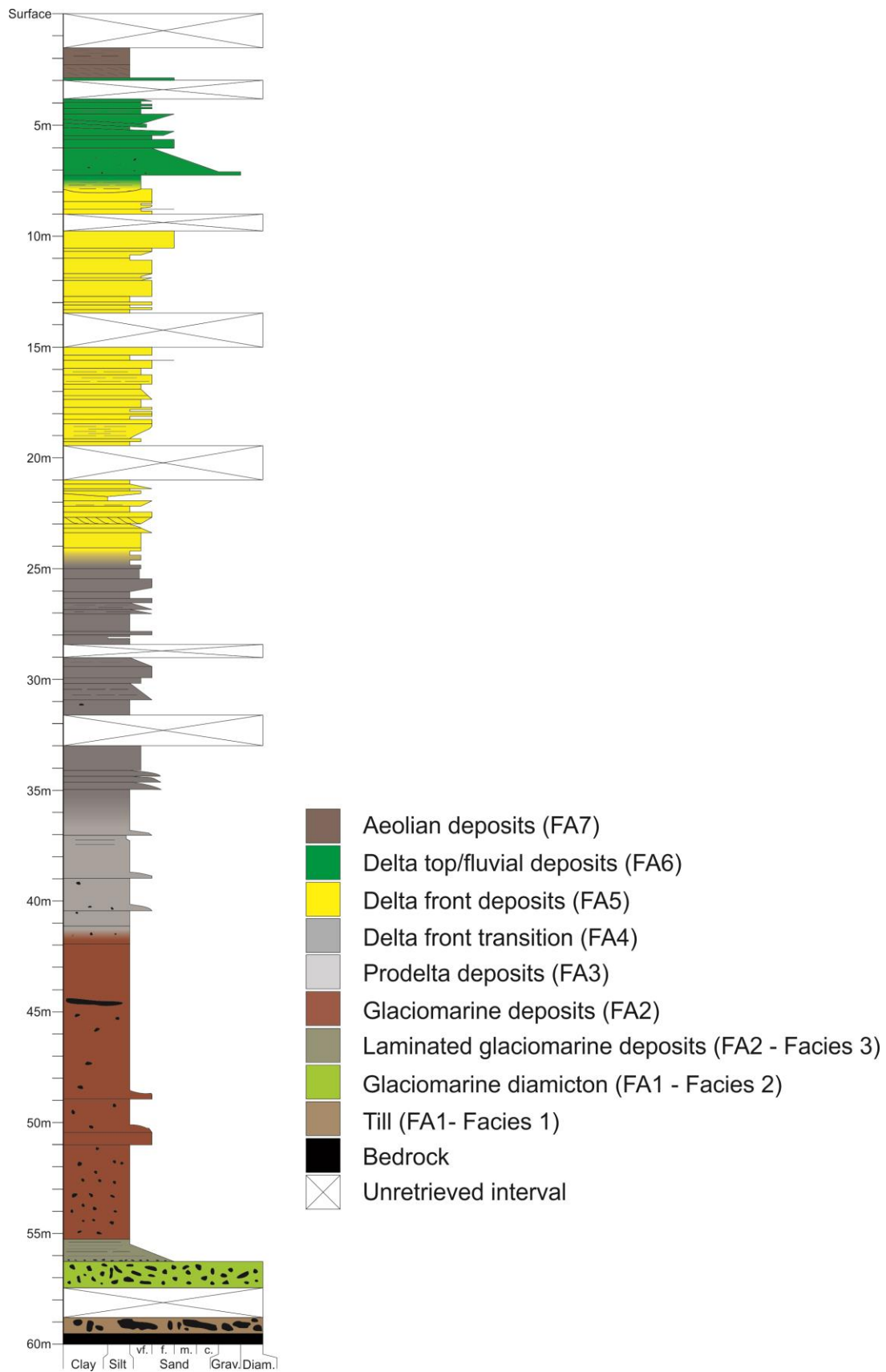








**Figure 8.1** Illustrations identifying the main sedimentary processes in Adventdalen from the late Weichselian to present. The distribution of these environments within a simplified sedimentary log is provided in **Figure 8.2**.



**Figure 8.2** Simplified sedimentary log used throughout this investigation with the approximate zonation of the depositional environments and facies associations from **Figure 8.1**.

*Stage 2: Glaciomarine environment (early Holocene)*

The deposition of glaciomarine sediments during the early Holocene coincides with a period of rapid RSL decline (Lønne and Nemeč 2004). Sediment was principally distributed to the basin by hyperpycnal plumes emanating from distant glaciers and/or fluvial sources. Deposits are punctuated by infrequent turbidites recording environmental instability during the early stages of paraglacial landscape response (Ballantyne 2002a). Sediment accumulation rates during this interval were low (ca. 3.1 m ka<sup>-1</sup>), permitting the establishment of an impoverished benthic faunal community. Bioturbation resulted in the homogenization of most deposits (**Figure 8.1d**). Evidence for continued ice rafting during this interval is provided by IRD distributed in these deposits. Sedimentation rates increased to 4.7 m ka<sup>-1</sup> towards the middle Holocene, reflecting the increasing proximity of the prograding Adventelva delta system.

*Stage 3: Progradation of the fjord-head delta (middle Holocene)*

Prodeltaic muds overlay the homogenous glaciomarine deposits beginning approximately 6.8 kya (**Figure 8.1e**). At this time, sea level in Adventfjord is estimated to be 10 m above present (Lønne and Nemeč 2004). Sedimentation rates increased during this interval to ca. 9.1 m ka<sup>-1</sup>. Deposits reflect the increasing importance of hyperpycnal underflows generated from gravitational instabilities on the distal delta front and fluvial generated undercurrents. A decrease in bioturbation documents the response of benthic fauna to stresses imparted by fluctuating sedimentation rates, turbidity, oxygen, and food availability.

From 6.1 kya to 4.6 kya, the delta front prograded past the study site (**Figure 8.1f**). During this interval, approximately 29 m of sediment was deposited at an average rate of 19 m ky<sup>-1</sup>. Delta progradation was rapid due to decreasing accommodation space and forced regression driven by isostatic sea-level changes. Sediment was supplied by glaciers in the hinterland and reworking by streams incised into abandoned fluvial and deltaic deposits. Overlaying deposits contain tidal signatures (rhythmites and mud drapes) and record prograding or meandering distributary channels or distributary bars active on the delta plain.

Warm boundary conditions in these subaquatic environments precluded the aggradation of permafrost. The earliest conceivable timing for the onset of permafrost development coincides with subaerial exposure following RSL decline or delta progradation.

*Stage 4: Aeolian sedimentation and permafrost aggradation (late Holocene – Recent)*

Preservation of the delta plain deposits is attributed to the emergence and abandonment associated with the gradual RSL decline during the middle Holocene. Active aeolian sedimentation occurs on surviving terrace segments which border Adventdalen (**Figure**

**8.1g).** These sediments probably originated from unvegetated fluvial bars in central Adventdalen (Bryant 1982).

Under prevailing climate conditions, this depositional regime favours the accumulation of segregated ground ice and syngenetic permafrost which forms concurrently with sedimentation. This cryostructures, interpreted to be aggradational ice, is in contrast to the characteristics of underlying permafrost. Below three meters depth, pore ice, infrequently punctuated by ice layers, indicates the post-depositional growth of permafrost. The timing of permafrost development is 3.0 kya and is supported by investigations of other characteristic permafrost landforms in the study area (Svensson 1971; Yoshikawa and Nakamura 1996).

## **8.2. Conclusions**

The following conclusions can be drawn from this examination of late Quaternary sediment and permafrost characteristics in Adventdalen:

- The successful application of the drilling technique utilized in this investigation is likely the most significant methodological outcome of this study. Though the logistical requirements and high operating costs associated with this method will preclude its widespread application, this study has demonstrated that retrieval of unlithified sediment cores from considerable depth is possible in permafrost areas. The success of this method is attributed to the presence of ground ice, which acts as a cement between individual grains.
- Late Quaternary sedimentary environments in Adventdalen were controlled by climate, relative sea level change, and sediment supply. The chronology of events contributing to the sedimentary and permafrost development of lower Adventdalen was determined from OSL and AMS  $^{14}\text{C}$  dating of cored deposits and correlation with the results of marine investigations in Isfjorden. The sedimentological development of the system that continues to fill Adventfjorden may be divided into four stages:

Stage 1: The late Weichselian glaciation and deglaciation which resulted in the deposition of till and glaciomarine sediments from a retreating ice sheet.

Stage 2: Glaciomarine environment during the early Holocene. During this interval, favorable marine conditions permitted the establishment of a diverse benthic faunal community.

Stage 3: Progradation of the fjord-head delta during the middle Holocene. Deltaic sedimentation was dominated by suspension settling from hypopycnal plumes, hyperpycnal underflows, and gravitational failures on the delta front. The intensity

of bioturbation decreases upwards in relation to coarsening and shallowing of these deposits.

Stage 4: Aeolian dominated sedimentary environment characterized by the deposition of wind-transported silts. This onset of these environmental conditions began 3.0 kya and coincides with permafrost aggradation in the valley bottom.

- Vertical changes in mean grain size, median, sorting, skewness, the first percentile, and lithology were used to identify grain size trends in the core. The results indicate that certain environments and processes are more easily distinguished than others. The range of depositional processes occurring in all subaquatic environments makes the determination of depositional environment problematic, on the basis of a single sample. However, results suggest that the identification of depositional agents is possible using grain size parameters.
- The complete description of frozen sediments requires the identification and classification of ice-related structures. Three main cryostructures are identified in the frozen sediments of Adventdalen, indicating the presence of both syngenetic and epigenetic permafrost. The establishment of conditions conducive to permafrost aggradation occurred during the Late Holocene, ca. 3.0 kya.

### **8.3. Research implications and directions for further investigations**

This is the first study to investigate the Holocene landscape and permafrost development of the sedimentary deposits in lower Adventdalen. Given the geomorphological similarities between Adventdalen and other large valleys in western and central Spitsbergen, the sedimentary and geocryological model presented in this investigation may be applicable to other areas. The results of this investigation have implications for infrastructure development in the Adventdalen area as well as future permafrost and sedimentological studies in Arctic environments.

Ground ice has implications for infrastructure development in permafrost terrain due to the effects of changes to the ground thermal regime on subsidence and slope stability. The presence of appreciable ground ice in the upper three meters of the Adventdalen deposits indicates that changes in the ground thermal regime, either as a result of climatic change or alteration to ground surface conditions, will result in subsidence. Observations made during this investigation suggest that the all retrieved deposits are ice-bonded under the thermal regime prevailing at the study site. Indeed, it is unlikely that retrieval of these deposits would have been possible without the presence of pore ice. Frozen deposits of this nature are likely

characterized by low permeability; a favorable trait for investigations interested in storing carbon dioxide below the ground surface.

High-Arctic Holocene deltas have received little attention due to the remoteness of study sites and difficulties in obtaining direct sedimentological observations. The observations presented in this thesis may have implications for the post-glacial development of valley-fjord systems in the circum-Arctic region. In particular few studies have investigated the characteristics and distributions of trace fossils in Arctic Holocene deltas. The results from this investigation may therefore be of interest in this regard.

Future investigations of these deposits may examine:

- 1) The vertical variations in density of the cored sediments. The outcome of this would prove valuable to near-surface seismic investigations seeking to accurately model and interpret the spatial variations of Quaternary deposits in Adventdalen.
- 2) The geochemical composition (salinity, pH, reduction potential) of the pore ice within the cored interval. This would hopefully provide an indication of the salinity during deposition as well as oxygen conditions.
- 3) Biostratigraphy (including macrofossils, pollen, and foraminifera) of these deposits. An investigation of this nature may complement existing palynological and foraminiferal studies in the Isfjorden area. Results may have bearing on the reconstruction of regional climatic and biotic conditions during the Holocene.
- 4) The manner in which sediment properties (eg. shear strength and unfrozen water content) change with temperature. This may provide an indication of the presence of cryopegs in the Adventdalen deposits. As laboratory investigations in this study were conducted at a temperature significantly lower than the natural ground temperature, a conclusion regarding the physical state of the sediments under prevailing thermal conditions is limited.

## LITERATURE

- Alexanderson H, Landvik JY, Ryen HT. 2010. Chronology and styles of glaciation in an inter-fjord setting, northwestern Svalbard. *Boreas* **10**: 10.1111.
- Ashley GM, Southard JB, Boothroyd JC. 1982. Deposition of climbing-ripple beds: a flume simulation. *Sedimentology* **29**: 67-79.
- Ballantyne CK. 2002a. A general model of paraglacial landscape response. *The Holocene* **12**: 371-376.
- Ballantyne CK. 2002b. Paraglacial geomorphology. *Quaternary Science Reviews* **21**: 1935-2017.
- Bann KL, Fielding CR. 2004. An integrated ichnological and sedimentological comparison of non-deltaic shorefaces and sub-aqueous delta deposits in Permian reservoir units of Australia. In *The Application of Ichnology to Palaeoenvironmental and Stratigraphic Analysis*. McIlroy D (ed). The Geological Society of London, Special Publication 228: 273-310.
- Beckman Coulter. 2011. *LS 13 320 Laser Diffraction Particle Size Analyzer: Instructions for use*. Beckman Coulter Inc: Brea, California. 246 p.
- Bhattacharya JP, MacEachern JA. 2009. Hyperpycnal rivers and prodeltaic shelves in the Cretaceous seaway of North America. *Journal of Sedimentary Research* **79**: 184-209.
- Benn DI, Evans DJA. 2010. *Glaciers & Glaciation*, Second Edition. Hodder education: Abingdon. 802 p.
- Birks HH. 1991. Holocene vegetational history and climatic change in west Spitsbergen – plant macrofossils from Skardtjørna, an Arctic lake. *The Holocene* **1**: 209-218.
- Björck S, Wohlfarth B. 2001.  $^{14}\text{C}$  chronostratigraphic techniques in paleolimnology. In *Tracking environmental change using lake sediments*. Last WM, Smol JP (eds). Klume Academic Press: Dordrecht; Vol. 1: 205-245.
- Blott SJ, Pye K. 2001. GRADISTAT: A grain size distribution and statistics package for the analysis of unconsolidated sediments. *Earth Surface Processes and Landforms* **26**: 1237-1248.
- Braathen A, Bælum K, Christiansen HH, Dahl T, Eiken O, Elvebakk H, Hansen F, Hanssen TH, Jochmann M, Johansen TA, Johnsen H, Larsen L, Lie T, Mertes J, Mørk A, Mørk MB, Nemec W, Olausson S, Oye V, Rød K, Titlestad GO, Tveranger J, Vagle K. 2012. The Longyearbyen CO<sub>2</sub> Lab of Svalbard, Norway – initial assessment of the geological conditions for CO<sub>2</sub> sequestration. *Norwegian Journal of Geology* **92**: 353-376.
- Brady NC, Weil RR. 2008. *The Nature and Properties of Soil*, 14<sup>th</sup> Edition. Prentice Hill: Upper Saddle River; New Jersey. 975 p.
- Bray MT, French HM, Shur Y. 2006. Further Cryostratigraphic Observations in the CRREL Permafrost Tunnel, Fox, Alaska. *Permafrost and Periglacial Processes* **17**: 233-243.
- Bromley RG. 1996. *Trace Fossils: Biology, taphonomy and applications*. Chapman & Hill; London. 361 p.
- Brouchkov A. 2002. Nature and Distribution of Frozen Saline Sediments on the Russian Arctic Coast. *Permafrost and Periglacial Processes* **13**: 53-90.



- Bryant ID. 1982. Loess deposits in lower Adventdalen, Spitsbergen. *Polar Research* **2**: 93-103.
- Bugantseva NA, Vasilchuk AC, Zemskova AM, Chizhova JN, Vasilchuk YK, Christiansen HH. 2012.  $\delta^{18}\text{O}$  Variations in Late Holocene Ice-Wedges and Winter Air Temperature Variability in the Yamal Peninsula, Russia, and in Adventdalen, Svalbard. In *Proceedings of the Tenth International Conference on Permafrost, 25-29 June 2012*. Melnikov VP (ed). The Northern Publisher: Salekhard; Vol. 2, 41-45.
- Burn CR. 1988. The development of near-surface ground ice during the Holocene at sites near Mayo, Yukon Territory, Canada. *Journal of Quaternary Science* **3**: 31-38.
- Burn CR, Kokelj SV. 2009. The environment and permafrost of the Mackenzie Delta Area. *Permafrost and Periglacial Processes* **20**: 83-105.
- Burn CR, Zhang Y. 2009. Permafrost and climate change at Herschel Island (Quikiqtaruq), Yukon Territory, Canada. *Journal of Geophysical Research* **114**: F02001.
- Cheng G. 1983. The mechanism of repeated-segregation for the formation of layered ground ice. *Cold Regions Science and Technology* **8**: 57-66.
- Christiansen HH. 2005. Thermal regime of ice-wedge cracking in Adventdalen, Svalbard. *Permafrost and Periglacial Processes* **16**: 87-98.
- Cowan EA, Powell RD. 1990. Suspended sediment transport and deposition in cyclically interlaminated sediment in a temperate glacial fjord, Alaska, USA. In *Glacimarine Environments: Processes and Sediments*. Dowdeswell JA, Scourse JD (eds.) Geol. Soc. London Spec. Publ.; 53: 75-89.
- Cowan EA, Seramur KC, Cai J, Powell RD. 1999. Cyclic sedimentation produced by fluctuations in meltwater discharge, tides and marine productivity in an Alaskan fjord. *Sedimentology* **46**: 1109-1126.
- Dallmann WK (ed). 1999. *Lithostratigraphic lexicon of Svalbard: Upper Palaeozoic to Quaternary bedrock; Review and recommendations for nomenclature use*. Norsk Polarinstitutt, Tromsø. 318p.
- Dallmann WK, Kjærnet T, Nøttvedt A. 2001. Geological map of Svalbard 1:100 000. Sheet C9G Advendalen. Explanatory text. *Norsk Polarinstitutt Temakart* **31/32**: 4-55.
- Elverhøi A, Liestøl O, Nagy J. 1980. Glacial erosion, sedimentation and microfauna in the inner part of Kongsfjorden, Spitsbergen. *Norsk Polarinstitutt Skrifter* **172**: 33-61.
- Elverhøi A, Svendsen JI, Solheim A, Andersen ES, Milliman J, Mangerud J, Hooke RL. 1995. Late Quaternary Sediment Yield from the High Arctic Svalbard Area. *Journal of Geology* **103**: 1-17.
- Eckerstorfer M, Christiansen HH. 2011. The “High Arctic Maritime Snow Climate” in Central Svalbard. *Arctic, Antarctic, and Alpine Research* **43**: 11-21.
- Fairbanks RG. 1989. A 17,000-year glacio-eustatic sea level record: influence of glacial melting rates on the Younger Dryas event and deep-ocean circulation. *Nature* **342**: 637-642.
- Felix M, Peakall J, McCaffrey WD. 2006. Relative importance of processes that govern the generation of hyperpycnal flows. *Journal of Sedimentary Research* **76**: 382-387.
- Folk RL, Ward WC. 1957. Brazos River bar: a study in the significance of grain size parameters. *Journal of Sedimentary Petrology* **27**: 3-26.

- Folk RL. 1966. A review of grain-size parameters. *Sedimentology* **6**: 73-93.
- Forman SL, Lubinski DJ, Ingólfsson Ó, Zeeberg JJ, Snyder JA, Siegert MJ, Matishov GG. 2004. A review of postglacial emergence on Svalbard, Franz Josef Land, and Novaya Zemlya, northern Eurasia. *Quaternary Science Reviews* **23**: 1391-1434.
- Forman SL. 1989. Late Weichselian glaciation and deglaciation of the Forlandsundet area, western Spitsbergen, Svalbard. *Boreas* **18**: 51-60.
- Forman SL. 1990. Post-glacial relative sea-level history of northwestern Spitsbergen, Svalbard. *Geological Society of America Bulletin* **102**: 1580-1590.
- Forwick M, Vorren TO. 2009. Late Weichselian and Holocene sedimentary environments and ice rafting in Isfjorden, Spitsbergen. *Palaeogeography, Palaeoclimatology, Palaeoecology* **280**: 258-274.
- Forwick M, Vorren TO. 2011. Stratigraphy and deglaciation of the Isfjorden area, Spitsbergen. *Norwegian Journal of Geology* **90**: 163-179.
- Fox D. 2011. Observations of massive ground ice, Herschel Island, Yukon Territory. MSc Thesis. Department of Geography, McGill University. 111p.
- French HM, Harry DG. 1990. Observations on buried glacier ice and massive segregated ice, Western Arctic Coast, Canada. *Permafrost and Periglacial Processes* **1**: 31-43.
- French HM. 2007. *The Periglacial Environment*, Third Edition. John Wiley & Sons Ltd; Chichester, England. 456 p.
- French HM, Shur Y. 2010. The principles of cryostratigraphy. *Earth-Science Reviews* **10**: 190-206.
- Friedman GM, Sanders JE. 1978. *Principles of Sedimentology*. Wiley, New York.
- Førland EJ, Hanssen-Bauer I, Nordli PØ. 1997. Climate statistics and longterm series of temperature and precipitation at Svalbard and Jan Mayen. *Report Series of the Norwegian Meteorological Institute* **21/97**.
- Førland EJ, Benestad R, Hanssen-Bauer I, Haugen JE, Skaugen TE. 2011. Temperature and Precipitation Development at Svalbard 1900-2100. *Advances in Meteorology*: 893790.
- Galloway WE. 1975. Process Framework for Describing the Morphologic and Stratigraphic Evolution of Deltaic Depositional Systems. In *Deltas - Models for Exploration*. Broussard ML (ed). Houston Geological Society: Houston: 87-98.
- García-García F, Corbí H, Soria JM, Viseras C. 2011. Architecture analysis of a river flood-dominated delta during an overall sea-level rise (early Pliocene, SE Spain). *Sedimentary Geology* **237**: 102-113.
- Gilbert R. 1990. Rafting in glacialmarine environments. In *Glacialmarine environments: processes and sediments*. Dowdeswell JA, Scourse JD (eds). Geological Society Special Publication No. 53: 105-120.
- Glaister RP, Nelson HW. 1974. Grain-size distributions, an aid in facies identification. *Bulletin of Canadian Petroleum Geology* **22**: 203-240.
- Harris C, Kern-Luetsch M, Christiansen HH, Smith F. 2011. The Role of Interannual Climate Variability in Controlling Solifluction Processes, Endalen, Svalbard. *Permafrost and Periglacial Processes* **22**: 239-253.

- Hald M, Ebbesen H, Forwick M, Godtliebsen F, Khomenko L, Korsun S, Olsen LR, Vorren TO. 2004. Holocene paleoceanography and glacial history of the West Spitsbergen area, Euro-Arctic Margin. *Quaternary Science Reviews* **23**: 2075-2088.
- Hansen L. 2004. Deltaic infill of a deglaciated arctic fjord, East Greenland: sedimentary facies and sequence stratigraphy. *Journal of Sedimentary Research* **74**: 422-437.
- Hanssen-Bauer I, Solås MK, Steffensen EL. 1990. The climate of Spitsbergen. *Report Series of the Norwegian Meteorological Institute* **39/90**.
- Hinkel KM, Nelson FE. 2003. Spatial and temporal patterns of active layer thickness at circumpolar active layer monitoring (CALM) sites in northern Alaska, 1995-2000. *Journal of Geophysical Research* **108 (D2)**: 8168.
- Hivon EG, Sego DC. 1993. Distribution of saline permafrost in the Northwest Territories, Canada. *Canadian Geotechnical Journal* **30**: 506-514.
- Holtedahl H. 1965. Recent turbidites in Hardangerfjord, Norway. In *Submarine Geology and Geophysics – Coulston Papers*. Whitter WP, Bradshaw R (eds). Butterworth; London: 107-141.
- Humlum O, Instanes A, Sollid JL. 2003. Permafrost in Svalbard: a review of research history, climatic background and engineering challenges. *Polar Research* **22**: 191-215.
- Humlum O. 2005. Holocene permafrost aggradation in Svalbard. In *Cryospheric systems: Glaciers and Permafrost*. Harris C, Murton JB (eds). Geological Society, London, Special Publications 242: 119-130.
- Humlum O, Christiansen HH, Juliussen H. 2007. Avalanche-derived rock glaciers in Svalbard. *Permafrost and Periglacial Processes* **18**: 75-88.
- Ingólfsson Ó, Landvik JY. 2013. The Svalbard-Barents Sea ice-sheet – Historical, current and future perspectives. *Quaternary Science Reviews* **64**: 33-60.
- Jaeger JM, Nittrouer CA. 1999. Sediment deposition in an Alaskan fjord: controls on the formation and preservation of sedimentary structures in an icy bay. *Journal of Sedimentary Research* **69**: 1011-1026.
- James NP, Dalrymple RW (eds). 2010. *Facies Models 4*. Geological Association of Canada; St. John's, Newfoundland. 586 p.
- Jeppesen JW. 2001. Palæoklimatiske indikatorer for central Spitsbergen, Svalbard. Eksemplificeret ved studier af iskiler og deres værtssedimenter. MSc thesis, University Center on Svalbard.
- Jillavenkatesa A, Dapkunas SJ, Lum L-SH. 2001. *NIST Recommended Practice Guide: Particle Size Characterization*. National Institute of Standards and Technology; Special publication 960-1; US Government Printing Office: Washington, DC. 165p.
- Johansen TA, Digranes P, van Schaack M, Lønne I. 2003. On seismic mapping and modeling of near-surface sediments in polar areas. *Geophysics* **68**: 1-8.
- Jull AJT. 2007. AMS Method. In *Encyclopedia of Quaternary Science*. Elias SA (ed). Elsevier: Amsterdam: 2911-2918.
- Kasse C. 2002. Sandy aeolian deposits and environments and their relation to climate during the Last Glacial Maximum and Lateglacial in northwest and central Europe. *Progress in Physical Geography* **26**: 507-532.

- Kelly RN, Kazanjian J. 2006. Commercial reference shape standards used in the study of particle shape effect on laser diffraction particle size analysis. *AAPS PharmSciTech* **7**: Article 42.
- Knaust D, Bromley RG. 2012. *Trace fossils as indicators of sedimentary environments*. Elsevier; Amsterdam. 960 p.
- Konert M, Vandenberghe J. 1997. Comparison of laser grain size analysis with pipette and sieve analysis: a solution for the underestimation of the clay fraction. *Sedimentology* **44**: 523-535.
- Kokelj SV, Burn CR. 2005. Geochemistry of the active layer and near-surface permafrost, Mackenzie delta region, Northwest Territories, Canada. *Canadian Journal of Earth Sciences* **42**: 37-48.
- Kostaschuk RA, McCann SB. 1983. Observations on delta-forming processes in a fjord-head delta, British Columbia, Canada. *Sedimentary Geology* **36**: 269-288.
- Kottek M, Grieser J, Beck C, Rudolf B, Rubel F. 2006. World map of the Koeppen-Geiger climate classification updated. *Meteorologische Zeitschrift* **15/3**: 259-263.
- Krbetschek MR, Gonser G, Schwamborn G. 2002. Luminescence Dating Results of Sediment Sequences of the Lena Delta. *Polarforschung* **70**: 83-88.
- Landvik JY, Bondevik S, Elverhøi A, Fjeldskaar W, Mangerud J, Salvigsen O, Siegert MJ, Svendsen JI, Vorren TO. 1998. The last glacial maximum of Svalbard and the Barents Sea area: Ice sheet extent and configuration. *Quaternary Science Reviews* **17**: 43-75.
- Landvik JY, Ingólfsson Ó, Meinert J, Lehman SJ, Solheim A, Elverhøi A, Ottesen D. 2005. Rethinking Late Weichselian ice-sheet dynamics in coastal NW Svalbard. *Boreas* **34**: 7-24.
- Le Roux JP, Rojas EM. 2007. Sediment transport patterns determined from grain size parameters: Overview and state of the art. *Sedimentary Geology* **202**: 473-488.
- Lønne I, Nemec W. 2004. High-arctic fan delta recording deglaciation and environment disequilibrium. *Sedimentology* **51**: 553-589.
- Lønne I. 2005. Faint traces of high Arctic glaciations: an early Holocene ice-front fluctuation in Bolterdalen, Svalbard. *Boreas* **34**: 308-323.
- Mackay JR. 1970. Disturbances to the tundra and forest tundra of the western Arctic. *Canadian Geotechnical Journal* **7**: 420-432.
- Mackay JR. 1972. The world of underground ice. *Annals of the Association of American Geographers* **62**: 1-22.
- Mackay JR, Dallimore SR. 1992. Massive ice of the Tuktoyaktuk area, western Arctic coast, Canada. *Canadian Journal of Earth Sciences* **29**: 1235-1249.
- MacEachern JA, Bann KL, Bhattacharya JP, Howell CD. 2005. Ichnology of deltas: organism responses to the dynamic interplay of rivers, waves, storms, and tides. In *River Deltas – Concepts, Models, and Examples*. Giosan L, Bhattacharya JP (eds). Society for Sedimentary Geology (SEPM) Special Publication 83; 49-85.
- Mackiewicz NE, Powell RD, Carlson PR, Molnia BF. 1984. Interlaminated ice-proximal glacial marine sediments in Muir Inlet, Alaska. *Marine Geology* **57**: 113-147.
- McCann SB, Kostaschuk RA. 1987. Fjord Sedimentation in Northern British Columbia. In *Glaciated Coasts*. Fitzgerald DM, Rosen PS (eds). Academic Press: London: 33-51.

- Major H, Haremo P, Dallmann WK, Andresen A. 2000. Geological map of Svalbard 1:100 000, sheet C9G Advendalen (revised after Major 1964). *Norsk Polarinstituttemakart* **31**.
- Mangerud J, Dokken T, Hebbeln D, Heggen B, Ingólfsson Ó, Landvik JY, Mejdahl V, Svendsen JI, Vorren TO. 1998. Fluctuations of the Svalbard-Barents Sea Ice Sheet during the last 150 000 years. *Quaternary Science Reviews* **17**: 11-42.
- McLaren P. 1981. An interpretation of trends in grain size measures. *Journal of Sedimentary Petrology* **51**: 611-624.
- McLaren P, Bowles D. 1985. The effects of sediment transport on grain-size distributions. *Journal of Sedimentary Petrology* **55**: 457-470.
- Morse PD, Burn CR, Kokelj SV. 2009. Near-surface ground-ice distribution, Kendal Island Bird Sanctuary, Western Arctic Coast, Canada. *Permafrost and Periglacial Processes* **20**: 155-171.
- Murton JB, French HM. 1994. Cryostructures in permafrost, Tuktoyaktuk coastlands, western arctic Canada. *Canadian Journal of Earth Sciences* **31**: 737-747.
- Mycielska-Dowgiałło E, Ludwikowska-Kędzia M. 2011. Alternative interpretations of grain-size data from Quaternary deposits. *Geologos* **17**: 189-203.
- Nagy J. 2005. Delta-influenced foraminiferal facies and sequence stratigraphy of Paleocene deposits in Spitsbergen. *Palaeogeography, Palaeoclimatology, Palaeoecology* **222**: 161-179.
- Nichols GJ, Fisher JA. 2007. Processes, facies and architecture of fluvial distributary system deposits. *Sedimentary Geology* **195**: 75-90.
- NORPERM (Norwegian Permafrost Database). 2014. Online ground temperature data from Svalbard. <http://www.tspnorway.com/> [accessed 10 February 2014]
- Norsk Polarinstituttt. 2013. Online map data. <http://toposvalbard.npolar.no/> [accessed 14 December 2013]
- Ó Cofaigh C, Lemmen DS, Evans DJA, Bednarski J. 1999. Glacial landform-sediment assemblages in the Canadian High Arctic and their implications for late Quaternary glaciation. *Annals of Glaciology* **28**: 195-201.
- Ó Cofaigh C, Dowdeswell JA. 2001. Laminated sediments in glacial marine environments: diagnostic criteria for their interpretation. *Quaternary Science Reviews* **20**: 1411-1436.
- Osterkamp TE. 2001. Sub-sea Permafrost. In *Encyclopedia of Ocean Sciences*. Steele JH, Thorpe SA, Turekian KK (eds). Academic Press: Waltham, Massachusetts: 2902-2912.
- Ottesen D, Dowdeswell JA, Rise L. 2005. Submarine landforms and the reconstruction of fast-flowing ice streams within a large Quaternary ice sheet: the 2500-km-long Norwegian-Svalbard margin (57°-80°N). *Geological Society of America Bulletin* **117**: 1033-1050.
- Passega R. 1957. Texture as characteristic of clastic deposition. *American Association of Petroleum Geologists Bulletin* **41**: 1952-1984.
- Passega R. 1964. Grain size representation by CM patterns as a geological tool. *Journal of Sedimentary Petrology* **34**: 830-847.
- Passega R, Byramjee R. 1969. Grain-size image of clastic deposits. *Sedimentology* **13**: 233-252.

- Pissart A, Vincent JS, Edlund SA. 1977. Dépôts et phénomènes éoliens sur l'île de Banks, Territoires du Nord-Ouest, Canada. *Canadian Journal of Earth Sciences* **14**: 2462-2480.
- Pollard WH, French HM. 1980. A first approximation of the volume of ground ice, Richards Island, Pleistocene Mackenzie Delta, Northwest Territories, Canada. *Canadian Geotechnical Journal* **17**: 509-516.
- Prior DB, Wiseman WJ, Bryant WR. Submarine chutes on the slopes of fjord deltas. *Nature* **290**: 326-328.
- Puthusserry JT, Murray AS, Kjær KH, Funder S, Larsen E. 2006. Optically Stimulated Luminescence (OSL) dating of glacial sediments from Arctic Russia – depositional bleaching and methodological aspects. *Boreas* **35**: 587-599.
- Rachold V, Bolshiyarov DY, Grigoriev MN, Hubberten HW, Junker R, Kunitsky VV, Merker F, Overduin P, Schneider W. 2007. Nearshore Arctic Subsea Permafrost in Transition. *EOS* **88**: 149-156.
- Reading HG (ed). 1996. *Sedimentary Environments: Processes, Facies and Stratigraphy*, Third Edition. Blackwell Publishing; Oxford. 688 p.
- Reineck HE, Wunderlich F. 1968. Classification and origin of flaser and lenticular bedding. *Sedimentology* **11**: 99-104.
- Rodríguez Tovar FJ, Nagy J, Reolid M. 2014. Palaeoenvironment of Eocene prodelta in Spitsbergen recorded by the trace fossil *Phycosiphon incertum*. *Unpublished manuscript*.
- Salvinsen O. 1984. Occurrence of pumice on raised beaches and Holocene shoreline displacement in the inner Isfjorden area, Svalbard. *Polar Research* **2**: 107-113.
- Salvinsen O, Forman SL, Miller GH. 1992. Thermophilous molluscs on Svalbard during the Holocene and their paleoclimatic implications. *Polar Research* **11**: 1-10.
- Salvinsen O. 2002. Radiocarbon-dated *Mytilus edulis* and *Modiolus modiolus* from northern Svalbard: Climatic implications. *Norsk Geografisk Tidsskrift* **56**: 56-61.
- Shur Y, French HM, Bray MT, Anderson DA. 2004. Syngenetic Permafrost Growth: Cryostratigraphic Observations from the CRREL Tunnel near Fairbanks, Alaska. *Permafrost and Periglacial Processes* **15**: 339-347.
- Sletten K, Lyså A, Lønne I. 2001. Formation and disintegration of a high-arctic ice-cored moraine complex, Scott Turnerbreen, Svalbard. *Boreas* **30**: 272-284.
- Smith MW, Riseborough DW. 2002. Climate and the Limits of Permafrost: A Zonal Analysis. *Permafrost and Periglacial Processes* **13**: 1-15.
- Solem K, Davidsen B, Grimstvedt AM, Schiellerup H. 1996. *NGU-SD 5.11: Kornfordelingsanalyse med coulter laser partikkelteller*. Faggruppe for laboratorier; Norges Geologiske Undersøkelse. 25 p.
- Steel RJ, Dalland A, Kalgraff K, Larsen V. 1981. The Central Tertiary Basin of Spitsbergen: sedimentary development of a sheared-margin basin. In *Geology of the North Atlantic Borderlands*. Kerr JW (ed). Canadian Society of Petroleum Geologists: 647-664.
- Streletskaia ID. 1998. Cryopeg response to periodic climate fluctuations.. In *Proceedings of the Seventh International Conference on Permafrost, 13-17 June 1998*. Université Laval, Centre d'études nordiques, Collection Nordicana 55, 1021-1025.

- Svendsen JI, Mangerud J, Elverhøi A, Solheim A, Schuttenhelm RTE. 1992. The Late Weichselian glacial maximum on western Spitsbergen inferred from offshore sediment cores. *Marine Geology* **104**: 1-17.
- Svendsen JI, Elverhøi A, Mangerud J. 1996. The retreat of the Barents Sea Ice Sheet on the western Svalbard margin. *Boreas* **25**: 244-256.
- Svendsen JI, Mangerud J. 1997. Holocene glacial and climatic variations on Spitsbergen, Svalbard. *The Holocene* **7**: 45-57.
- Svensson H. 1971. Pingos i yttre delen av Adventdalen. *Norsk Polarinstitutt Årbok* **1969**: 168-174.
- Syvitski JPM, Farrow GE. 1983. Structures and processes in bayhead deltas: Knight and Bute inlet, British Columbia. *Sedimentary Geology* **36**: 217-244.
- Syvitski JPM, Shaw J. 1995. Sedimentology and geomorphology of fjords. In *Geomorphology and Sedimentology of Estuaries, Development in Sedimentology 53*. Perillo GME (ed). Elsevier, Amsterdam: 113-178.
- Sørbel L, Tolgensbakk J, Hagen JO, Høgvard K. 2001. Geomorphological and Quaternary Geological Map of Svalbard: 1:100 000. Skeet C9Q Adventdalen. Explanatory text. *Norsk Polarinstitutt Temakart* **31/32**: 57-78.
- Taylor AM, Goldring R. 1993. Description and analysis of bioturbation and ichnofabric. *Journal of the Geological Society, London* **150**: 141-148.
- Tessier B. 1993. Upper intertidal rhythmites in the Mont-Saint-Michel Bay (NW France): Perspectives for paleoreconstruction. *Marine Geology* **110**: 355-367.
- Tolgensbakk J, Sørbel L, Høgvard K. 2000. Adventdalen, Geomorphological and Quaternary Geological Map, Svalbard 1:100 000, Spitsbergen sheet C9Q. *Norsk Polarinstitutt Temakart* **32**.
- Williams PJ, Smith MW. 1989. *The Frozen Earth: Fundamentals of Geocryology*. Cambridge University Press: Cambridge. 306 p.
- Włodarska-Kowalczyk M, Szymalfenig M, Zajączkowski M. 2007. Dynamic sedimentary environments of an Arctic glacier-fed river estuary (Adventfjorden, Svalbard). II: Meio- and macrobenthic fauna. *Estuarine, Coastal and Shelf Science* **74**: 274-284.
- Yoshikawa K, Harada K. 1995. Observations of Nearshore Pingo Growth, Adventdalen, Svalbard. *Permafrost and Periglacial Processes* **6**: 361-372.
- Yoshikawa K, Nakamura T. 1996. Pingo growth ages in the delta area, Adventdalen, Svalbard. *Polar Record* **32**: 347-352.
- Zajączkowski M, Szczuciński W, Bojanowski R. 2004. Recent changes in sediment accumulation rates in Adventfjorden, Svalbard. *Oceanologica* **46**: 217-231.
- Zajączkowski M, Włodarska-Kowalczyk M. 2007. Dynamic sedimentary environments of an Arctic glacier-fed river estuary (Adventfjorden, Svalbard). I: Flux, deposition, and sediment dynamics. *Estuarine, Coastal and Shelf Science* **74**: 285-296.
- Zajączkowski M. 2008. Sediment supply and fluxes in glacial and outwash fjords, Kongsfjorden and Adventfjorden, Svalbard. *Polish Polar Research* **29**: 59-72.
- Zhang R, Wang Y, Gao J, Shaoming P. 2009. Sediment texture and grain-size implications: the Changjiang subaqueous delta. *Acta Oceanologica Sinica* **28**: 38-49.

# Appendix A: Sedimentary log

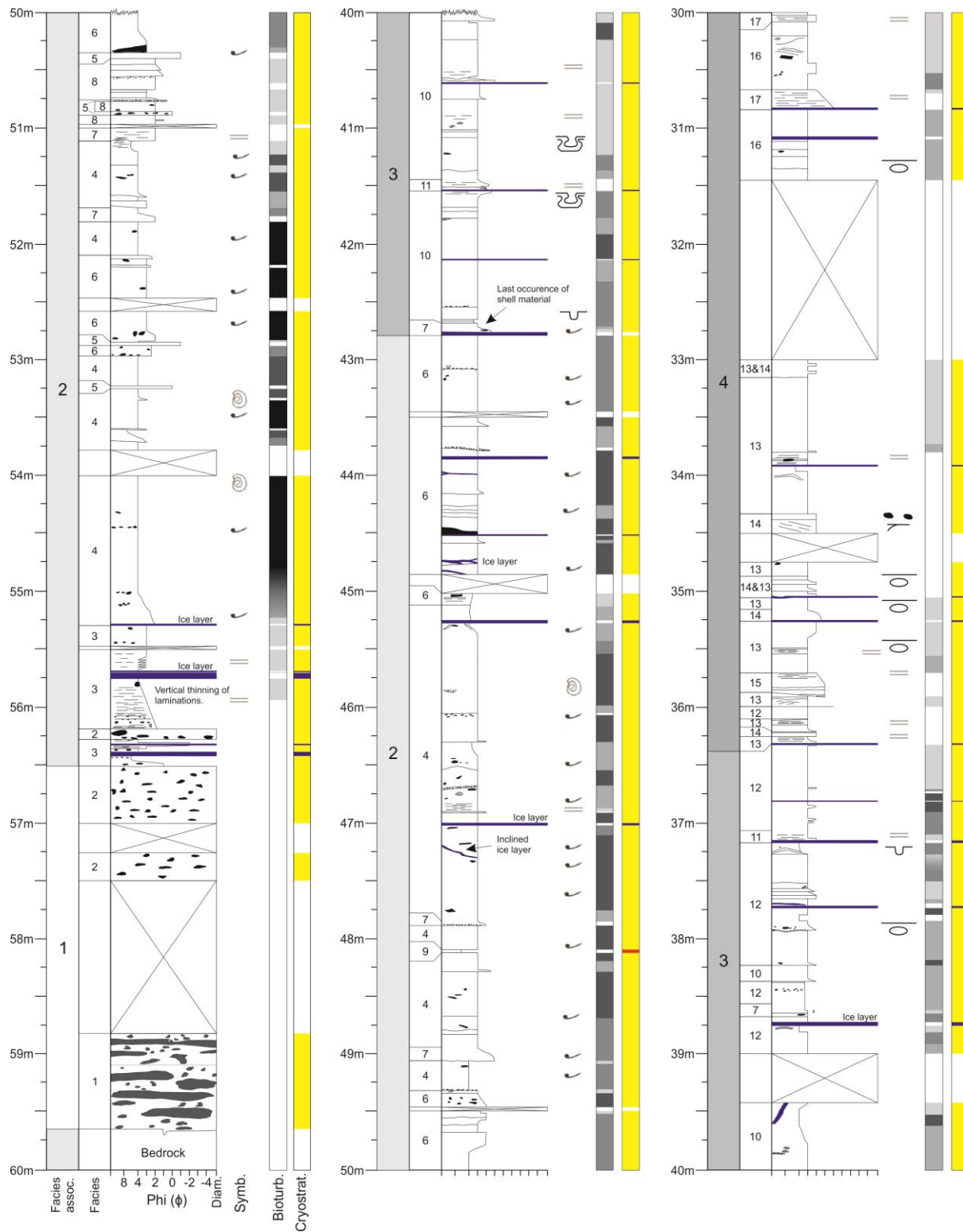


Figure A.1 continued...



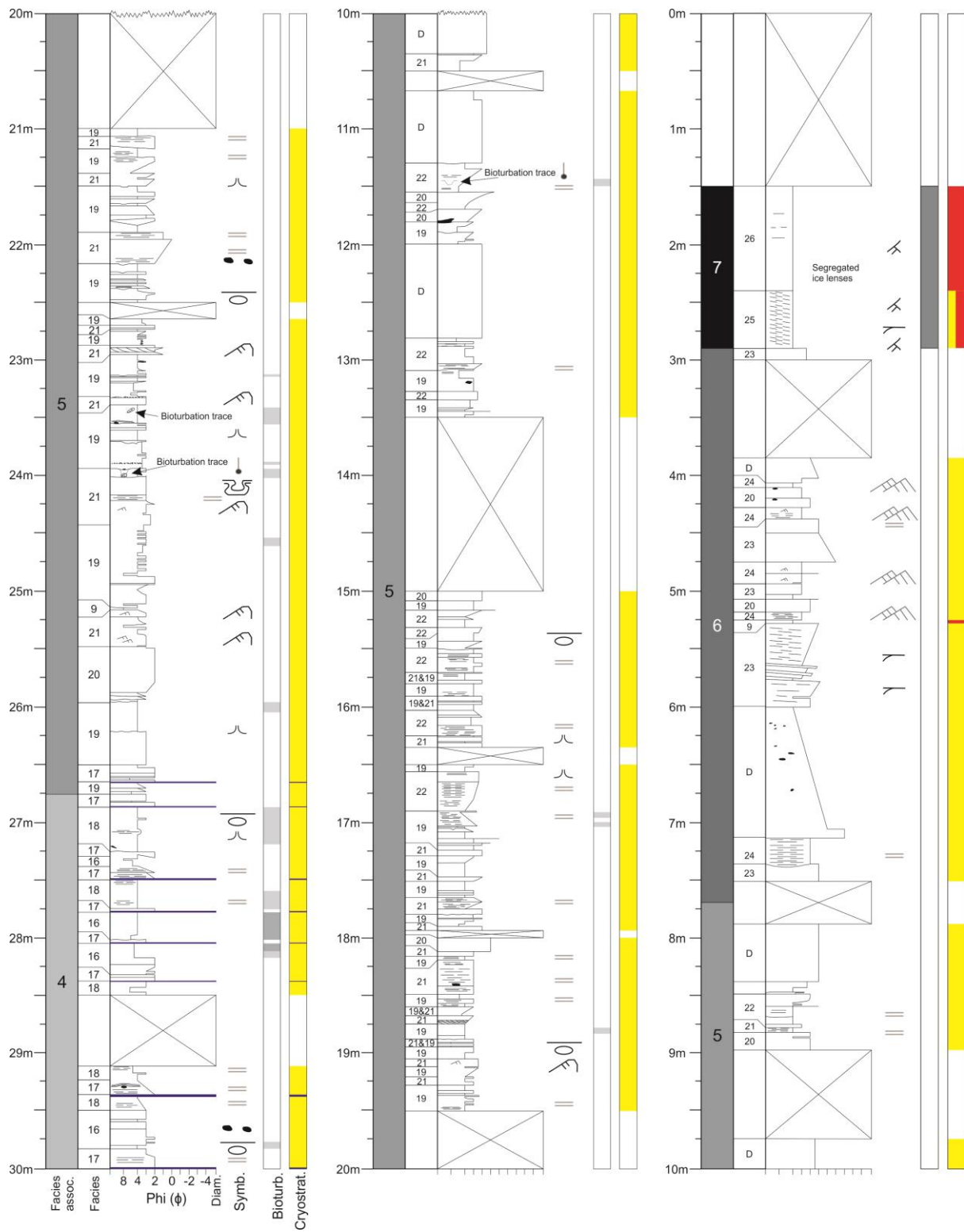
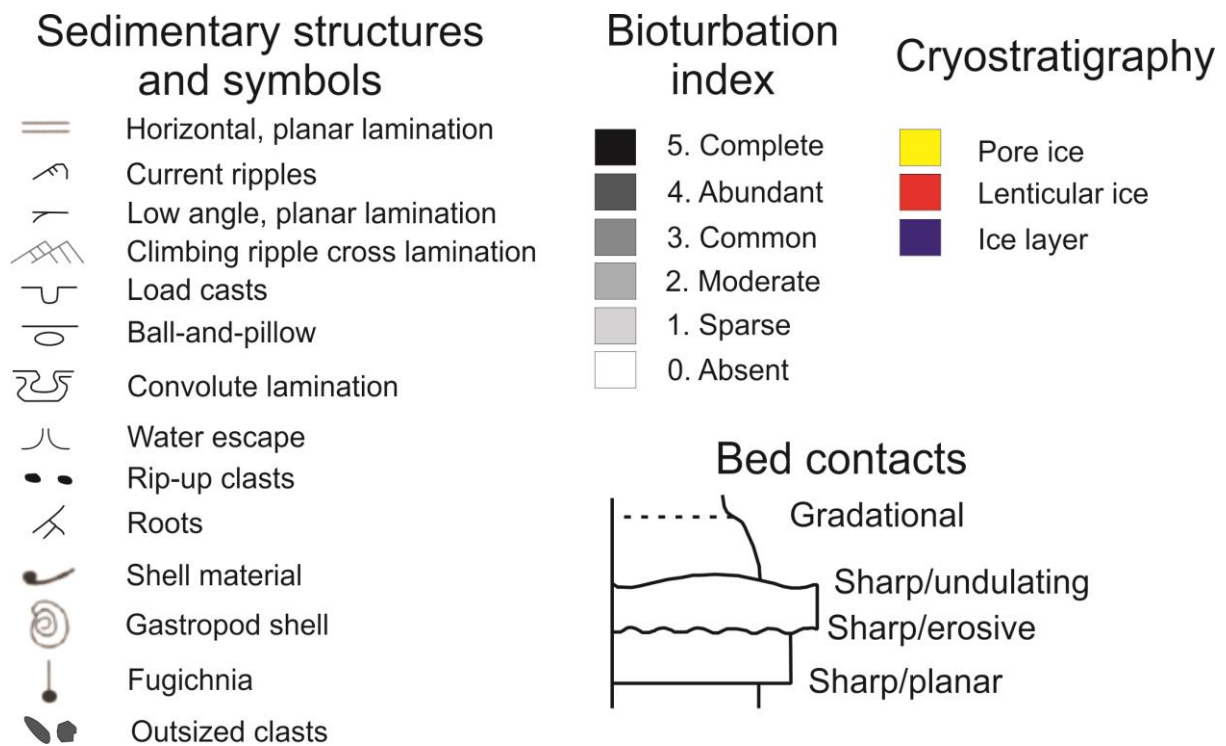
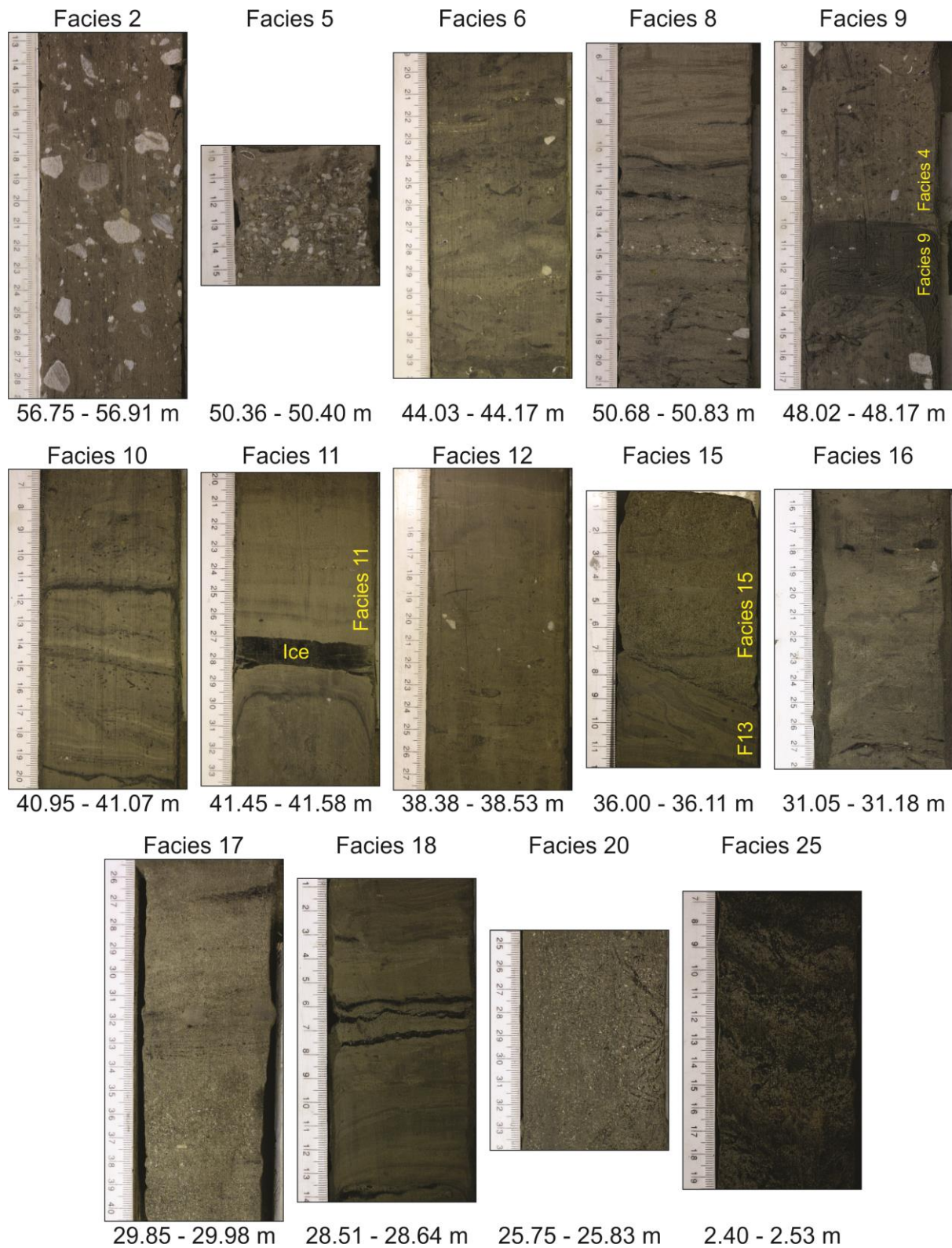


Figure A.1 continued...



**Figure A.1** Detailed sedimentary log of the ice-bonded 60 m core.

**Appendix B: Images of additional facies**



**Figure B.1** Images of additional facies not included in Chapter Five.

## **Appendix C: Core ichnology**

This section will provide a brief overview of the trace fossil and ichnological interpretations acquired from the sediment core under study. A basic summary is included in the main body of this thesis (Chapter Six).

### **Introduction**

Ichnology refers to the study of trace fossils (McIlroy 2004). Trace fossils form a morphologically diverse record of the activity of organisms within the environments they occupy. In assessing the strengths of ichnology to palaeoenvironmental reconstruction, McIlroy (2004) notes trace fossils are almost always found *in situ* and may occur in deposits otherwise devoid of body fossils. The identification and classification of trace fossils provides information regarding faunal response to environmental stimuli. Resultant conclusions are often invaluable additions to complete sedimentological descriptions, assisting in the qualitative evaluation of sedimentation rates, salinity, oxygenation, substrate consistency, turbidity, and, to a lesser extent, bathymetry (Tonkin 2012).

At present, the application of trace fossils to improving palaeoenvironmental interpretations in glacial environments is a relatively unexplored corner of ichnology. Ichnological studies of glacial landscapes have principally focused on the Gondwana and Quaternary ice ages (Netto et al. 2012).

In Arctic fjord environments, sedimentation rates, freshwater input, turbidity, substrate characteristics, and oxygen content exhibit a controlling influence on benthic faunal assemblages (Netto et al. 2012). Fjords are typified by high sedimentation rates, owing to input from fluvial, aeolian, and mass-transport sources. In inner-fjord settings, high sedimentation rates constrain bioturbation by increasing environmental stress, resulting in a decline in benthic faunal abundance and diversity (Eg. Włodarska-Kowalczyk et al. 2007). Additionally, high concentrations of suspended sediments impede the activity of suspension feeding organisms (Feder and Matheke 1980; Netto et al. 2012). Netto et al. (2012) suggest fjords are therefore preferentially bioturbated in the distal zones, where trace fossils are typically horizontal in inclination and reflect deposit feeding ethologies.

The impact of melt-water and sediment input on benthic communities in the Adventfjord has been investigated by Włodarska-Kowalczyk et al. (2007). This study demonstrates that the abundance and diversity of benthic species increases with distance from the fjord head. Generally, trace fossils in fjords are attributed the activity of annelids and molluscs (Netto et

al. 2012). Indeed, these are the dominant members of macrobenthic assemblages in the contemporary Adventfjord (Włodarska-Kowalczyk et al. 2007).

#### *Glaciomarine trace fossil assemblages*

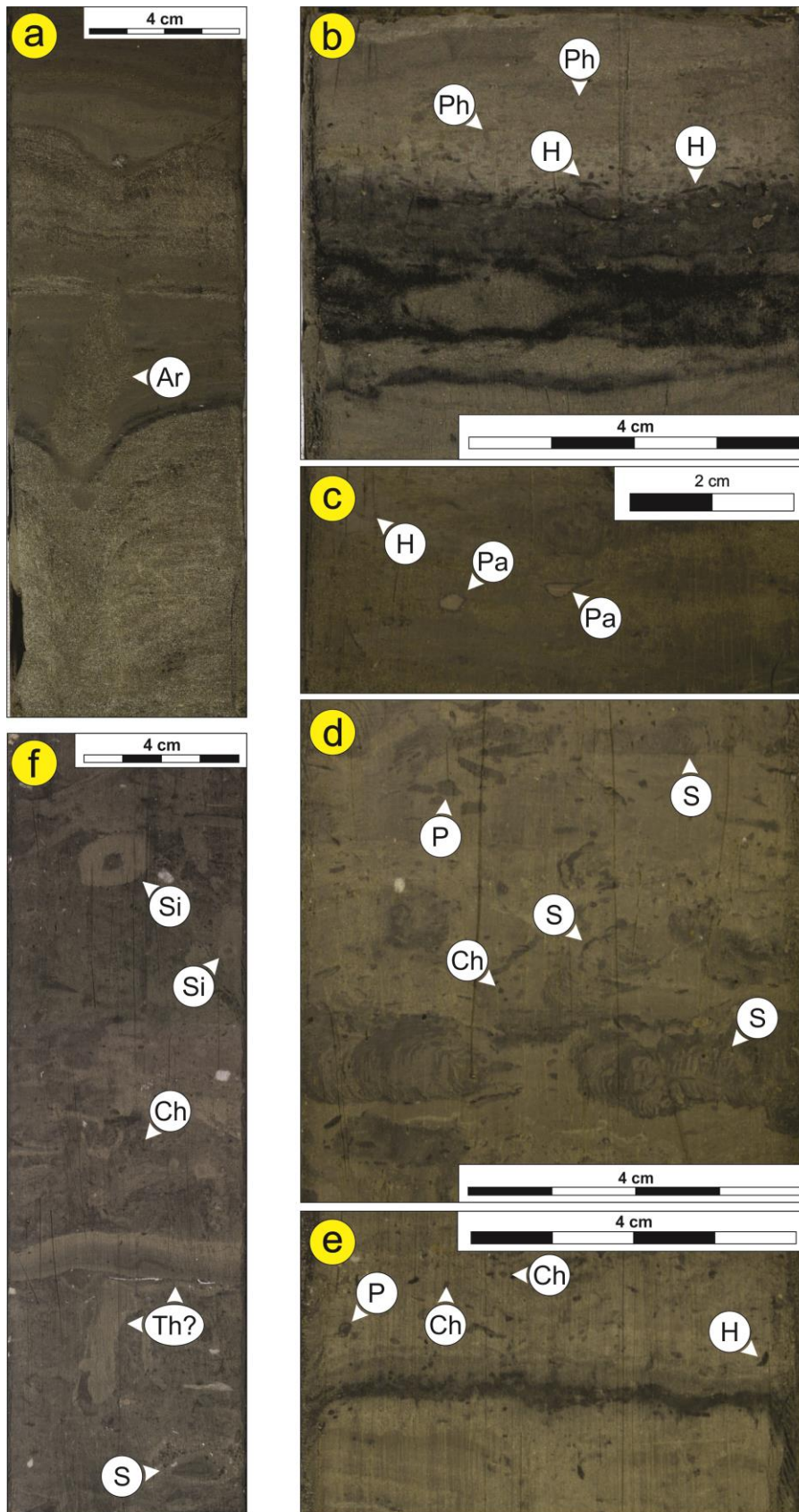
Glaciomarine ichnofauna are typically small when compared with those from temperate settings (Netto et al. 2012). Netto et al. (2012: 317) note trace fossil assemblages of fine-grained sediments in shallow glaciomarine environments are mainly composed of *Arenicolites*, *Chondrites*, *Diplocraterion*, *Palaeophycus*, *Phycosiphon*, *Planolites*, *Rhizocorallium*, and *Thalassinoides*. Trace fossils are sporadically distributed and assemblages reflect those of an impoverished *Cruziana* Ichnofacies suite, otherwise associated with brackish environments (James and Dalrymple 2010; Netto et al. 2012:317).

### **Results and interpretation**

The Late Quaternary sediments in Adventdalen contain a restricted assemblage of trace fossils principally belonging to the *Cruziana* Ichnofacies suite (James and Dalrymple 2010). Nine trace fossils are identified at the genus level: *Arenicolites*, *Chondrites*, *Helminthopsis*, *Palaeophycus*, *Phycosiphon*, *Planolites*, *Scolicia*, *Siphonichnus*, and *Thalassinoides* (**Figure C.1**). Fugichnia, a structure resulting from an animal evacuating its burrow, is also noted. Trace fossils are described in **Table C.1**, and are used to construct five trace fossil assemblages (A1 – A5; **Figure C.2**). Assemblages are not defined for intervals where no trace fossils are observed or in terrestrial deposits. Terrestrial deposits are characterized by the relatively uniform distribution of roots; no terrestrial faunal traces are discerned.

#### *A1: Glacial proximal trace fossil assemblage*

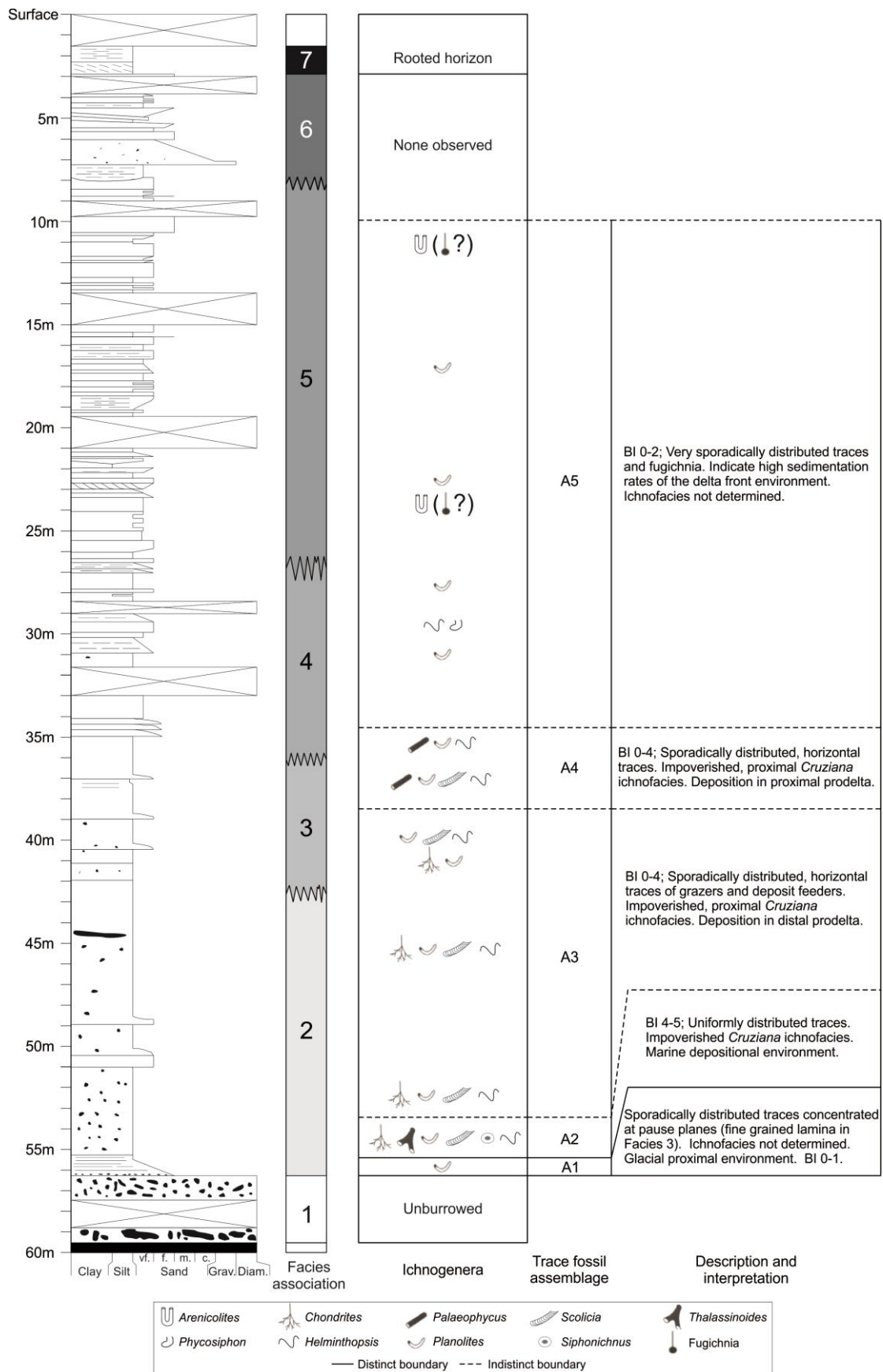
A1 is associated with the laminated silt deposits of Facies 3. Trace fossils sporadically distributed, increasing in abundance towards the upper portion of this facies. This assemblage is dominated by the presence of *Planolites* which occur at pause planes (fine grained lamina) deposited during quiescent periods. Trace fossils are exclusively horizontal in inclination. Due to the low diversity of A1, no ichnofacies is determined. In combination with sedimentological evidence, trace fossils within this association likely reflect the rapid colonization of glaciomarine sediments following deglaciation. Ó Cofaigh and Dowdeswell (2001) have previously observed the intensification of bioturbation in laminated glaciomarine sediments with increasing distance from the ice margin.



**Figure C.1** Identified trace fossils, primarily belonging to the *Cruziana* Ichnofacies. Approximate depth of each image: a – 23.9 m; b – 29.1 m; c – 35.38 m; d – 39.6 m; e – 41.0 m; f – 54.5 m. Trace-fossil abbreviations are as follows: Ar – *Arenicolites*; Ch – *Chondrites*; H – *Helminthopsis*; Pa – *Palaeophycus*; Ph – *Phycosiphon*; P – *Planolites*; S – *Scolicia*; Si – *Siphonichus*; Th – *Thalassinoides*.

**Table C.1** Descriptions of the trace fossils identified in the core. Refer to **Figure C.1** for images.

Trace fossils ( <i>Ichnogenus</i> )	Description	Behaviour represented	Discussion
<i>Arenicolites</i> – Ar	Unlined U-shaped tubes, ca. 3 cm in diameter, and 5-15 cm in depth.	Suspension feeding (Eyles et al. 1992)	<i>Arenicolites</i> shares morphological characteristics of escape structures ( <i>Fugichnia</i> ). Fill reflects surrounding lithology, forming a concave-up, chevron pattern.
<i>Chondrites</i> – Ch	Small branching tunnel networks filled with dark sediment (?mud) and, occasionally, lighter sands. Tunnel diameter 1 – 2 mm.	Deposit feeding	<i>Chondrites</i> is believed to represent the feeding traces ( <i>fodinichnia</i> ) of burrowing worms (Eyles et al. 1992).
<i>Fugichnia</i> – Fu	Vertical to near-vertical burrows with strata collapsing into them. Typically 1-3 cm in diameter and up to 10 cm depth.	Escape from burial	Escape traces ( <i>fugichnia</i> ) provide indication of an organism's response to maintain a favorable position in relation to the sediment-water interface. May be indicative of high (or variable) sedimentation rates (Bromley 1996).
<i>Helminthopsis</i> – H	Irregularly winding, unbranching, horizontal burrows with dark fill; ca. 1mm in diameter.	Grazing	<i>Helminthopsis</i> is a grazing trace ( <i>pascichnia</i> ) possibly produced by annelids in brackish to marine environments (Bromley 1996; Buatois et al. 1998).
<i>Palaeophycus</i> – Pa	Lined horizontal burrows. Diameter is less than 1 cm, lining ca. 1 mm in thickness.	Dwelling structure of a suspension feeding or predaceous worm (Eyles et al. 1992)	Dwelling structure likely produced by annelids in a marine environment. Differentiated from <i>Planolites</i> by the presence of passive infill (similar to host material) and the presence of a distinct lining (Eyles et al. 1992).
<i>Phycosiphon</i> – Ph	Hook-shaped burrows ca. 0.5 mm in diameter. Fill is typically darker than surrounding sediment.	Grazing and deposit feeding	The <i>Phycosiphon</i> tracemaker exhibits opportunistic behaviour and common occurs in dysoxic sediments where food is available (Rodríguez Tovar et al. 2014).
<i>Planolites</i> – P	Unlined, horizontal to slightly inclined burrows with active fill different from enclosing sediments. Diameter commonly less than 5 mm.	Deposit feeding	Meandering, locomotion traces ( <i>pascichnia</i> ) indicating that an organism has exploited a particular region in search of food (Bromley 1996). In proximal expressions of the <i>Cruziana</i> ichnofacies, planolites are observed in association with dark, organic-rich (?) horizons.
<i>Scolicia</i> – S	Bilaterally symmetrical trace with spreiten. 1-2 cm in diameter. Orientation is typically parallel or slightly oblique to bedding.	Grazing	<i>Scolicia</i> likely represent the activity of deposit feeding urchans (Smith and Crimes 1983).
<i>Siphonichnus</i> – Si	Unlined, inclined (?) 1-2 cm in diameter with smaller tube characterized by dark infill.	Dwelling	Dwelling traces ( <i>domichnia</i> ) of an infaunal bivalve (Zonneveld and Gingras 2013).
<i>Thalassinoides</i> – Th	Horizontal tunnel network only observed in cross section. Fill appears cleaner than the enclosing sediments. Vertical sediments also possibly observed. Tunnel diameter ca. 1-2 cm.	Deposit feeding and dwelling	<i>Thalassinoides</i> is often attributed to the activity of burrowing crustaceans. These combined feeding and dwelling traces document an organism's exploitation of the substrate in search of food (Bromley 1996).



**Figure C.2** Simplified sedimentological log with trace fossil assemblages. The intensity of biogenic activity decreases upwards in relation to coarsening and shallowing of the deposits. The trace fossil assemblages illustrate a glacial proximal to open fjord basin to delta transition.



#### *A2: Glaciomarine trace fossil assemblage*

A2 occurs above A1, in the lower portions of Facies Association 2. High degrees of bioturbation are noted in this interval (BI 4-5). A2 generally corresponds to Facies 4. *Chondrites*, *Helminthopsis*, *Planolites* are common. Moderate numbers of *Scolicia* and (?)*Thalassinoides* are observed. Trace fossils are predominantly horizontal in inclination and uniformly distributed and reflect the activity of grazing and deposit feeding organisms (Bromley 1996). This assemblage is classified as an impoverished *Cruziana* ichnofacies, indicating marine conditions (Netto et al. 2012).

#### *A3: Distal prodelta trace fossil assemblage*

A3 displays common numbers of *Chondrites*, *Helminthopsis*, and *Planolites*, and moderate numbers of *Scolicia*. *Scolicia* appear diminutive in size towards the top of A3, particularly when compared with A2. As in A2, trace fossils relate to grazing and deposit feeding and are primarily horizontal in inclination, indicating low energy depositional environments. However, the trace fossil distribution is non-uniform and appears to be facies controlled. This implies fluctuations in environmental variables (Gingras et al. 1998). Traces occur in association with fine grained (silt) deposits. The BI values of bioturbated intervals range between 1 and 4. Deposits of sediment gravity flows (ex. Facies 7), are characterized by bioturbated tops but are otherwise unburrowed. This assemblage is hesitantly classified as an impoverished, proximal *Cruziana* ichnofacies, signifying stressed marine conditions within the distal prodelta.

#### *A4: Proximal prodelta trace fossil assemblage*

A4 is differentiated from A3 by the presence of *Palaeophycus* and the absence of *Chondrites*. A4 displays common numbers of *Helminthopsis* and *Planolites*, while *Palaeophycus* and *Scolicia* occur rarely. As in A3, traces are sporadically distributed and concentrated in silt-rich facies. Burrows are primarily horizontal in inclination. Again, this association is classified as an impoverished, proximal *Cruziana* ichnofacies, signifying stressed marine conditions within the proximal prodelta.

#### *A5: Delta front trace fossil assemblage*

Trace fossils in A5 are very sporadic in distribution. *Arenicolites*, *Helminthopsis*, *Planolites*, and *Phycosiphon* occur rarely, in association with fine grained deposits. Fugichnia, vertically oriented escape traces, are observed in heterolithic sediments and likely signify high sedimentation rates (Bromley 1996). Significant thicknesses of unbioturbated strata provide further indication of high sedimentation rates in this environment (Gingras et al. 1998). The

low diversity of trace fossils precludes the determination of an ichnofacies association. The assemblage is interpreted as occurring within the delta front based on the sporadic distribution of burrows and presence of fugichnia indicative of high, albeit variable, sedimentation rates. The virtual absence of trace fossils in delta front deposits has also been made by Gingras et al. (1998).

### **Summary**

Ten distinct biogenic traces are identified within the core deposits studied here and grouped into five trace fossil assemblages. Ichnogenera primarily represent deposit feeding and grazing ethologies (Bromley 1996; James and Dalrymple 2010). The limited number of suspension feeding organisms is likely due to the high concentrations of suspended sediment, characteristic of fjord environments (Włodarska-Kowalczyk et al. 2007; Netto et al. 2012). The vertical distribution of trace fossils indicates the presence of strong palaeoenvironmental controls on benthic faunal communities. In A1, the controlling variable is likely the vicinity to a palaeo-ice sheet. The proximity to a prograding delta is suggested as the principal factor governing the characteristics of ichnogenera in A2 – A5. With decreasing depth, trace fossil assemblages show a gradual reduction in ichnogenera diversity, trace fossil abundance and distribution. The trace fossil associations presented above are interpreted to represent the development of a prograding delta in the palaeo-Adventfjord.

## References for Appendix C

- Bromley RG. 1996. *Trace fossils: Biology, taphonomy and applications*, Second Edition. Chapman & Hall: London.
- Buatios LA, Mangano MG, Maples CG, Lanier WP. 1998. Ichnology of an Upper Carboniferous Fluvio-Estuarine Paleovalley: The Tonganoxie Sandstone, Buildex Quarry, Eastern Kansas, USA. *Journal of Paleontology* **72(1)**: 152-180.
- Eyles N, Vossler SM, Lagoe MB. 1992. Ichnology of a glacially-influenced continental shelf and slope; the Late Cenozoic Gulf of Alaska (Yakatage Formation). *Palaeogeography, Palaeoclimatology, Palaeoecology* **94**: 193-221.
- Feder HM, Matheke GEM. 1980. Distribution, abundance, community structure and tropic structure of the benthic infauna of the northeast Gulf of Alaska. *Institute of Marine Science Report* **R78-8**.
- Gingras MK, MacEachern JA, Pemberton SG. 1998. A comparative analysis of the ichnology of wave- and river-dominated allomembers of the Upper Cretaceous Dunvegan Formation. *Bulletin of Canadian Petroleum Geology* **46 (1)**: 51-73.
- James NP, Dalrymple RW (eds). 2010. *Facies Models 4*. Geological Association of Canada; St. John's, Newfoundland. 586p.
- MacEachern JA, Bann KL, Bhattacharya JP, Howell CD. 2005. Ichnology of deltas: organism responses to the dynamic interplay of rivers, waves, storms, and tides. In *River Deltas – Concepts, Models, and Examples*. Giosan L, Bhattacharya JP (eds). Society for Sedimentary Geology (SEPM) Special Publication 83; 49-85.
- McIlroy D. 2004. The application of ichnology to palaeoenvironmental and stratigraphic analysis: introduction. In *The Application of Ichnology to Palaeoenvironmental and Stratigraphic Analysis*. Geological Society; London: 237-272.
- Netto RG, Benner JS, Buatios LA, Uchman A, Mangano MG, Ridge JC, Kazakauskas V, Gaigalas A. 2012. Glacial Environments. In *Trace fossils as indicators of sedimentary environments*. Knaust D, Bromley RG (eds). Elsevier; Amsterdam: 299-327.
- Ó Cofaigh C, Dowdeswell JA. 2001. Laminated sediments in glacial marine environments: diagnostic criteria for their interpretation. *Quaternary Science Reviews* **20 (13)**: 1411-1436.
- Rodríguez Tovar FJ, Nagy J, Reolid M. 2014. Palaeoenvironment of Eocene prodelta in Spitsbergen recorded by the trace fossil *Phycosiphon incertum*. *Unpublished manuscript*.
- Smith AB, Crimes P. 1983. Trace fossils formed by heart urchins – a study of *Scolicia* and related traces. *Lethaia* **16**: 79-92.
- Tonkin NS. 2012. Deltas. In *Trace fossils as indicators of sedimentary environments*. Knaust D, Bromley RG (eds). Elsevier; Amsterdam: 507-528.
- Włodarska-Kowalczyk M, Szymalfenig M, Zajczkowski M. 2007. Dynamic sedimentary environments of an Arctic glacier-fed river estuary (Adventfjorden, Svalbard). II: Meio- and macrobenthic fauna. *Estuarine, Coastal and Shelf Science* **74**: 274-284.
- Zonneveld JP, Gingras MK. 2013. The ichnotaenonomy of vertically oriented, Bivalve-generated equilibrichnia. *Journal of Paleontology* **87(2)**: 243-253.

## Appendix D: Grain size results

**Table D.1** Distribution of grain size and statistical parameters calculated in the GRADISTAT program using the equations proposed by Folk and Ward (1957) and methods suggested by Passege (1957; 1964). Each sample consists of a 1-3 cm slice of half-core selected from a homogenous unit.

Sample Id	Mean depth (m)	Facies association	% Clay $\leq 2\mu\text{m}$	% Silt 2 - 63 $\mu\text{m}$	% Sand 63 $\mu\text{m}$ - 2mm	Mean grain size ( $\phi$ )	Standard deviation ( $\phi$ )	Skewness	Median ( $\phi$ )	C ( $\phi$ )
294	1.60	FA7	2.3	67.0	30.7	4.90	1.73	0.37	4.48	2.20
292	1.80	FA7	1.9	66.7	31.4	5.01	1.80	0.37	4.53	2.16
282	2.95	FA7	2.2	63.2	34.6	4.88	1.84	0.33	4.47	2.16
281	3.98	FA6	4.1	35.4	60.5	3.28	3.28	0.43	2.22	-0.85
280	4.06	FA6	3.8	70.0	26.2	5.63	2.00	0.13	5.45	2.25
279	4.08	FA6	1.9	58.9	39.2	4.59	1.47	0.53	4.15	2.47
278	4.10	FA6	2.3	77.5	20.2	5.42	1.94	0.11	5.20	0.97
276	4.27	FA6	3.7	48.8	47.5	4.52	2.73	0.14	4.21	0.21
265	5.22	FA6	2.4	30.0	67.7	4.16	1.93	0.67	3.28	2.05
264	5.26	FA6	7.5	86.7	5.8	6.83	1.63	-0.12	6.88	2.55
263	5.29	FA6	3.6	64.7	31.7	5.33	2.07	0.24	4.95	2.19
262	5.45	FA6	1.9	40.0	58.1	4.29	1.69	0.59	3.67	2.39
261	5.59	FA6	1.3	81.1	17.7	4.56	1.03	0.46	4.41	3.24
260	5.64	FA6	3.6	90.7	5.7	6.04	1.57	0.23	5.77	3.06
258	5.74	FA6	3.3	90.1	6.6	6.16	1.58	0.13	5.97	2.46
257	5.77	FA6	3.6	41.9	54.6	4.30	2.57	0.45	3.37	0.62
255	7.17	FA6	3.6	52.4	44.0	4.94	2.26	0.29	4.47	1.89
252	7.49	FA6	4.3	46.7	49.0	4.46	2.86	0.14	4.16	0.17
251	8.1	FA6	5.6	56.8	37.6	5.07	2.68	0.00	5.04	0.28
250	8.22	FA6	4.7	50.4	45.0	4.35	3.10	-0.04	4.48	-0.41
249	8.50	FA6	3.7	87.1	9.2	6.18	1.69	0.02	6.12	2.40
247	8.58	FA6	4.1	42.4	53.6	4.48	2.57	0.41	3.61	0.55
245	8.76	FA6	3.6	44.5	52.0	4.54	2.43	0.43	3.72	0.74
244	8.77	FA6	4.4	64.5	31.1	5.46	2.34	-0.08	5.67	1.86
243	8.80	FA5	2.5	56.0	41.5	4.96	1.97	0.43	4.33	2.12
240	10.10	FA5	3.6	39.9	56.5	4.43	2.31	0.56	3.46	1.76
239	10.31	FA5	2.9	34.4	62.7	4.06	2.38	0.59	2.99	0.75
235	11.07	FA5	5.1	75.5	19.4	5.83	2.04	0.02	5.77	2.16
232	11.57	FA5	3.6	40.1	56.3	4.30	2.58	0.44	3.39	0.55
231	11.59	FA5	3.5	32.4	64.2	3.93	2.63	0.56	2.79	0.43
230	11.66	FA5	2.6	48.8	48.6	4.70	1.96	0.51	3.99	2.22
229	11.79	FA5	3.6	77.7	18.7	5.69	1.91	0.13	5.49	2.28
227	12.05	FA5	4.4	54.3	41.3	4.97	2.48	0.13	4.72	0.68
225	12.80	FA5	3.6	47.3	49.1	4.66	2.48	0.30	4.02	0.52
224	13.06	FA5	3.4	88.2	8.4	6.06	1.64	0.13	5.86	2.25
223	13.07	FA5	2.7	61.5	35.8	5.03	1.96	0.31	4.61	2.26
222	13.47	FA5	3.2	68.3	28.5	5.32	1.99	0.22	5.00	2.25
221	15.14	FA5	3.8	81.9	14.3	5.80	1.80	0.17	5.55	2.25
220	15.16	FA5	3.9	60.5	35.6	5.24	2.12	0.25	4.85	2.21
219	15.18	FA5	2.6	51.3	46.1	4.76	2.03	0.44	4.13	2.22
218	16.07	FA5	2.1	42.2	55.7	4.47	1.91	0.57	3.72	2.21
216	16.15	FA5	3.9	87.6	8.5	6.12	1.68	0.10	5.96	2.61
215	16.17	FA5	2.6	43.0	54.4	4.49	2.12	0.54	3.66	2.01
214	16.60	FA5	2.5	34.2	63.3	4.26	2.07	0.63	3.32	1.93
213	16.79	FA5	3.1	73.0	24.0	5.31	1.79	0.44	4.73	2.49
212	16.80	FA5	4.4	87.6	8.0	5.98	1.70	0.24	5.68	2.62
210	17.01	FA5	3.7	68.8	27.5	5.40	2.06	0.16	5.13	1.93
209	17.65	FA5	3.2	72.4	24.4	5.55	1.96	0.08	5.46	2.34
206	17.68	FA5	2.2	45.2	52.6	4.53	1.77	0.58	3.85	2.31
203	17.71	FA5	1.7	36.8	61.5	4.08	1.48	0.58	3.65	2.41
200	17.74	FA5	3.5	89.9	6.6	6.07	1.58	0.17	5.87	2.89
199	17.85	FA5	5.8	86.7	7.6	6.50	1.73	-0.06	6.50	2.53
198	17.89	FA5	5.2	83.3	11.6	6.49	1.81	-0.17	6.64	2.41
197	17.9	FA5	3.2	49.2	47.6	4.81	2.08	0.50	4.05	2.16
195	18.19	FA5	2.9	44.9	52.2	4.64	2.13	0.55	3.77	2.12
190	18.73	FA5	2.6	39.9	57.5	4.51	1.96	0.65	3.60	2.31
187	18.92	FA5	2.1	60.3	37.6	4.82	1.72	0.46	4.30	2.47
186	19.15	FA5	3.1	45.9	51.0	4.72	2.06	0.56	3.87	2.23
185	19.18	FA5	3.2	63.7	33.1	5.06	1.90	0.43	4.48	2.32
183	21.13	FA5	3.1	52.5	44.4	4.86	2.09	0.41	4.24	2.13
182	21.18	FA5	4.9	88.2	6.9	6.28	1.67	0.09	6.14	2.66
181	21.47	FA5	3.2	67.5	29.4	5.17	1.85	0.39	4.66	2.51
179	21.97	FA5	4.0	50.9	45.1	4.74	2.59	0.16	4.36	0.21
178	22.13	FA5	3.8	43.4	52.8	4.69	2.23	0.56	3.74	1.96

176	22.91	FA5	3.0	40.0	57.0	4.51	2.07	0.59	3.61	2.06
175	22.93	FA5	3.7	46.3	50.0	4.61	2.45	0.36	3.92	0.82
173	23.29	FA5	5.1	94.9	0.0	6.79	1.34	0.05	6.74	4.32
172	23.31	FA5	4.8	81.9	13.3	6.13	1.92	-0.02	6.05	1.94
171	23.32	FA5	3.5	46.5	50.0	4.77	2.14	0.52	3.92	2.07
166	24.42	FA5	3.7	61.8	34.5	5.22	2.05	0.35	4.68	2.29
157	25.44	FA5	3.6	46.7	49.7	4.79	2.19	0.51	3.95	2.13
150	26.51	FA5	3.1	52.1	44.8	4.89	2.14	0.38	4.31	2.24
147	26.87	FA5	2.2	51.0	46.8	4.72	1.90	0.50	4.05	2.32
145	27.25	FA5	2.7	67.9	29.4	5.20	1.86	0.32	4.79	2.47
143	27.57	FA5	3.8	81.7	14.5	5.85	1.79	0.12	5.69	2.57
140	27.73	FA5	6.3	86.7	7.0	6.56	1.70	-0.06	6.58	2.75
142	27.75	FA5	2.7	49.3	48.0	4.75	1.98	0.51	4.02	2.33
139	28.13	FA4	4.5	86.0	9.5	6.15	1.73	0.07	6.04	2.69
138	28.36	FA4	2.6	42.1	55.3	4.51	2.00	0.57	3.69	2.09
136	28.4	FA4	5.0	81.3	13.7	6.07	1.86	0.01	6.02	2.47
134	29.36	FA4	2.0	44.8	53.2	4.49	1.83	0.55	3.81	2.25
132	29.41	FA4	7.4	88.8	3.8	6.89	1.51	-0.07	6.92	2.63
128	29.95	FA4	4.3	34.2	61.6	4.05	2.66	0.57	2.84	0.55
124	30.67	FA4	3.3	43.1	53.6	4.61	2.19	0.58	3.67	2.05
120	31.06	FA4	5.2	81.9	12.9	6.13	1.87	0.00	6.10	2.37
118	31.1	FA4	4.1	89.8	6.1	6.27	1.61	0.07	6.18	2.90
114	33.87	FA4	4.5	84.1	11.4	6.12	1.79	0.03	6.06	2.37
113	34.48	FA4	2.3	43.9	53.8	4.52	2.10	0.53	3.70	1.99
110	35.7	FA4	1.8	44.9	53.4	4.33	1.87	0.46	3.79	1.92
108	35.85	FA4	2.1	43.5	54.4	4.44	2.04	0.53	3.68	2.05
107	35.89	FA4	5.3	87.0	7.8	6.37	1.72	-0.02	6.35	2.53
106	36.12	FA4	5.9	92.3	1.8	6.75	1.44	0.03	6.71	3.57
105	36.22	FA4	4.2	84.4	11.5	5.99	1.76	0.12	5.82	2.61
103	37.12	FA3	5.9	88.6	5.6	6.61	1.63	-0.06	6.64	2.50
101	37.17	FA3	6.6	88.8	4.6	6.82	1.54	-0.07	6.84	2.55
100	37.63	FA3	4.8	86.3	8.9	6.29	1.72	0.00	6.25	2.37
98	37.74	FA3	5.2	85.9	9.0	6.30	1.75	0.01	6.23	2.43
97	37.8	FA3	5.7	89.5	4.8	6.55	1.60	0.02	6.49	2.70
96	38.22	FA3	6.2	86.2	7.6	6.52	1.73	-0.08	6.57	2.57
95	38.7	FA3	5.0	84.4	10.6	6.21	1.79	0.00	6.17	2.25
93	38.76	FA3	6.7	90.3	3.0	6.70	1.53	0.00	6.69	3.37
92	38.83	FA3	6.0	87.5	6.5	6.53	1.68	-0.05	6.55	2.40
89	40.6	FA3	2.8	81.0	16.2	5.54	1.70	0.27	5.22	2.61
87	40.63	FA3	4.9	89.8	5.3	6.51	1.58	0.01	6.45	2.53
86	41	FA3	5.8	91.1	3.1	6.77	1.43	0.01	6.74	2.66
85	41.35	FA3	6.0	90.7	3.3	6.76	1.48	-0.01	6.74	2.78
84	41.5	FA3	4.6	90.1	5.3	6.23	1.64	0.12	6.08	3.24
81	42.35	FA3	6.8	89.3	3.9	6.83	1.51	-0.05	6.85	2.70
80	42.76	FA2	4.7	91.3	4.0	6.71	1.47	-0.02	6.73	2.63
78	42.79	FA2	7.0	89.4	3.6	6.98	1.44	-0.08	7.02	2.64
77	43.08	FA2	7.7	87.6	4.7	6.95	1.53	-0.11	7.01	2.51
76	43.52	FA2	7.6	91.7	0.7	6.92	1.45	-0.04	6.96	4.11
72	45.02	FA2	7.3	86.6	6.1	6.72	1.71	-0.12	6.78	2.53
71	45.21	FA2	5.9	87.4	6.7	6.50	1.70	-0.03	6.47	2.47
69	45.37	FA2	6.6	89.3	4.1	6.77	1.53	-0.04	6.77	2.57
66	46.52	FA2	6.6	80.0	13.4	6.41	2.02	-0.19	6.55	1.69
65	46.98	FA2	7.2	86.3	6.5	6.71	1.69	-0.12	6.79	2.39
63	47.02	FA2	7.4	86.4	6.2	6.85	1.66	-0.17	6.97	2.49
61	47.59	FA2	7.8	89.6	2.6	6.93	1.51	-0.10	7.03	2.97
60	48.08	FA2	8.5	86.9	4.6	6.88	1.61	-0.13	7.00	2.90
59	48.1	FA2	11.5	85.6	2.9	7.00	1.63	-0.14	7.16	3.10
58	48.24	FA2	7.2	86.8	6.1	6.55	1.75	-0.05	6.55	2.25
57	48.34	FA2	7.2	88.2	4.6	6.71	1.62	-0.06	6.75	2.97
56	48.74	FA2	6.4	83.1	10.5	6.44	1.87	-0.11	6.49	2.18
55	49.05	FA2	3.0	53.4	43.6	5.01	2.09	0.35	4.50	2.32
54	49.09	FA2	5.8	82.4	11.8	6.30	1.86	-0.06	6.33	2.41
49	50.25	FA2	5.2	73.2	21.6	5.86	2.06	0.02	5.84	2.22
48	50.37	FA2	3.8	27.5	68.7	2.82	3.29	0.69	1.02	-0.72
47	50.5	FA2	8.0	57.4	34.6	5.62	2.49	-0.01	5.61	1.67
46	50.7	FA2	4.6	68.8	26.6	5.72	2.11	-0.02	5.80	2.40
41	51.06	FA2	3.2	50.5	46.3	4.85	2.17	0.41	4.19	2.05
40	51.13	FA2	6.0	84.8	9.2	6.46	1.78	-0.08	6.49	2.37
39	51.25	FA2	6.4	85.4	8.2	6.57	1.76	-0.11	6.64	2.43
38	51.75	FA2	5.7	82.1	12.2	6.36	1.87	-0.12	6.47	2.30
37	51.79	FA2	2.7	37.6	59.7	4.45	2.11	0.67	3.39	2.18
36	51.81	FA2	7.0	86.0	7.1	6.58	1.71	-0.07	6.63	2.62
33	52.84	FA2	5.6	86.0	8.4	6.39	1.75	-0.04	6.40	2.47
32	52.86	FA2	5.6	71.8	22.7	5.75	2.41	-0.22	6.13	1.49
31	52.94	FA2	4.9	80.5	14.6	6.23	1.93	-0.15	6.40	2.40

27	54.45	FA2	5.7	88.8	5.5	6.51	1.64	0.01	6.46	2.51
25	54.8	FA2	6.9	87.5	5.6	6.78	1.63	-0.11	6.84	2.51
24	55.02	FA2	7.7	88.1	4.2	6.92	1.54	-0.10	6.99	2.70
21	55.66	FA2	16.2	83.7	0.1	7.24	1.69	-0.29	7.65	4.21
20	55.76	FA2	13.8	85.7	0.5	7.27	1.53	-0.18	7.45	4.13
18	56.16	FA2	11.0	80.5	8.5	6.76	1.88	-0.17	6.94	2.41
16	56.36	FA2	10.6	82.6	6.8	6.82	1.79	-0.15	6.96	2.40
15	56.49	FA2	7.9	79.4	12.7	6.36	1.97	-0.09	6.42	2.25
14	56.51	FA2	7.2	70.3	22.5	5.86	2.22	-0.04	5.92	1.99
12	56.93	FA1	5.8	60.9	33.3	5.32	2.36	0.08	5.21	0.95
11	57.38	FA1	7.4	63.0	29.6	5.57	2.37	0.04	5.48	1.59
7	59.42	FA1	5.5	67.7	26.8	5.46	2.28	0.05	5.33	0.93
6	59.61	FA1	5.6	64.8	29.6	5.39	2.32	0.06	5.27	1.01

**Table D.2** Distribution of grains > 2 mm. Sample id corresponds to those presented in **Table D.1**. The fraction of samples > 2mm was determined by dry sieving and samples are reported in % weight. Note this differs to samples in **Table D.1** which are presented in % volume.

<b>Sample Id.</b>	<b>Mean depth (m)</b>	<b>Clast content &gt; 2 mm (%; g/g)</b>
281	3.98	18.9
252	7.49	1.4
250	8.22	7.2
247	8.58	0.8
245	8.76	1.5
244	8.77	4.9
240	10.10	1.0
221	15.14	4.8
220	15.16	4.2
97	37.80	0.3
66	46.52	1.8
63	47.02	1.1
60	48.08	3.2
58	48.24	6.9
56	48.74	4.4
54	49.09	1.3
49	50.25	6.3
48	50.37	39.0
47	50.50	1.8
40	51.13	0.4
39	51.25	1.9
38	51.75	5.0
36	51.81	1.1
32	52.86	15.8
16	56.36	3.2
15	56.49	4.9
14	56.51	4.1
12	56.93	12.2
11	57.38	40.1

## Appendix E: Results of AMS $^{14}\text{C}$ and OSL dating

**Table E.1** List of radiocarbon (AMS  $^{14}\text{C}$ ) dates for the core sediments. Analysis conducted by the AMS  $^{14}\text{C}$  Dating Center (Aarhus University, Denmark).

<b>Facies association</b>	<b>Depth (m)</b>	<b>Laboratory Id.</b>	<b>Material</b>	<b><math>^{14}\text{C}</math> age (years BP; <math>\pm 1\sigma</math>)</b>	<b>Calibrated age BP (<math>2\sigma</math>)</b>
FA5	10.44	04092012	Plant	$4207 \pm 28$	4828 – 4755
FA4	28.50	04092012	Plant	$4561 \pm 27$	5250 – 5123



**Table E.2** List of Optically Stimulated Luminescence (OSL) dates for the core sediments. Analysis conducted by the Nordic Laboratory for Luminescence Dating (Aarhus University, Denmark).

Facies association	Depth (m)	Laboratory Id.	Measured age (Quartz; kya; $\pm$ std. err)	Measured age (K Feldspar; kya; $\pm$ std. err)
FA7	2.15	133022	1.79 $\pm$ 0.14	2.01 $\pm$ 0.17
FA6	2.98	131517	2.96 $\pm$ 0.23	3.22 $\pm$ 0.28
FA6	4.15	131518	4.53 $\pm$ 0.24	
FA6	4.45	131519	4.41 $\pm$ 0.31	3.65 $\pm$ 0.53
FA6	5.22	131520	4.47 $\pm$ 0.31	4.79 $\pm$ 0.52
FA6	7.18	131522	4.06 $\pm$ 0.29	3.74 $\pm$ 0.74
FA5	8.58	131523	5.37 $\pm$ 0.30	
FA5*	8.85	131524	6.37 $\pm$ 0.58	7.18 $\pm$ 2.47
FA5	10.18	131525	5.43 $\pm$ 0.27	
FA5	11.05	131526	4.53 $\pm$ 0.29	4.39 $\pm$ 0.91
FA5	11.95	131527	5.19 $\pm$ 0.52	
FA5	12.87	131528	4.04 $\pm$ 0.43	5.34 $\pm$ 0.44
FA5	13.49	131529	5.24 $\pm$ 0.29	
FA5	15.03	131530	4.54 $\pm$ 0.26	4.09 $\pm$ 0.43
FA5	15.91	131531	5.79 $\pm$ 0.36	
FA5	16.27	133023	5.20 $\pm$ 0.45	5.92 $\pm$ 0.55
FA5	17.2	131532	4.55 $\pm$ 0.31	6.64 $\pm$ 1.09
FA5	17.95	131533	5.29 $\pm$ 0.33	
FA5	18.73	131534	5.09 $\pm$ 0.42	5.88 $\pm$ 0.41
FA5	19.44	131535	4.93 $\pm$ 0.26	
FA5	21.09	131536	3.74 $\pm$ 0.28	6.04 $\pm$ 0.36
FA5	22.45	131537	5.17 $\pm$ 0.38	7.18 $\pm$ 0.80
FA5	23.56	131538	5.44 $\pm$ 0.30	
FA5	24.93	131539	4.80 $\pm$ 0.29	6.48 $\pm$ 0.65
FA5	26.54	131540	5.20 $\pm$ 0.34	6.46 $\pm$ 0.29
FA4	28.35	131541	5.52 $\pm$ 0.32	
FA4	29.37	131542	6.10 $\pm$ 0.35	8.09 $\pm$ 0.92
FA4	30.06	133026	5.28 $\pm$ 0.51	4.37 $\pm$ 0.87
FA4	30.78	133025	4.45 $\pm$ 0.39	5.22 $\pm$ 0.79
FA4	31.4	133024	6.87 $\pm$ 0.72	5.82 $\pm$ 0.72
FA4	33.8	131501	3.93 $\pm$ 0.55	6.10 $\pm$ 0.34
FA4	34.98	131502	5.69 $\pm$ 0.39	
FA3*	36.55	131503	10.69 $\pm$ 0.94	30.94 $\pm$ 5.21
FA3	38.05	131504	6.35 $\pm$ 0.76	
FA3	42.2	131507	6.74 $\pm$ 1.20	6.10 $\pm$ 0.77
FA2*	44.05	131508	2.94 $\pm$ 0.24	
FA2	46.05	131509	7.58 $\pm$ 0.77	4.54 $\pm$ 0.57
FA2	49.65	131511	8.74 $\pm$ 0.56	11.42 $\pm$ 1.46
FA2*	51.8	131512	17.87 $\pm$ 1.64	21.57 $\pm$ 1.18
FA2†	54.45	131513		10.03 $\pm$ 3.04
FA2†	55.15	131514		
FA1†	56.15	131515		
FA1†	59.19	131516		

\* Not included in analysis due to incomplete bleaching (resulting in an age overestimate) or anomalously high background dose rates (resulting in an age underestimate). Exclusion of these samples was at the recommendation of lab personnel.

† Samples could not be dated as they appear to never have been exposed to sufficient light to reset the luminescence signal.

## Appendix F: Gravimetric moisture content and excess ice content results

**Table F.1** Gravimetric moisture content of all samples determined by methods and equation presented in Chapter Four. Note that each sample is a 1-3 cm slice of half core.

Sample id.	Mean depth (m)	Gravimetric-water content (%)			
294	1.55	52.1	230	11.66	31.5
293	1.70	52.4	229	11.79	29.9
292	1.80	49.4	228	11.82	32.2
291	1.90	138.4	227	12.05	42.4
290	2.10	80.0	226	12.49	34.3
289	2.34	160.3	225	12.80	30.7
288	2.38	97.9	224	13.06	34.5
287	2.46	122.1	223	13.07	29.2
286	2.50	73.6	222	13.47	29.5
285	2.68	77.8	221	15.14	23.0
284	2.70	144.6	220	15.16	23.5
283	2.80	118.2	219	15.18	29.7
282	2.95	30.3	218	16.07	25.4
281	3.98	17.5	217	16.09	25.3
280	4.06	33.7	216	16.15	24.8
279	4.08	26.9	215	16.17	30.9
278	4.10	31.6	214	16.60	33.8
277	4.12	28.3	213	16.79	25.8
276	4.27	29.0	212	16.80	24.5
275	4.37	30.5	211	17.00	30.7
274	4.39	24.8	210	17.01	27.2
273	4.50	26.4	209	17.65	27.6
272	4.51	24.9	208	17.66	26.9
271	4.60	18.2	207	17.67	24.8
270	4.69	14.6	206	17.68	25.2
269	4.79	29.2	205	17.69	29.1
268	4.80	27.7	204	17.70	26.3
267	5.03	53.5	203	17.71	28.5
266	5.09	33.2	202	17.72	25.9
265	5.22	29.5	201	17.73	29.1
264	5.26	32.8	200	17.74	28.3
263	5.29	33.2	199	17.85	26.8
262	5.45	32.0	198	17.89	30.0
261	5.59	32.6	197	17.90	33.6
260	5.64	34.1	196	18.17	27.2
259	5.67	39.3	195	18.19	31.4
258	5.74	35.0	194	18.34	35.3
257	5.77	32.0	193	18.39	29.0
256	5.91	36.0	192	18.65	29.7
255	7.17	30.9	191	18.67	32.2
254	7.33	26.8	190	18.73	34.4
253	7.39	27.8	189	18.83	28.7
252	7.49	29.3	188	18.91	30.7
251	8.10	26.8	187	18.92	29.1
250	8.22	30.7	186	19.15	36.3
249	8.50	27.8	185	19.18	30.0
248	8.52	16.4	184	19.48	30.8
247	8.58	29.0	183	21.13	35.2
246	8.60	28.5	182	21.18	24.8
245	8.76	18.7	181	21.47	37.5
244	8.77	13.0	180	21.50	30.0
243	8.80	28.1	179	21.97	28.6
242	8.87	23.5	178	22.13	36.0
241	8.98	45.1	177	22.65	31.2
240	10.10	35.2	176	22.91	35.0
239	10.31	35.8	175	22.93	32.2
238	10.42	34.7	174	22.97	28.2
237	10.44	22.2	173	23.29	29.1
236	10.92	36.9	172	23.31	27.1
235	11.07	47.2	171	23.32	31.6
234	11.13	23.1	170	23.80	27.0
233	11.16	20.4	169	23.83	26.0
232	11.57	7.3	168	23.84	27.9
231	11.59	28.8	167	24.18	34.0
			166	24.42	32.5
			165	24.45	28.0

164	24.87	27.9	76	43.52	30.6
163	24.89	32.8	75	43.94	26.1
162	24.90	27.6	74	44.34	28.4
161	25.04	26.3	73	44.53	27.8
160	25.15	30.4	72	45.02	28.2
159	25.29	27.5	71	45.21	27.8
158	25.35	25.2	70	45.26	28.8
157	25.44	27.8	69	45.37	29.6
156	25.70	35.0	68	46.04	25.2
155	25.87	28.5	67	46.12	25.2
154	26.20	28.8	66	46.52	23.1
153	26.22	33.3	65	46.98	30.0
152	26.25	29.0	63	47.02	33.9
151	26.49	25.9	62	47.12	27.9
150	26.51	33.1	61	47.59	28.1
149	26.63	32.0	60	48.08	20.3
148	26.68	24.6	59	48.10	28.2
147	26.87	41.1	58	48.24	23.8
145	27.25	30.0	57	48.32	28.8
144	27.27	39.6	56	48.74	21.8
143	27.57	27.7	55	49.05	26.9
140	27.73	32.6	54	49.09	18.9
142	27.75	28.6	53	49.30	27.4
139	28.13	29.0	52	49.35	21.3
138	28.34	35.0	51	49.72	22.7
136	28.40	27.4	50	49.87	21.9
135	28.48	29.8	49	50.25	19.1
134	29.36	30.3	48	50.37	22.4
132	29.41	30.2	47	50.50	21.2
131	29.58	32.9	46	50.70	24.0
130	29.79	28.8	45	50.86	23.2
129	29.82	30.8	44	50.88	13.6
128	29.95	28.4	43	50.92	17.1
126	30.36	32.9	42	50.94	15.0
125	30.63	32.0	41	51.06	26.8
124	30.67	37.1	40	51.13	26.7
123	30.81	32.4	39	51.25	26.1
121	30.84	26.9	38	51.75	26.6
120	31.06	32.4	36	51.81	27.5
118	31.10	29.3	35	52.10	26.1
117	31.43	29.5	34	52.63	27.1
116	33.47	28.5	33	52.84	24.8
115	33.84	37.4	32	52.86	19.7
114	33.87	37.5	31	52.94	27.7
113	34.48	29.5	30	52.99	28.1
112	35.14	26.3	29	53.48	26.1
111	35.68	25.3	28	54.00	26.3
110	35.70	25.3	27	54.45	29.9
109	35.73	26.5	26	54.60	25.3
108	35.85	30.8	25	54.80	32.0
107	35.89	26.9	24	55.02	29.2
106	36.12	28.0	21	55.66	18.7
105	36.22	23.7	20	55.76	52.8
104	36.73	25.3	17	56.31	15.7
103	37.12	32.5	16	56.36	22.0
101	37.17	36.5	15	56.49	20.0
100	37.63	29.2	14	56.51	14.8
98	37.74	30.1	13	56.62	12.5
97	37.80	26.1	12	56.93	10.3
96	38.22	26.4	11	57.38	19.7
95	38.70	27.4	10	58.97	13.6
93	38.76	31.0	9	59.13	16.6
92	38.83	23.4	8	59.32	6.9
91	39.76	28.2	7	59.42	14.0
90	40.14	25.9	6	59.61	8.4
88	40.62	30.7			
87	40.63	28.3			
86	41.00	29.2			
85	41.35	30.6			
84	41.50	27.1			
82	41.53	33.0			
81	42.35	32.4			
80	42.76	29.4			
78	42.79	50.7			
77	43.08	25.5			

**Table F.2** Excess ice content. The values for samples in grey were measured using the methods and equation presented in Chapter Four. Remaining samples (with excess ice content of 100%) are ice-layers. An estimate of 100% excess ice was based on the absence of observable bubbles or sediments contained in the ice.

<b>Mean depth (m)</b>	<b>Excess-ice content (%)*</b>
1.9	36.64
2.1	13.81
4.27	9.54
8.98	22.37
11.57	20.74
26.24	100.00
26.65	100.00
27.74	100.00
28.39	100.00
29.39	100.00
29.99	100.00
30.83	100.00
31.08	100.00
37.15	100.00
37.22	100.00
38.72	100.00
40.62	100.00
41.52	100.00
42.78	100.00
45.23	100.00
47.01	100.00
55.68	100.00
56.32	100.00

\* Excess-ice contents of 100% indicate sediment-free ice layers (1-2 cm thick) which were not measured. These samples were kept frozen to facilitate analysis of gas content in the ice.

## **Appendix G: Core photographs (CD)**